MOTION TOMOGRAPHY PERFORMED BY AUTONOMOUS UNDERWATER VEHICLES

A Thesis
Presented to
The Academic Faculty

by

Meriam Ouerghi

In Partial Fulfillment
of the Requirements for the Degree
of Master of Mechanical Engineering in the
School of Mechanical Engineering

Georgia Institute of Technology
August 2017

MOTION TOMOGRAPHY PERFORMED BY AUTONOMOUS UNDERWATER VEHICLES

Approved by:

Professor Fumin Zhang, Advisor
School of Electrical and Computer Engineering
Georgia Institute of Technology

DR. Jonathan Rogers
School of Mechanical Engineering
Georgia Institute of Technology

Professor Oliver Sawodny
The Institute for System Dynamics
Stuttgart University

Professor Cristina Tarin
The Institute for System Dynamics
Stuttgart University

Date Approved: 27 July 2016

TABLE OF CONTENTS

LIST OF FIGURES

SUMMARY

Motion Tomography (MT) is a novel method to estimate an ambient flow field. Based on collective data obtained from the autonomous underwater vehicles (AUV), MT formulates a specific nonlinear system of equations as an inverse problem.

In this thesis, we redesign the MT algorithm by using a local approximation of the gradient of AUV position. We establish a theoretical study of motion tomography (MT) problem, where we focus on the evolution of the AUV predicted trajectory, computed by the MT algorithm, to derive the MT error dynamics.

A main result of this thesis illustrates a fundamental connection between the trajectory tracing mechanism and the flow update. This insight is not only relevant for proving the convergence of the MT algorithm, but provides a new perspective on inverse problems in general. To overcome the complexity of the underlying problem, we follow a systematic scheme: We start by analyzing one vehicle MT and then we enlarge the scope to multiple vehicle MT.

Therein, we looked for an appropriate way to incorporate the collected data from AUVs and accounting for several reasons, discussed in this work, we focused on Motion Tomography Correction per Cycle (MTCC). We proved the convergence of the redesigned algorithm MTCC without imposing the Lipschitz continuity property.

Furthermore, we improved the accuracy of ambient flow field estimation by extending the MT algorithm with second part. We modified the AUV predicted velocity so that the simulated final time converges to the measured travel time. Finally, the simulations are in good agreement with the theoretical study and underpin the derived conclusions.

CHAPTER I

INTRODUCTION

Autonomous Underwater Vehicles (AUV) have reached a considerable maturity in reliability and agility. They have been developed and constantly improved to serve the changing needs of oceanography in different applications, ranging from short term applications for rapid assesment and sampling, to persistent networks for continuous long-term monitoring and mapping of the ocean [21], [30].

One of the major challenges in AUV deployment is to follow the planned trajectory in an unfamiliar dynamic underwater. As a matter of fact, water current instabilities can deflect the vehicle to an undesired direction and perturb AUVs safety. Furthermore, Global Positioning System (GPS) becomes totally ineffectual underwater because their transmitted signals cannot propagate through seawater. Therefore the vehicles robustness to strong environmental variations is extremely crucial for mission accomplishment. One solution is to estimate and predict the underwater positions based on a priori knowledge of the flow field. However, modeling the ocean field is a sophisticated task that involves many factors. Continuously changing currents and an inaccurate or delayed flow estimate prevents the vehicles from reaching their targets to acquire data [15].

Inspired by the Computerized Tomography (CT), [27] a novel method, called Motion Tomography (MT), is proposed in [2, 4] to improve the underwater navigation by estimating the ambient flow. The MT fuses the data collected by AUVs along their paths, in particular, the effect of the flow on the trajectory to create a spatial map of a flow field through multiple AUVs scanning a region of interest. Compared to other types of algorithms [1, 8] MT defines the Motion Integration Error (MT error) as the

difference between GPS surfacing position of the AUV and predicted position. The obtained MT error is formulated into an inverse problem to infer the underlying flow which is computationally faster and in higher resolution than existing flow models. Accounting for the nonlinear feature of the resulting problem, MT algorithm is an iterative process that consists of trajectory tracing and flow field estimation. However, relying only on the measured end position is not enough to estimate the strength of the flow.

In this regard, the GPS provides in addition to the surfacing position highly accurate estimate of travel time. This thesis exploits this fact and extends MT algorithm with a new phase that incorporates time of travel to improve the accuracy of the flow estimate.

Nonetheless, it turns out that the MT problem is inherently ill-posed. The lack of uniqueness and continuous dependence of the solution on data, impedes the convergence study [37]. Challenges arise not only because the derivative of the MT error function is not continuous and not defined on the whole data space, but also because it is not a locally Lipschitz function, a fundamental prerequisite to prove the convergence of inverse problem. The most conventional choices of nonlinear iterative algorithms are the family of variants on Newton's method e.g. Damped Gauss-Newton and Levenburg-Marquardt [25].

Accounting for its wide application, there exists a substantial literature devoted to study the convergence of nonlinear Newton's method in its various forms. The interested readers are referred to the excellent survey paper [40] for detailed accounts. The convergence theory of Newton's method assumes at least continuous differentiability of the nonlinear function and nonsingularity of the Jacobian [24]. However, some relaxations have been made to extend the application of the classical Newton method, just to name a few: Newton-like methods for solving nonlinear equations with non differentiable terms in [7] or the calm solution mappings in [10–12]. The

existing theoretical justifications of the inverse problem convergence revolve mainly around the Lipschitz property in different forms and these do not hold for the MT algorithm. Therefore, we approach the MT problem with a different perspective and we redesign the MT algorithm.

For data incorporation, we construct a set of non linear constraints and we apply the Kaczmarz method which is an iterative approach to solve a non linear system of equations. Concerning the convergence analysis, we limit the scope first on one vehicle in order to elucidate the trajectory tracing mechanism and the associated features. We provide a compact form for the error dynamics by computing the necessary derivatives for the algorithm. Based on one vehicle analysis we raise the challenge by considering the one axis analysis and finally the general MT problem. We prove the convergence of the proposed algorithm without requiring the Lipschitz continuity condition. In an analogous way to CT, see [8], we propose two versions of the MT algorithm that account multiple vehicle incorporation: Motion Tomography Correction per Cycle (MTCC) and Motion Tomography Correction Per Projection (MTCP). Adding to that, this thesis incorporates the time information into the MT problem, to provide more accurate results than previous work [2].

The rest of the document is organized as follows. Chapter 2 introduces some background material that is relevant for the main results of this thesis and provides a short review of MT algorithm introduced in [2]. In Chapter 3, we redesign the MT algorithm and derive the MT error dynamics. The convergence of the redesigned MT algorithm is proved without imposing the Lipschitz continuity property. Chapter 4 extends the MT algorithm with a new phase by incorporating time of travel. Convergence analysis is established as well. Chapter 5 addresses the multiple vehicle problem. We propose two versions of MT algorithm and we establish the convergence of the MT error. Finally, we prove the theoretical conclusions by simulations in Chapter 6 and we conclude the thesis in Chapter 7.

CHAPTER II

PRELIMINARY RESEARCH

Autonomous Underwater Vehicles (AUVs) are characterized by relatively slow speed. Hence, the motion of (AUVs) is strongly affected by ocean currents, and consequently the surfacing position deviates from the planned position. Motion Tomography (MT) takes into account this fact to estimate the depth-averaged flow velocity using GPS surfacing positions $r^* \in \mathbb{R}^2$.

This chapter aims to provide detailed literature review of the research domains relevant to motion tomography. The research challenges and difficulties associated with each of the domains will be discussed.

2.1 Formulation of MT

In this section, we define the MT framework by making the following assumptions:

Assumption 2.1.1. *The flow field is time-invariant over one observation interval $\mathcal{T}$. As a result, the flow is now represented by $F(r,t) = F(r)$.*

Assumption 2.1.2. *The horizontal through-water speeds (as opposed to ground speeds) of all vehicles are identically s_{h}, which is a constant.*

2.1.1 Vehicle Motion Under Flow

We consider the depth averaged horizontal motion of AUVs subject to ambient time invariant flow $F(r(t)) \in \mathbb{R}^2_+$. Assuming that the AUV motion is a first order particle model with constant speed s_{h} and heading angle $\theta \in \mathbb{R}_+$, then the velocity of the AUV $V(t) \in \mathbb{R}^2_+$ varies according to the flow $F(r(t))$ such that the final position $r^f \in \mathbb{R}^2_+$

follows:

$$r^f = r^0 + \int_{t_0}^{t^f} V(t)\mathrm{d}t = r^0 + \int_{t_0}^{t^f} \left(S + F(r(t))\right) \mathrm{d}t, \tag{1}$$

where $S = s_\mathrm{h}[\cos\theta, \sin\theta]^\top$, $r^0 \in \mathbb{R}^2_+$ refers to the initial position, t_0 the start time of observation and t^f to the time of travel.

MT estimates a flow field map from the motion-integration error and trajectory information of the AUV. Suppose the AUV position is available only at time t_0 and t^f and the flow $F(r(t))$ is unknown, then an offset between the estimated and real trajectories is observed. So the motion-integration error along the vehicle trajectory $\gamma(t), t \in \mathcal{T}$ is defined in as:

$$d(\gamma,\mathcal{T}) = \int_{t_0}^{t^f} \left(\dot{r}(\tau,F) - \dot{\tilde{r}}(\tau,\tilde{F})\right) d\tau = \int_{t_0}^{t^f} \left(F(r)\right) \mathrm{d}\tau, \tag{2}$$

where $F(r(t))$ is the real flow, $\mathcal{T} = t^f - t_0$ is the observation interval and $\tilde{F}$ is prior flow information which is assumed to be zero.

2.1.2 MT Problem Formulation

In order to estimate the spatial distribution of a flow field, the previous work [2] incorporates the motion-integration errors of multiple AUVs. N vehicles are deployed in a domain $\mathcal{D}$ (see Figure 1). We denote their surfacing positions by ${}^i r$, $i = \{1, \cdots, V\}$ and the trajectories of each vehicle by curve ${}^v\gamma$. Let ${}^i d$ be the motion-integration error of vehicle v which is determined after one observation interval $\mathcal{T}$.

Chang et al.all introduce the arc-length parameter ${}^i\ell$ for curve ${}^i\gamma$ to describe the MT error along the AUV trajectory as follows:

$$\mathrm{d}^i\ell = \|{}^iV(F(r(t)))\|\mathrm{d}t. \tag{3}$$

Combining Eq.(3) with Eq.(2) yields:

$${}^i d = \int_{{}^i\gamma} \frac{1}{\|V(F({}^i r))\|} F({}^i r)\mathrm{d}^i\ell. \tag{4}$$

Now discretize domain $\mathcal{D}$ into $\mathbf{P}=n\times n$ grid cells, as illustrated in Fig.1. For the kth cell, let us denote flow velocity by F^k. Since the vehicle heading θ is constant, the traced trajectory is piecewise linear over the domain $\mathcal{D}$. For the vth vehicle in C^k, we assume that vehicle heading ${}^i\theta^k$ is constant within C^k. Then, the speed of the ith vehicle along the trajectory is given by

$$\left\|{}^iV^k(F)\right\| = \left\| s_{\mathrm{h}} \begin{bmatrix} \cos{}^i\theta^k \\ \sin{}^i\theta^k \end{bmatrix} + F^k \right\|. \tag{5}$$

We assume that vehicle heading ${}^i\theta^k$ is available to us or can be estimated with small bounded error. For the vth vehicle passing through the kth cell, C^k, the length of the vehicle trajectory, ${}^iL^k$, can be obtained by

$${}^iL^k = \int_{{}^i\gamma[C^k]} \mathrm{d}{}^i\ell, \tag{6}$$

in which ${}^i\gamma[C^k]$ represents curve ${}^i\gamma$ within the spatial interval for C^k in a planar space. Based on the discretization setting designed above, Eq (4) can be discretized into the following form:

$${}^id = \sum_{k=1}^{\mathbf{P}} \frac{{}^iL^k(F)}{\|{}^iV^k(F)\|} F^k, \quad i = \{1,\cdots,N\}. \tag{7}$$

Considering the flow velocity along the x and y directions separately, we have

$$\begin{aligned} {}^id_x &= \sum_{k=1}^{\mathbf{P}} \frac{{}^iL^k(F)}{\|{}^iV^k(F)\|} F_x^k, \\ {}^id_y &= \sum_{k=1}^{\mathbf{P}} \frac{{}^iL^k(F)}{\|{}^iV^k(F)\|} F_y^k \end{aligned} \tag{8}$$

By constructing vectors $\mathbf{d}_x = [{}^1d_x, {}^2d_x, \cdots, {}^Nd_x]^T$ and $\mathbf{d}_y = [{}^1d_y, {}^2d_y, \cdots, {}^Nd_y]^T$, we can rewrite Eq (8) as

$$\begin{aligned} \mathbf{d}_x &= L(F)F_x \\ \mathbf{d}_y &= L(F)F_y, \end{aligned} \tag{9}$$

where $F = [F_x^T, F_y^T]^T$, and

$$L(F) = \begin{bmatrix} \frac{{}^1L^1(F)}{\|{}^1V^1(F)\|} & \cdots & \frac{{}^1L^{\mathbf{P}}(F)}{\|{}^1V^{\mathbf{P}}(F)\|} \\ \vdots & \ddots & \vdots \\ \frac{{}^NL^1(F)}{\|{}^NV^1(F)\|} & \cdots & \frac{{}^NL^{\mathbf{P}}(F)}{\|{}^NV^{\mathbf{P}}(F)\|} \end{bmatrix}. \tag{10}$$

Hence, the obtained equation (9) is an inverse problem that uses the measured motion integration error d to estimate the flow F. Inspecting Eq (9) reveals that the MT problem is nonlinear, non differentiable and even inherently ill-posed. The lack of uniqueness and continuous dependence of the solution on data brings challenges to MT [37]. The work [2] proposes the Trajectory Tracing mechanism to circumvent the non linearity, a key step to solve the MT problem.

2.1.3 Trajectory Tracing and Its Error Bound

Since real vehicle trajectories are nonlinear, computing $L(F)$ under the assumption that the trajectories are linear jeopardizes the accuracy of flow mapping. Trajectory Tracing constructs new AUV trajectory based on the predicted flow. The vehicle trajectory is traced at iteration i through simulation that embeds the current estimate of the flow field F_i. For the ith vehicle, the vehicle velocity is obtained as follows:

$${}^iV_j(t) = s_{\mathrm{h}} \begin{bmatrix} \cos{}^i\theta \\ \sin{}^i\theta \end{bmatrix} + F_i({}^ir_j(t)), \tag{11}$$

Hence the traced vehicle trajectory γ_j is obtained as follows:

$${}^i\gamma_j = \int_{t^0}^{t^f} \left(s_{\mathrm{h}} \begin{bmatrix} \cos{}^i\theta \\ \sin{}^i\theta \end{bmatrix} + F_i({}^ir_j(t)) \right) \mathrm{d}t, \tag{12}$$

Plugging Eq (12) in (7) provides the motion integration error d_j to update the predictive flow at iteration $j+1$. Accordingly, MT comprises two key steps: iteratively alternates between flow estimation and trajectory tracing.

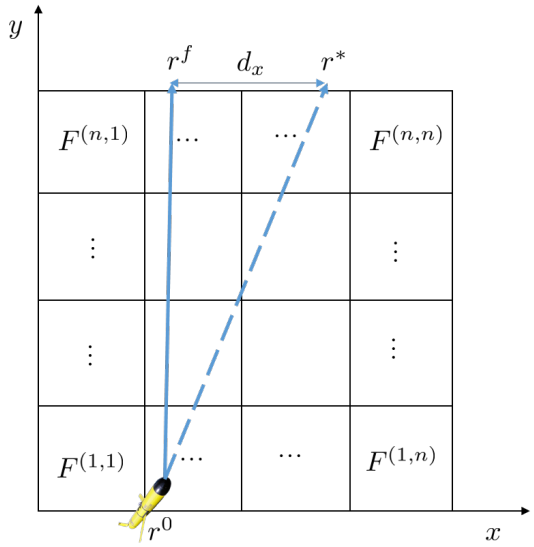

Figure 1: Illustration of MT mapping formulation. Actual (the blue dashed line) and predicted (the blue solid line) vehicle trajectories are displayed in a discretized domain.

2.2 A Kaczmarz-Type Method for Flow Field Estimation by MT

Adding to the non-linearity and the non-differentiability of (4), the number of obtained trajectories is significantly smaller than the number of cells crossed by one AUV. Therefore, the MT problem is a highly underdetermined nonlinear system. To deal with these challenges, an iterative flow field estimation algorithm is derived in [2]. The method is based on the Kaczmarz method [17, 18], an iterative method for solving a linear system of equations. The Kaczmarz method, also known as the algebraic reconstruction technique [13] in the medical imaging community, has been used for computerized tomography [26].

The proposed Kaczmarz method iterates the following optimization process:

$$\begin{aligned} F_{j+1} &= \underset{F}{\operatorname{argmin}} \frac{1}{2} \|F - F_j\|^2 \\ \text{subject to} \quad & {}^i d = {}^i L(F) \end{aligned} \tag{13}$$

where ${}^iL_j$ is the ith row of matrix L, ${}^id$ the ith element of vector $\mathbf{d}$. Solving (13)

Algorithm 1: MT flow field estimation

Data: Motion-integration errors ${}^i\mathbf{d} = \{{}^1\mathrm{d}, \cdots, {}^N d\}$

Set $i = 0$. Make an initial guess of the solutions, $F_{x,0}$ and $F_{y,0}$.

repeat

  for $v = 1$ **to** N **do**

    Update the solutions by

$$F_{x,j+1} = F_{x,j} + \lambda_j \frac{{}^i d_{x,j} - {}^i L(F_j) F_{x,j}}{\|{}^i L(F_j)\|^2} \left({}^p L(F_j)\right)^T,$$

$$F_{y,j+1} = F_{y,j} + \lambda_j \frac{{}^i d_{y,j} - {}^j L(F_j) F_{y,j}}{\|{}^i L(F_j)\|^2} \left({}^i L(F_j)\right)^T,$$

    Let $i = i + 1$.

  end

  ${}^i e_{x,j} =^i L(F_j) F_{x,j} -^i \mathrm{d}_{x,j}$.

  ${}^i e_{y,i} =^i L(F_j) F_{y,j} -^i \mathrm{d}_{y,j}$.

until *a stopping condition is met (e.g.,* $\|{}^i e_{x,i}\|, \|{}^i e_{y,i}\| \leq \epsilon_{\mathbf{F}}$*)*

yields the following formula to update F:

$$F^{k+1} = F^k + \lambda_k \frac{d_j - \mathbf{L}_j F^k}{\|\mathbf{L}_j\|^2} \mathbf{L}_j^T, \tag{14}$$

where λ_k is a relaxation parameter for the convergence rate of the method. Furthermore, the convergence of Motion Integration Error d has been analyzed in previous work [2]. However, the proposed proof requires the following assumptions:

Assumption 2.2.1. *Given any real numbers* $0 < \epsilon, \beta < 1$ *and a true solution* $F^\star$ *to Equation* (7)*, there exists a ball* $\mathcal{B}(F^\star, \delta)$ *around* $F^\star$ *with radius* $\delta > 0$ *such that the following hold for all* $f \in \mathcal{B}(F^\star, \delta)$*:*

1) $\dfrac{\gamma_L \|F^\star\|}{\|{}^i L(F)\|} < \sqrt{\epsilon}$ *for all* $i = \{1, \cdots, N\}$.

2) *For a sequence* F_j *generated by Equation* (14)*, let* $\mathbf{e}_j = F_j - F^\star$ *and* $M_j = I -^i \mathbf{L}^+(F_j)\,{}^i\mathbf{L}(F_j)$ *where* $j = \mathrm{mod}(j, N) + 1$*. For every* N *iterations, there exists at least one* $i \in \{nN, nN+1, \cdots, (n+1)N - 1\}$*,* $n = \{0, 1, 2, \cdots\}$ *such that* $\mathbf{e}_j$ *satisfies* $\langle M_j \mathbf{e}_j, \mathbf{e}_j \rangle \leq (1 - \beta) \langle \mathbf{e}_j, \mathbf{e}_j \rangle$ *where* $\beta > 1 + \epsilon - \dfrac{1}{(1+\epsilon)^{N-1}}$.

Assumption 2.2.2. *${}^iL(F)$ in Equation* (7) *is Lipschitz continuous for all $i = \{1, \cdots, N\}$ with the largest Lipschitz constant $\gamma_L = \max_i {}^i\gamma_L$, where ${}^i\gamma_L$ is the Lipschitz constant for ${}^iL(F)$.*

Based on the proposed Assumptions, the convergence of MT algorithm is presented in the following Theorem:

Theorem 2.2.1. *Suppose Assumptions 2.2.2 and 2.2.1 hold for Equation* (9) *and its solution $\boldsymbol{F}^\star$. Starting from any initial point $\boldsymbol{F}_0$ within a ball $\mathfrak{B}(\boldsymbol{F}^\star,\delta)$, e.g., $\|\boldsymbol{F}^\star - \boldsymbol{F}_0\| < \delta$, the sequence $\boldsymbol{F}_j$ generated by Algorithm 2 converges to $\boldsymbol{F}^\star$ as $j \to \infty$.*

A thorough review of the proof of Theorem 2.2.1, see [2] reveals its invalidity because it assumes that the optimal solution is isolated, and this assumption does not hold for the tomography application. As a matter of fact the problem has uncountably infinite solutions. Thus, in any ball of radius δ around $\mathbf{F}^\star$ there are uncountable many other solutions.

Moreover, Assumption 2.2.2 does not hold in general case. Due to the non-continuity of the estimated flow, the MT pronblem is not Lipschitz. As it is well known that if the optimal problem is non differentiable or not Lipschitz continuous, analyzing the underlying algorithm turns out to be a challenging task.

For the reasons given above, we approach the MT problem with different perspective using different techniques that we will suggest in the following chapter. We reconsider the formulation of MT problem and accordingly we redesign the algorithm to establish the convergence of MT algorithm.

CHAPTER III

CONVERGENCE ANALYSIS OF MOTION INTEGRATION ERROR

This chapter extends previous work on Motion Tomography (MT). We redesign the MT algorithm using a local approximation of the gradient of the AUV position. Furthermore, we establish the trajectory tracing mechanism and derive the MT error dynamics. The convergence of the redesigned MT algorithm is proved without imposing the Lipschitz continuity property.

3.1 Formulation of MT

We consider the horizontal trajectory of AUVs subject to ambient time invariant flow $F(r(t)) \in \mathbb{R}^2_+$. Assuming that the AUV motion is a first order particle model with constant speed and heading angle $s_{\mathrm{h}}, \theta \in \mathbb{R}_+$, the velocity of the AUV $V(r(t)) \in \mathbb{R}^2_+$ varies according to the flow $F(r(t))$ such that the final position $r^f \in \mathbb{R}^2_+$ follows:

$$r^f = r^0 + \int_{t_0}^{t^f} V(r(t))\mathrm{d}t = r^0 + \int_{t_0}^{t^f} S + F(r(t))\mathrm{d}t, \tag{15}$$

where $S = s_{\mathrm{h}}[\cos\theta, \sin\theta]^\top$, $r^0 \in \mathbb{R}^2_+$ refers to the initial position and t^f to the time of travel.

For the sake of self-containment, let us briefly recall the principles of MT. Suppose the AUV position is available only at time t_0 and t^f and the flow $F(r(t))$ is unknown, then an offset between the estimated and actual trajectories is observed. So the motion-integration error $d(\gamma,\mathcal{T})$ along the vehicle trajectory $\gamma(t), t \in \mathcal{T}$ is defined in as:

$$d(\gamma,\mathcal{T}) = \int_{t_0}^{t^f} \dot{r}(\tau,F) - \dot{\tilde{r}}(\tau,\tilde{F})d\tau = \int_{t_0}^{t^f} F(r)d\tau, \tag{16}$$

where $F(r,t)$ is real flow, and prior flow information $\tilde{F}$ is assumed to be zero. The MT method creates a map of the underlying flow field F by solving the motion-integration error equation (16) through an iterative process that consists of trajectory tracing and flow field estimation. The traced trajectory $\tilde{\gamma}$ is obtained by iteratively simulating the vehicle trajectory using the current estimate of the flow as follows:

$$\tilde{\gamma} = \int_{t_0}^{t^f} \left(S + \tilde{F}(r) \right) \mathrm{d}t. \tag{17}$$

We keep the original formulation of the MT problem but we solve it in a different way that enables us to later analyze the trajectory tracing and to study the convergence of MT error d. We simplify (15) by making the following assumption:

Assumption 3.1.1. *We assume that input velocity S is constant, the heading angle varies between $0 \leq \theta \leq \frac{\pi}{2}$ and the AUV velocity $V(t)$ is componentwise positive.*

We discretize domain $\mathcal{D}$ into $P = n \times n$ grid cells with $C^{(h,s)}$ referring to the (h,s)th cell and define index $k = (h-1)n + s$ such that $C^k \equiv C^{(h,s)}$, $k = \{1, \cdots, P\}$, as illustrated in Fig.1. For the kth cell, let us denote flow velocity by F^k. Since the vehicle heading θ is constant, the traced trajectory is piecewise linear over the domain $\mathcal{D}$. Furthermore, $\mathcal{C}_i$ denotes the ordered set of cells that the AUV crosses at iteration $i : \mathcal{C}_i = \{C^0, \cdots, C^f\}$. Since only the flow in cells crossed by the AUV intervenes in the corresponding MT error, the flow $F_i^k(r_i(t))$ at iteration i in cell k can be defined along the traced trajectory $\tilde{\gamma}_i$ as:

$$F_i^k(r_i(t)) = \begin{cases} [F_{x,i}^k, F_{y,i}^k]^\top, & r_i(t) \in C^k \\ [0,0]^\top & otherwise \end{cases} \tag{18}$$

where $r_i(t)$ is the positon of the AUV along the traced trajectory $\tilde{\gamma}_i$. Next we use the step function U to formulate $F_i^k(r_i(t))$:

$$F_i(r_i(t)) = \sum_{h=1}^{n} \sum_{s=1}^{n} F_i^{(h,s)} M^{(h,s)}(t), \tag{19}$$

where $r_i(t) = [x_i(t), y_i(t)]^\top$, Δ is length of the edge of one cell and $M^{(h,s)}(t)$ is equal to $((1 - U(x_i(t) - h\Delta))(1 - U(y_i(t) - s\Delta))U(x_i(t) - (h-1)\Delta)U(y_i(t) - (s-1)\Delta)))$. Plugging this expression in (15) yields:

$$\begin{aligned} r_i^f &= r^0 + \int_{t_0}^{t_i^f} S + F_i(r_i(t))\mathrm{d}t \\ &= r^0 + \sum_{h=1}^{n}\sum_{s=1}^{n}\int_{t_0}^{t_i^f}(S + F_i^{(h,s)}M^{(h,s)}(t))\mathrm{d}t. \end{aligned} \tag{20}$$

Let $\mathbf{F}_i$ denote $\mathbf{F}_i^\top = [F_i^{(1,1)}, \cdots, F_i^{(n,n)}]^\top$ and r^* the final measured position, we define the MT inverse problem solving the following equation for $\mathbf{F}_i$ for each iteration i:

$$d_i = r^* - r_i^f(\mathbf{F}_i). \tag{21}$$

Since F_i^k depends on the position of AUV r_i^k, according to (18), the obtained MT inverse problem (21) is nonlinear. Thus, we use the Newton-type method to compute $\mathbf{F}^*$ such that $d_i \to 0$ as $i \to \infty$. However, this apprach requires gradient computation [24].

Noting that (21) is not differentiable and its corresponding solution is nonisolated, we define $\mathcal{F}^*$ as the set of solutions that fulfill $r^* - r_i^f(\mathbf{F}_i) = 0$ and we propose a suitable substitute for the gradient:

Let us define $\nabla r(F_i^k)$ as a local gradient of r with respect to the flow $F_i^{k\top} = [F_{x,i}^k, F_{y,i}^k]^\top$, and we define t_i^k the duration of travel in cell C^k such that when the AUV reaches one side of cell C^k $(x_i^k - h\Delta).(y_i^k - s\Delta) = 0$ holds. Hence, we integrate the AUV velocity in cell C^k and compute x_i^k in recursive way as follows:

$$x_i^k = x_i^{k-1} + \int_0^{t_i^k}(S_x + F_{x,i}^k)M^{(h,s)}(t)\mathrm{d}t. \tag{22}$$

We remark from Equations (22) and (18) that there is a nonlinear relationship between the AUV position and the predicted flow. In order to estimate the flow, we need the corresponding set of cells that the AUV crossed. Hence, we can compute the gradient of the AUV position to predict the flow. Assuming the underlying trajectory includes

cell C^k, we get $\frac{\partial x_i^k}{\partial F_{x,i}^k}$

$$\frac{\partial x_i^k}{\partial F_{x,i}^k} = \int_0^{t_i^k} M^{(h,s)}(t) + (S_{x,i} + F_{x,i}^k)\frac{\partial M^{(h,s)}(t)}{\partial F_{x,i}^k}\mathrm{d}t. \tag{23}$$

We insert the definition of Dirac delta function δ into (23) to get:

$$\int_0^{t_i^k} \frac{\partial U(x(t) - h\Delta)}{\partial F_{x,i}^k}\mathrm{d}t = \int_0^{t_i^k} \delta(x(t) - h\Delta)\frac{\partial x(t)}{\partial F_{x,i}^k}\mathrm{d}t. \tag{24}$$

Since the gradient approximation is locally defined inside the cell C^k, $\delta(x(t)-h\Delta) = 0$ inside C^k. Hence we get:

$$\int_0^{t_i^k} \frac{\partial U(x(t) - h\Delta)}{\partial F_{x,i}^k}\mathrm{d}t = \int_0^{t_i^k} \delta(x(t) - h\Delta)\frac{\partial x(t)}{\partial F_{x,i}^k}\mathrm{d}t = 0. \tag{25}$$

Hence, (23) is reduced to $\int_0^{t_i^k} M(t)^{(h,s)}\mathrm{d}t$ where $M(r(t)) = 1$ for $r(t) \in C^k$. This means that $\int_0^{t_i^k} M(t)\mathrm{d}t = t_i^k$.

Similarly we finish computing the local gradient:

$$\begin{aligned} \frac{\partial x(t_i^k)}{\partial F_{x,i}^k} &= t_i^k, \quad \frac{\partial x(t_i^k)}{\partial F_{y,i}^k} = 0 \\ \frac{\partial y(t_i^k)}{\partial F_{y,i}^k} &= t_i^k, \quad \frac{\partial y(t_i^k)}{\partial F_{x,i}^k} = 0. \end{aligned} \tag{26}$$

Let us stack all the flow vectors F_i^k for the grid cells in $\mathbf{F}_i$. We solve the MT inverse problem using first order Taylor expansion around $\mathbf{F}_i$:

$$r_i^f(\mathbf{F}^*) = r_i^f(\mathbf{F}_i) + \nabla r_i^f(\mathbf{F}_i)^\top(\mathbf{F}^* - \mathbf{F}_i) \tag{27}$$

Let $\mathbf{F}_{i+1} = \mathbf{F}^*$ and $\|T_i\|^2 = \sum_{k=1}^f t_i^{k^2}$ applying the technique proposed in [24] we update the predicted flow at step $i+1$:

$$F_{i+1}^k = F_i^k + \frac{t_i^k}{\|T_i\|^2} d_i. \tag{28}$$

Algorithm 2: MT flow field estimation

Data: Measured final position r^*

Set $i = 0$. Initialize the flow $F_0^k = \mathbf{0} \in \Re^2$; **repeat**

  Trajectory tracing to get T_i, t_i^k and d_i

  Update the flow in all cells k:

$$F_{i+1}^k = F_i^k + \frac{t_i^k}{\|T_i\|^2} d_i. \tag{29}$$

until $\| d_i\| \leq \epsilon_{\mathbf{f}}$

3.2 Trajectory Tracing

As we discussed above, the flow update requires the underlying trajectory, which can be obtained by the Trajectory Tracing Mechanism. This is an approach that constructs new AUV trajectory based on the predicted flow and provides the set of crossed cells and the gradient of AUV position. The vehicle trajectory is traced at iteration i through simulation that embeds the current estimate of the flow field F_i. We suggest in this section an explicit formulation for trajectory tracing, that we can use not only to update the inputs for the MT algorithm but to establish the convergence analysis. As a matter of fact, computing the AUV end position r_i^k in the cell C_i^k allows to determine the corresponding travel time t_i^k as follows:

$$t_i^k = \frac{y_i^k - y_i^{k-1}}{V_{y,i}^k}, \quad V_{y,i}^k > 0 \tag{30}$$

Adding to that, we can compute the resulted MT error $d_i = r^* - R_i^f$ and $\|T_i\|^2$, since $\|T_i\|^2 = \sum_{k=1}^{f} {t_i^k}^2$ and t_i^k is known.

The trajectory tracing formulation holds in the intersection cells $\mathcal{C}_{i-1} \cap \mathcal{C}_i$, which means the part of traced trajectory that crosses the same cells in iteration i and $i-1$. Furthermore, we need to have an explicit form for the final position in order to establish a motion estimation recursion. Accounting for the discontiunity of the flow, we consider the cells $\mathcal{C}_{i-1} \cap \mathcal{C}_i = \{C^1, \cdots, C^m\}$ where the AUV navigates at iteration

i and $i-1$. Hence, the AUV will cross the same side of the k^{th} cell, $k < m$:

$$(x_i^k - x_{i-1}^k).(y_i^k - y_{i-1}^k) = 0 \tag{31}$$

For convenience, we define $\varepsilon_{x,i}^k = \frac{t_i^k}{\|T_i\|^2} d_{x,i}$, $\varepsilon_{y,i}^k = \frac{t_i^k}{\|T_i\|^2} d_{y,i}$, and $\varepsilon_i^k = [\varepsilon_{x,i}^k, \varepsilon_{y,i}^k]^\top$, the AUV velocity as $V_i^k = [V_{x,i}^k, V_{y,i}^k]^\top$ and we use $\times$ for the 2 dimension cross product.

Theorem 3.2.1. *Let the flow be updated according to (28), Assumption 3.1.1 holds and suppose $\mathcal{C}_{i-1} \cap \mathcal{C}_i = \{C^1, \cdots, C^p\}$. Let $C^m \in \{C^1, \cdots, C^p\}$. Then, there exists three different ways of cell crossing:*

- *The first case is when the AUV crosses opposite sides: On the one hand, if $y_i^m - y_i^{m-1} = \Delta$ holds, then:*

$$\begin{aligned} y_i^m &= y_{i-1}^m \\ x_i^m &= x_{i-1}^m - \frac{t_{i-1}^m}{V_{y,i}^m} V_{i-1}^m \times \varepsilon_{i-1}^m + x_i^{m-1} - x_{i-1}^{m-1}. \end{aligned} \tag{32}$$

  On the one hand, if $x_i^m - x_i^{m-1} = \Delta$ is valid, the AUV position is:

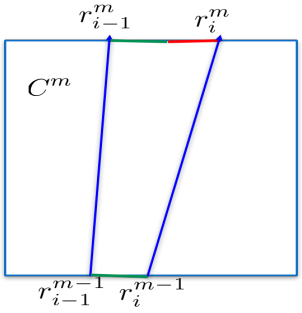

Figure 2: Case one:Vertical crossing.

$$\begin{aligned} x_i^m &= x_{i-1}^m \\ y_i^m &= y_{i-1}^m - \frac{t_{i-1}^m}{V_{x,i}^m} V_{i-1}^m \times \varepsilon_{i-1}^m + y_i^{m-1} - y_{i-1}^{m-1} \end{aligned} \tag{33}$$

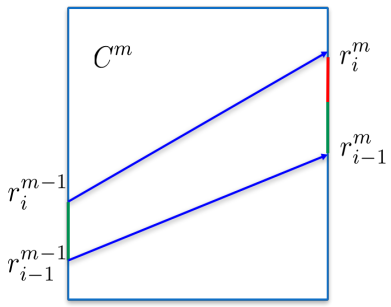

Figure 3: Case one:Vertical crossing.

- *The second case is when the AUV crosses two consecutive sides in the following order:* $y_i^{m-1} = h\Delta \cap x_i^m = (s+1)\Delta$.

$$\begin{aligned} x_i^m &= x_{i-1}^m \\ y_i^m &= y_{i-1}^m - \frac{t_{i-1}^m}{V_{x,i}^m} V_{i-1}^m \times \varepsilon_{i-1}^m + \frac{V_{y,i}^m}{V_{x,i}^m}(x_{i-1}^{m-1} - x_i^{m-1}). \end{aligned} \tag{34}$$

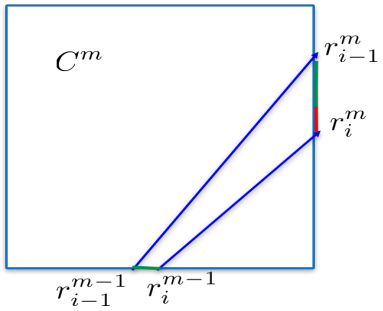

Figure 4: Second Case of cell crossing

- *The third case follows when* $y_i^m = (h+1)\Delta \cap x_i^{m-1} = s\Delta$

$$\begin{aligned} y_i^m &= y_{i-1}^m \\ x_i^m &= x_{i-1}^m - \frac{t_{i-1}^m}{V_{y,i}^m} V_{i-1}^m \times \varepsilon_{i-1}^m + \frac{V_{x,i}^m}{V_{y,i}^m}(y_{i-1}^{m-1} - y_i^{m-1}). \end{aligned} \tag{35}$$

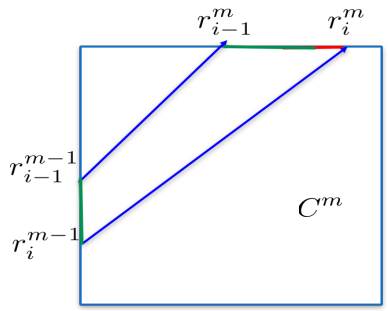

Figure 5: Third Case of cell crossing.

Based on the discussed cases, the AUV predicted position r_i^m *can be traced in iterative way up to cell* C^m*. If* $y_i^m = y_{i-1}^m$ *holds, we have:*

$$\begin{aligned} y_i^m &= y_{i-1}^m \\ x_i^m &= x_{i-1}^m - \sum_{k=1}^{m} \prod_{j=k}^{m} \alpha_i^j \frac{t_{i-1}^k}{V_{y,i}^k} V_i^k \times \varepsilon_{i-1}^k, \end{aligned} \tag{36}$$

Elsewhere,

$$\begin{aligned} x_i^m &= x_{i-1}^m \\ y_i^m &= y_{i-1}^m - \sum_{k=1}^{m} \frac{t_{i-1}^k}{V_{x,i}^k} \prod_{j=k}^{m} \alpha_i^j V_i^k \times \varepsilon_{i-1}^k, \end{aligned} \tag{37}$$

where

$$alpha_i^j = \begin{cases} 1 & if \quad y_i^j - y_i^{j-1} = \Delta \cup x_i^j - x_i^{j-1} = \Delta \\ \frac{V_{y,i}^j}{V_{x,i}^j} & if \quad y_i^j = h\Delta \cap x_i^{j-1} = s\Delta \\ \frac{V_{x,i}^j}{V_{y,i}^j} & otherwise \end{cases} \tag{38}$$

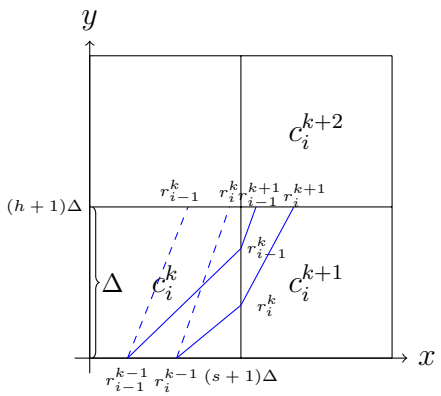

Figure 6: Illustration of different traced trajectories.

Proof. Concerning trajectory tracing, we notice from figure 6, that there exist 6 different cases to cross one cell. However, the symmetry of the grid reduces them to 3 cases:

First scenario, depicted by the dashed line in Figure 6, is when the AUV traverses the cell through vertical opposite sides; in other terms $y_i^k - y_i^{k-1} = \Delta$. The ordinate y_i^{k-1} remains equal to y_{i-1}^{k-1} and the change of the estimated flow will be reflected in x_i^k as follows:

$$\begin{aligned} x_i^k &= t_i^k V_{x,i}^k + x_i^{k-1} \\ &= \Delta \frac{V_{x,i}^k}{V_{y,i}^k} + x_i^{k-1}. \end{aligned} \tag{39}$$

We formulate $x_{i-1}^k = \Delta \frac{V_{x,i-1}^k}{V_{y,i-1}^k} + x_{i-1}^{k-1}$ and we add x_{i-1}^k and subtract $\Delta \frac{V_{x,i-1}^k}{V_{y,i-1}^k} + x_{i-1}^{k-1}$ in the above equation:

$$\begin{aligned} x_i^k &= \Delta(\frac{V_{x,i}^k}{V_{y,i}^k} - \frac{V_{x,i-1}^k}{V_{y,i-1}^k}) + x_i^{k-1} - x_{i-1}^{k-1} + x_{i-1}^k \\ &= x_{i-1}^k + t_{i-1}^k(\frac{V_{x,i}^k V_{y,i-1}^k - V_{x,i-1}^k V_{y,i}^k}{V_{y,i}^k}) + x_i^{k-1} - x_{i-1}^{k-1} \\ &= x_{i-1}^k + t_{i-1}^k(\frac{\varepsilon_{x,i-1}^k V_{y,i-1}^k - V_{x,i-1}^k \varepsilon_{y,i-1}^k}{V_{y,i}^k}) + x_i^{k-1} - x_{i-1}^{k-1} \\ &= x_{i-1}^k - \frac{t_{i-1}^k}{V_{y,i}^k} V_{i-1}^k \times \varepsilon_{i-1}^k + x_i^{k-1} - x_{i-1}^{k-1}. \end{aligned} \tag{40}$$

Hence first case of cell crossing satisfies the following dynamic:

$$\begin{aligned} y_i^k &= y_{i-1}^k \\ x_i^k &= x_{i-1}^k - \frac{t_{i-1}^k}{V_{y,i}^k} V_{i-1}^k \times \varepsilon_{i-1}^k + x_i^{k-1} - x_{i-1}^{k-1}. \end{aligned} \tag{41}$$

The same reasoning provides the vehicle position if the AUV traverses the cell through horizontal opposite sides, in other terms $x_i^k - x_i^{k-1} = \Delta$

$$x_i^k = x_{i-1}^k$$

$$y_i^k = y_{i-1}^k - \frac{t_{i-1}^k}{V_{x,i}^k} V_{i-1}^k \times \varepsilon_{i-1}^k + y_i^{k-1} - y_{i-1}^{k-1} \tag{42}$$

Concerning the second case, depicted by the solid line in cell $C^k = C^{(h,s)}$ in Figure 6, where the AUV crosses 2 consecutive sides such that $y_i^{k-1} = h\Delta \cap x_i^k = (s+1)\Delta$. In this case $t_i^k = \frac{\Delta - x_i^{k-1}}{V_{x,i}^k}$:

$$\begin{aligned}
y_i^k &= t_i^k V_{y,i}^k + y_i^{k-1} \\
&= \frac{\Delta - x_i^{k-1}}{V_{x,i}^k} V_{y,i}^k + y_i^{k-1} \\
&= \frac{\Delta - x_{i-1}^{k-1}}{V_{x,i}^k} V_{y,i}^k - \frac{\Delta - x_{i-1}^{k-1}}{V_{x,i-1}^k} V_{y,i-1}^k + y_i^{k-1} - y_{i-1}^{k-1} + y_{i-1}^k + \frac{V_{y,i}^k}{V_{x,i}^k}(x_{i-1}^{k-1} - x_i^{k-1}) \\
&= y_{i-1}^k + t_{i-1}^k \left(\frac{V_{x,i-1}^k V_{y,i}^k - V_{x,i}^k V_{y,i-1}^k}{V_{x,i}^k}\right) + y_i^{k-1} - y_{i-1}^{k-1} + \frac{V_{y,i}^k}{V_{x,i}^k}(x_{i-1}^{k-1} - x_i^{k-1}).
\end{aligned} \tag{43}$$

Hence, $y_i^{k-1} = y_{i-1}^{k-1} = h\Delta$. Plugging $y_i^{k-1} = y_{i-1}^{k-1}$ yields:

$$\begin{aligned}
y_i^k &= y_{i-1}^k + t_{i-1}^k \left(\frac{\varepsilon_{y,i-1}^k V_{x,i-1}^k - V_{y,i-1}^k \varepsilon_{x,i-1}^k}{V_{x,i}^k}\right) + \frac{V_{y,i}^k}{V_{x,i}^k}(x_{i-1}^{k-1} - x_i^{k-1}) \\
&= y_{i-1}^k - \frac{t_{i-1}^k}{V_{x,i}^k} V_{i-1}^k \times \varepsilon_{i-1}^k + \frac{V_{y,i}^k}{V_{x,i}^k}(x_{i-1}^{k-1} - x_i^{k-1}).
\end{aligned} \tag{44}$$

Consecutively, case two can be described in the following dynamics:

$$\begin{aligned}
x_i^k &= x_{i-1}^k \\
y_i^k &= y_{i-1}^k - \frac{t_{i-1}^k}{V_{x,i}^k} V_{i-1}^k \times \varepsilon_{i-1}^k + \frac{V_{y,i}^k}{V_{x,i}^k}(x_{i-1}^{k-1} - x_i^{k-1}).
\end{aligned} \tag{45}$$

Finally, case three happens when the transition can be formulated as follows $y_i^{k+1} = (h+1)\Delta \cap x_i^k = (s+1)\Delta$, see cell C^{k+1} in Figure 6. The deviation along x axis follows:

$$\begin{aligned}
x_i^{k+1} &= t_i^{k+1} V_{x,i}^{k+1} + x_i^k \\
&= \frac{\Delta - y_i^k}{V_{y,i}^{k+1}} V_{x,i}^{k+1} + x_i^k.
\end{aligned} \tag{46}$$

We formulate $x_{i-1}^{k+1} = \frac{\Delta - y_{i-1}^k}{V_{y,i-1}^{k+1}} V_{x,i-1}^{k+1} + x_{i-1}^k$ and we add x_{i-1}^{k+1} and subtract $\frac{\Delta - y_{i-1}^k}{V_{y,i-1}^{k+1}} V_{x,i-1}^{k+1} + x_{i-1}^k$ from the above equation to get the following expression:

$$x_i^{k+1} = \frac{\Delta - y_i^k}{V_{y,i}^{k+1}} V_{x,i}^{k+1} - \frac{\Delta - y_{i-1}^k}{V_{y,i-1}^{k+1}} V_{x,i-1}^{k+1} + x_i^k - x_{i-1}^k + x_{i-1}^{k+1}. \tag{47}$$

We substitute $\frac{\Delta-y_i^k}{V_{y,i}^{k+1}}V_{x,i}^{k+1}$ with $\frac{\Delta-y_{i-1}^k}{V_{y,i}^{k+1}}V_{x,i}^{k+1}+\frac{V_{x,i}^{k+1}}{V_{y,i}^{k+1}}(y_{i-1}^k-y_i^k)$ to obtain:

$$\begin{aligned}
x_i^{k+1} &= \frac{\Delta-y_{i-1}^k}{V_{y,i}^{k+1}}V_{x,i}^{k+1}-\frac{\Delta-y_{i-1}^k}{V_{y,i-1}^{k+1}}V_{x,i-1}^{k+1}+x_i^k-x_{i-1}^k+x_{i-1}^{k+1}+\frac{V_{x,i}^{k+1}}{V_{y,i}^{k+1}}(y_{i-1}^k-y_i^k)\\
&= x_{i-1}^{k+1}+t_{i-1}^{k+1}(\frac{V_{y,i-1}^{k+1}\varepsilon_{x,i-1}^{k+1}-\varepsilon_{y,i-1}^{k+1}V_{x,i-1}^{k+1}}{V_{y,i}^{k+1}})+\frac{V_{x,i}^{k+1}}{V_{y,i}^{k+1}}(y_{i-1}^k-y_i^k)\\
&= x_{i-1}^{k+1}-\frac{t_{i-1}^{k+1}}{V_{y,i}^{k+1}}V_{i-1}^{k+1}\times\varepsilon_{i-1}^{k+1}+\frac{V_{x,i}^{k+1}}{V_{y,i}^{k+1}}(y_{i-1}^k-y_i^k). \qquad (48)
\end{aligned}$$

Case three implies the following dynamics:

$$\begin{aligned}
y_i^{k+1} &= y_{i-1}^{k+1}\\
x_i^{k+1} &= x_{i-1}^{k+1}-\frac{t_{i-1}^{k+1}}{V_{y,i}^{k+1}}V_{i-1}^{k+1}\times\varepsilon_{i-1}^{k+1}+\frac{V_{x,i}^{k+1}}{V_{y,i}^{k+1}}(y_{i-1}^k-y_i^k). \qquad (49)
\end{aligned}$$

Thus, inserting (44) into (46) results in:

$$\begin{aligned}
x_i^{k+1} &= x_{i-1}^{k+1}-\frac{t_{i-1}^{k+1}}{V_{y,i}^{k+1}}V_{i-1}^{k+1}\times\varepsilon_{i-1}^{k+1}+\frac{V_{x,i}^{k+1}}{V_{y,i}^{k+1}}(y_{i-1}^k-y_i^k)\\
&= x_{i-1}^{k+1}-\frac{t_{i-1}^{k+1}}{V_{y,i}^{k+1}}V_{i-1}^{k+1}\times\varepsilon_{i-1}^{k+1}-\frac{V_{x_i}^{k+1}}{V_{y,i}^{k+1}}\frac{t_{i-1}^k}{V_{x,i}^k}V_{i-1}^k\times\varepsilon_{i-1}^k \qquad (50)\\
&+\frac{V_{x,i}^{k+1}}{V_{y,i}^{k+1}}\frac{V_{y,i}^k}{V_{x,i}^k}(x_i^{k-1}-x_{i-1}^{k-1}).
\end{aligned}$$

Let us define $\mathcal{C}_{i-1}\cap\mathcal{C}_i=\{C^1,\cdots,C^m\}$ and by combining the described cases and exploiting the above formulations, we compute r_i^m in iterative way starting from r^0. After some algebraic manipulations, we get the predicted position r_i^m in C^m:

$$\begin{aligned}
y_i^m &= y_{i-1}^m\\
x_i^m &= x_{i-1}^m-\sum_{k=1}^{m}\prod_{j=k}^{m}\alpha_i^j\frac{t_{i-1}^k}{V_{y,i}^k}V_i^k\times\varepsilon_{i-1}^k. \qquad (51)
\end{aligned}$$

$$\begin{aligned}
x_i^m &= x_{i-1}^m\\
y_i^m &= y_{i-1}^m-\sum_{k=1}^{m}\frac{t_{i-1}^k}{V_{x,i}^k}\prod_{j=k}^{m}\alpha_i^jV_i^k\times\varepsilon_{i-1}^k. \qquad (52)
\end{aligned}$$

$$\alpha_i^j = \begin{cases} 1 & \text{if} \quad y_i^j - y_i^{j-1} = \Delta \cup x_i^j - x_i^{j-1} = \Delta \\ \frac{V_{y,i}^j}{V_{x,i}^j} & \text{if} \quad y_i^j = h\Delta \cap x_i^{j-1} = s\Delta \\ \frac{V_{x,i}^j}{V_{y,i}^j} & \text{otherwise} \end{cases} \tag{53}$$

□

3.3 Convergence Analysis

Based on the explicit formulation of trajectory tracing, we can deduce the MT error dynamics in the following Lemma:

Lemma 3.3.1. *Let the flow be updated according to (28), Assumption 3.1.1 holds and suppose the set of explored cells remains constant $\mathcal{C}_{i-1} = \mathcal{C}_i$. Then, the MT error $d_{x,i}$ evolves according to the following dynamic: If $y_i^f = y_{i-1}^f$*

$$\begin{aligned} d_{y,i} &= d_{y,i-1} \\ d_{x,i} &= d_{x,i-1} + \sum_{k=1}^{f} \prod_{j=k}^{f} \alpha_i^j \frac{t_{i-1}^k}{V_{y,i}^k} V_i^k \times \varepsilon_{i-1}^k, \end{aligned} \tag{54}$$

Elsewhere,

$$\begin{aligned} d_{x,i} &= d_{x,i-1} \\ d_{y,i} &= d_{y,i-1} + \sum_{k=1}^{f} \frac{t_{i-1}^k}{V_{x,i}^k} \prod_{j=k}^{f} \alpha_i^j V_i^k \times \varepsilon_{i-1}^k, \end{aligned} \tag{55}$$

where

$$\alpha_i^j = \begin{cases} 1 & \textit{if} \quad y_i^j - y_i^{j-1} = \Delta \cup x_i^j - x_i^{j-1} = \Delta \\ \frac{V_{y,i}^j}{V_{x,i}^j} & \textit{if} \quad y_i^j = h\Delta \cap x_i^{j-1} = s\Delta \\ \frac{V_{x,i}^j}{V_{y,i}^j} & \textit{otherwise} \end{cases} \tag{56}$$

Proof. Let $\mathcal{C}_{i-1} = \mathcal{C}_i$ holds, hence C^m in (52) is the final crossed cell C^f. By means of $d_{x,i} = x^* - x_i^f$ and $d_{y,i} = y^* - y_i^f$, we get the MT error dynamics as follows:

If $y_i^f = y_{i-1}^f$

$$\begin{aligned} d_{y,i} &= d_{y,i-1} \\ d_{x,i} &= d_{x,i-1} + \sum_{k=1}^{f} \prod_{j=k}^{f} \alpha_i^j \frac{t_{i-1}^k}{V_{y,i}^k} V_i^k \times \varepsilon_{i-1}^k, \end{aligned} \tag{57}$$

If $x_i^f = x_{i-1}^f$

$$\begin{aligned} d_{x,i} &= d_{x,i-1} \\ d_{y,i} &= d_{y,i-1} + \sum_{k=1}^{f} \frac{t_{i-1}^k}{V_{x,i}^k} \prod_{j=k}^{f} \alpha_i^j V_i^k \times \varepsilon_{i-1}^k, \end{aligned} \tag{58}$$

where

$$\alpha_i^j = \begin{cases} 1 & \text{if} \quad y_i^j - y_i^{j-1} = \Delta \cup x_i^j - x_i^{j-1} = \Delta \\ \frac{V_{y,i}^j}{V_{x,i}^j} & \text{if} \quad y_i^j = h\Delta \cap x_i^{j-1} = s\Delta \\ \frac{V_{x,i}^j}{V_{y,i}^j} & \text{otherwise} \end{cases} \tag{59}$$

□

The explicit form for the motion integration error $d_{x,i}$ allows us to analyze the dynamic of MT error under the assumption of $\mathcal{C}_i = \mathcal{C}_{i-1}$. Consider the prediction error dynamic:

$$\begin{aligned} d_{y,i} &= d_{y,i-1} \\ d_{x,i} &= d_{x,i-1} + \sum_{k=1}^{m} \prod_{j=k}^{m} \alpha_i^j \frac{t_{i-1}^k}{V_{y,i}^k} V_i^k \times \varepsilon_{i-1}^k. \end{aligned} \tag{60}$$

Accounting for Assumption 3.1.1 and the symmetry of the grid, we consider only one case in the following assumption as it includes all necessary techniques to study the other initial conditions:

Assumption 3.3.1. *We assume that AUV velocity* $S_x = 0$, $S_y > F_x^k \geq 0$, $r^* = [x^*, L]^\top$, $r^0 = [x^0, 0]^\top$ *and* $x^* > x^0$

Since Assumption 3.3.1 implies $d_{y,i} = d_{y,i-1} = 0$, we focus on $d_{x,i}$ and we simplify the analysis of convergence. We get rid of the cross product in trajectory tracing as follows:

$$x_i^f = x_{i-1}^f + \sum_{k=1}^{f} \prod_{j=k}^{f} \alpha_i^j \frac{{t_{i-1}^k}^2}{\|T_{i-1}\|^2} d_{x,i-1}. \tag{61}$$

Plugging $d_{x,i} = x^* - x_i^f$ leads:

$$d_{x,i} = \sum_{k=1}^{f} (1 - \prod_{j=k}^{f} \alpha_i^j) \frac{{t_{i-1}^k}^2}{\|T_{i-1}\|^2} d_{x,i-1}, \tag{62}$$

where

$$\alpha_i^j = \begin{cases} 1 & \text{if} \quad y_i^j - y_i^{j-1} = \Delta \cup x_i^j - x_i^{j-1} = \Delta \\ \frac{V_{y,i}^j}{V_{x,i}^j} & \text{if} \quad y_i^j = h\Delta \cap x_i^{j-1} = s\Delta \\ \frac{V_{x,i}^j}{V_{y,i}^j} & \text{otherwise} \end{cases} \tag{63}$$

An immediate result from the trajectory tracing analysis is that the MT error converges trivially by the first iteration if the crossed cells includes only one column. In other terms, if $l\Delta \leq x_0 \leq (l+1)\Delta$ and $l\Delta \leq x^* \leq (l+1)\Delta$ holds, then only the first case of cell crossing occurs.

Lemma 3.3.2. *Let the flow be updated according to (28), Assumption 3.1.1 and 3.3.1 hold and suppose* $l\Delta \leq x_0 \leq (l+1)\Delta$ *and* $l\Delta \leq x^* \leq (l+1)\Delta$. *Then* $d_{x,1} = x^* - x_1^f = 0$.

Proof. Since $l\Delta \leq x^0, x^* \leq (l+1)\Delta$ and $F_x^k = 0 \forall k$ then $\mathcal{C}_0 = \mathcal{C}_1$ holds. The AUV crosses the cells from the opposite sides. Thus, case one implies $\prod_{j=k}^{f} \alpha_i^j = 1$

$$d_{x,1} = \sum_{k=1}^{f} (1 - \prod_{j=k}^{f} \alpha_1^j) \frac{{t_0^k}^2}{\|T_0\|^2} d_{x,0}$$

$$d_{x,1} = 0. \tag{64}$$

□

We notice that error dynamic d_i depends on $\beta_i^k = 1 - \prod_{j=k}^{f} \alpha_i^j$ described in (62). In fact, this factor reflects the effect of the three different ways of cell crossing on the convergence of MT algorithm. For better understanding we can formulate β_i^k using the notation that C^k corresponds to $C^{(h,s)}$, which describes the cell position in terms of column and row number. If the cell C^k corresponds to $C^{(h,s)}$ and C^f corresponds to $C^{(p,q)}$ and recalling that case one of trajectory tracing implies $\frac{V_{x,i}^{j+1}}{V_{x,j}^k} = 1$, then there exists $p - h$ column crossings that are included in β_i^k as follows:

$$\beta_i^k = 1 - \prod_{j=k}^{f} \alpha_i^j = 1 - \prod_{j=h}^{p} \frac{V_{x,i}^{j+1}}{V_{x,i}^j}, \tag{65}$$

where the cells C^j satisfies $C^{j+1} = C^{(h,s)}$ and $C^j = C^{(h+1,s)}$. Consequently, if we show that $0 \leq \frac{V_{x,i}^{j+1}}{V_{x,i}^j} \leq 1$ holds $\forall 1 \leq j \leq f$, then $0 \leq \beta_i^k \leq 1$ is true. As the AUV trajectory comprises consecutive column crossings we can divide the path into unit parts and consider one part to study the convergence of MT algorithm. Therefore, we consider one part of the trajectory where the AUV crosses one column. We apply the error dynamics on the traced trajectory where we account that cells $\{C^{m+2}, \cdots, C^f\}$ are in the same column:

$$\begin{aligned} d_{x,i} &= \sum_{j=1}^{f} \beta_i^j \frac{{t_i^j}^2}{\|T_i\|^2} d_{x,i-1} \\ &= \sum_{j=1}^{m+1} (1 - \frac{V_{x,i}^{k+1}}{V_{x,i}^k}) \frac{{t_i^j}^2}{\|T_i\|^2} d_{x,i-1} + \sum_{j=m+2}^{f} (1 - \frac{1}{1}) \frac{{t_i^j}^2}{\|T_i\|^2} d_{x,i-1} \\ &= \sum_{j=1}^{m+1} (1 - \frac{V_{x,i}^{k+1}}{V_{x,i}^k}) \frac{{t_i^j}^2}{\|T_i\|^2} d_{x,i-1}. \end{aligned} \tag{66}$$

As $V_{x,i}^k > 0$ $\forall k,i$, three cases can happen according to the ratio $\frac{V_{x,i}^{k+1}}{V_{x,i}^k}$:

- If $V_{x,i}^{k+1} = V_{x,i}^k$: then $d_{x,i} = 0$, MT error converges at iteration i .
- If $V_{x,i}^{k+1} < V_{x,i}^k$: then $d_{x,i} < d_{x,i-1}$ and the MT error decreases at iteration i .
- If $V_{x,i}^{k+1} > V_{x,i}^k$: then $d_{x,i} < 0$ and there will be an overshoot in error.

The previous example illustrates the crucial effect of the variation of AUV velocity along the horizontal axis, presented in $\frac{V_{x,i}^{k+1}}{V_{x,i}^{k}}$. A potential overshoot raises the difficulty in the study of MT algorithm. Therefore we relate the convergence of MT error to the value β_i^k and we focus on the ratio $\frac{V_{x,i}^{k+1}}{V_{x,i}^{k}}$.

In this regard, we want to show in the following Lemma that if the AUV crosses two

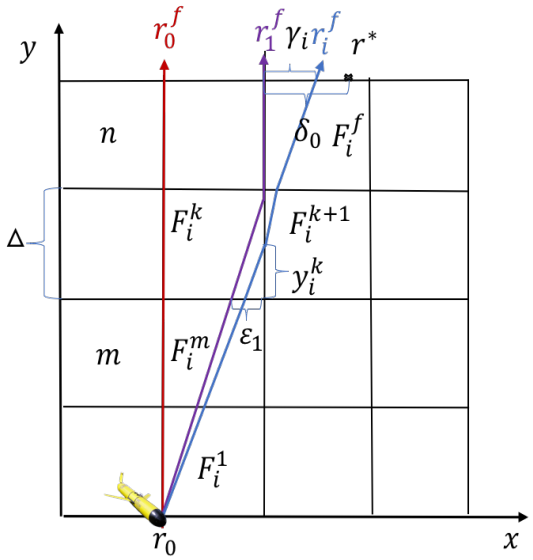

Figure 7: Illustration of trajectory tracing at different iterations. Initial trajectory (the red solid line) and traced trajectories (the purple and blue solid line) after first and second iteration are displayed in a discretized domain.

cells in the same row, $C^k = C^{(h,m)}$ and $C^{k+1} = C^{(h+1,m)}$, then $V_{x,i}^{k+1} \leq V_{x,i}^k \ \forall i$.

For better understanding, we provide the two following Lemmas, that we will use later in the analysis and we present Figure 8 as concrete illustration of trajectory tracing. For clarity, let us recall the flow update:

$$F_{i+1}^k = F_i^k + \frac{t_i^k}{\|T_i\|^2} d_i, \tag{67}$$

where t_i^k is the travel time to cross the cell k, $\|T_i\|^2 = \sum_{k=1}^{f} t_i^{k2}$ and d_i the MT error $d_i = r^* - r_i^f$. Let μ_i denote the distance $\mu_i = (h+1)\Delta - x_i^{k-1}$, $\delta_{x,0} = x^* - (h+1)\Delta$ and n the total number of cells in one column, see Figure 8. Furthermore, we notice that the second form of β_i^k implies if $0 \leq \frac{V_{x,i}^{j+1}}{V_{x,j}^{k}} \leq 1$ holds $\forall 1 \leq j \leq f$, then $0 \leq \beta_i^k \leq 1$ is

true. Since the ratio $\frac{V_{x,i}^{j+1}}{V_{x,i}^{j}}$ involves two columns and we do not impose an upper bound on $\delta_{x,0}$, we can consider in the following analysis w.l.o.g. one transition between two columns for simpler calculation.

Lemma 3.3.3. *Let the predicted flow be updated according to (28). Suppose Assumptions 3.1.1, and 3.3.1 hold. Let cells C^k and C^{k+1} correspond to $C^{(h,m)}$ and $C^{(h+1,m)}$ respectively and the following conditions hold*

- $V_{x,1}^{k} \leq V_{x,i}^{k+1}$.
- $V_{x,j}^{k+1} < V_{x,j}^{k} \ \forall j < i$.
- $n > m + 1$
- $t_i^{k+1} \geq t_i^k$

then $\frac{\Delta}{m}(n-m) < \delta_{x,0}$ *is valid.*

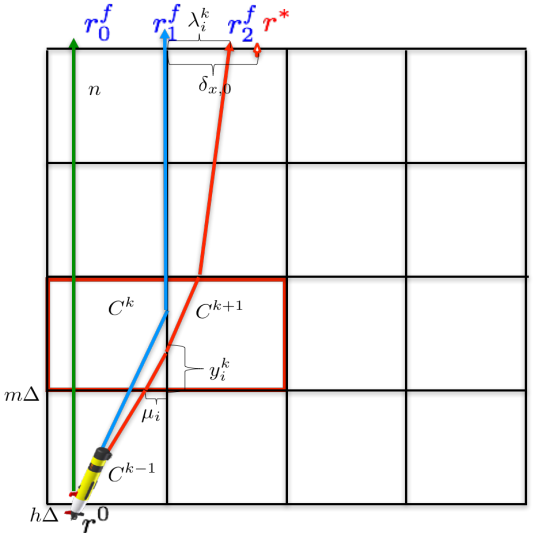

Figure 8: Illustration of trajectory tracing as described in Lemma 3.3.3.

Proof. The Lemma requires that the traveling time in cell k, t_i^k is less than the traveling time in cell $k+1$, t_i^{k+1}. Since $t_i^{k+1} + t_i^k = \frac{\Delta}{V_y}$ and $t_i^{k+1} \geq t_i^k$, then, $\frac{\Delta}{V_y} =$

$t_i^{k+1} + t_i^k \geq 2t_i^k$. Moreover, we can write $t_i^k = \frac{\mu_i}{V_{x,i}^k} = \frac{(h+1)\Delta - x_i^{k-1}}{V_{x,i}^k}$. Hence we get:

$$\frac{\Delta/2}{V_y} \geq \frac{\mu_i}{V_{x,i}^k}. \tag{68}$$

Since the AUV velocity $V_{x,i}^k = F_{x,i}^k$, we get a recursive form as follows:

$$\begin{aligned} V_{x,i}^k &= F_{x,i-1}^k + \frac{t_{i-1}^k}{\|T_{i-1}\|^2} d_{x,i-1} \\ &= \sum_{j=0}^{i-1} t_j^k \frac{d_{x,j}}{\|T_j\|^2}. \end{aligned} \tag{69}$$

We know that the flow is updated in the cell only if it is crossed by the AUV. At iteration $i = 1$, only column h is updated. Then at iteration $i = 2$, columns $h + 1$ and h are updated. let $\lambda_{x,i} = x_i^f - (h + 1)\Delta$, as depicted in Figure 8. Since the cells starting from C^{k+2} till cell C^f are crossed by the AUV in vertical direction, then the travel time is constant $t_i^{k+p} = \frac{\Delta}{V_y}$, $\forall 2 \leq k \leq f - k \ \forall 2 \geq i$.

$$V_{x,i}^{k+p} = \sum_{j=2}^{i-1} \frac{\Delta}{V_y} \frac{d_{x,j}}{\|T_j\|^2} \quad \forall 2 \leq p \leq f - k. \tag{70}$$

Concerning cell $C^{k+1} = C^{(h+1,m)}$, the velocity is updated starting from iteration $j = 2$ and the AUV crosses according to the third case of trajectory tracing. We see from Figure 8 that $y_j^{k+1} = (m + 1)\Delta$ the travel time in cell C^{k+1},

$$t_j^{k+1} = \frac{y_j^{k+1} - y_j^k}{V_y} = \frac{(m + 1)\Delta - y_j^k}{V_y}. \tag{71}$$

Plugging (71) in (69) yields:

$$V_{x,i}^{k+1} = \sum_{j=2}^{i-1} \frac{(m + 1)\Delta - y_j^k}{V_y} \frac{d_{x,j}}{\|T_j\|^2}. \tag{72}$$

Recalling that $C^{k+1} = C^{(h+1,m)}$ and $x^* < (h + 2)\Delta$, the number of cells in column $h + 1$ that are crossed by the AUV are $n - m$ and there exists $n - m - 1$ cells that are crossed in vertical way starting from cell c^{k+2} until c^f. In other terms, $f = n + 1$, because there exists only one transition that combines case 2 and 3. Based on the

aforementioned reasons λ_i, as depicted in Figure 8, follows:

$$\begin{aligned}\lambda_i &= \sum_{j=k+1}^{f} V_{x,i}^{j} t_i^{k+1} \\ &= (f-k+1)(V_{x,i}^{k+2})(t_i^{k+2}) + (V_{x,i}^{k+1})(t_i^{k+1}) \\ &= (f-m)(V_{x,i}^{k+2})(t_i^{k+2}) + (V_{x,i}^{k+1})(t_i^{k+1}) \\ &= (n-m-1)(V_{x,i}^{k+2})(t_i^{k+2}) + (V_{x,i}^{k+1})(t_i^{k+1}). \end{aligned} \tag{73}$$

Let us now compare $V_{x,i}^{k+p}$ and $V_{x,i}^{k+1}$:

$$\begin{aligned} V_{x,i}^{k+p} &= \sum_{j=2}^{i-1} \frac{\Delta}{V_y} \frac{d_{x,j}}{\|T_j\|^2} \quad \forall 2 \le p \le f-k \\ V_{x,i}^{k+1} &= \sum_{j=2}^{i} \frac{(m+1)\Delta - y_j^k}{V_y} \frac{d_{x,j}}{\|T_j\|^2}. \end{aligned} \tag{74}$$

We know that the AUV crosses the cell $C^k = C^{(m,h)}$ according to the second case of trajectory tracing then

$$t_j^k = \frac{(y_j^k - y_j^{k-1})}{V_y} = \frac{(y_j^k - m\Delta)}{V_y} = \frac{\mu_j}{V_{x,j}^k} \tag{75}$$

Hence, $y_j^k - m\Delta = \frac{\mu_j V_y}{V_{x,j}^k}$ holds. The first condition in Lemma is $V_{x,j}^{k+1} < V_{x,j}^k \ \forall j < i$, then $\alpha_j^q \le 1$ for all cells C^q. Applying the error dynamics (62), then $0 \le d_j$ and $x_j^f \le x^* \ \forall j < i$. Since the Mt error remains positive, $\frac{d_{x,j}}{\|T_j\|^2} \ge 0$ implies that the flow is increasing along x-axis resulting in non decrease of x_j^q and non increase of y_j^q in every cell $C^q \in \mathcal{C}_j$ after every iteration. As $\mu_j = (h+1)\Delta - x_j^{k-1}$, then μ_i is decreasing and accordingly $\frac{\Delta}{(m+1)\Delta - y_j^k}$ is also decreasing for all $j < i$, which implies that $(m+1)\Delta - y_i^k$ the maximum of $(m+1)\Delta - y_j^k$. Let us consider $V_{x,i}^{k+1}$

$$\begin{aligned} V_{x,i}^{k+1} &= \sum_{j=2}^{i-1} \frac{(m+1)\Delta - y_j^k}{V_y} \frac{d_{x,j}}{\|T_j\|^2} \\ &\le \frac{(m+1)\Delta - y_{i-1}^k}{V_y} \sum_{j=2}^{i-1} \frac{d_{x,j}}{\|T_j\|^2}. \end{aligned} \tag{76}$$

Consequently, a lower bound for $V_{x,i}^{k+p}$ $\forall 2 \leq p \leq f-k$ follows:

$$\begin{aligned} V_{x,i}^{k+p} &= \frac{\Delta}{V_y} \sum_{j=2}^{i-1} \frac{d_{x,j}}{\|T_j\|^2} \\ &\geq \frac{\Delta}{V_y} \frac{V_y}{(m+1)\Delta - y_{i-1}^k} V_{x,i}^{k+1} \\ &\geq \frac{\Delta}{(m+1)\Delta - y_{i-1}^k} V_{x,i}^{k+1} \quad \forall 2 \leq p \leq f-k. \end{aligned} \tag{77}$$

Plugging (77) in (73) yields:

$$\begin{aligned} \lambda_{x,i} &= (n-m-1) V_{x,i}^{k+2} t_i^{k+2} + V_{x,i}^{k+1} t_i^{k+1} \\ &\geq (n-m-1) \frac{\Delta}{(m+1)\Delta - y_{i-1}^k} V_{x,i}^{k+1} \frac{\Delta}{V_y} + V_{x,i}^{k+1} \frac{(m+1)\Delta - y_{i-1}^k}{V_y} \\ &\geq V_{x,i}^{k+1} \frac{\Delta}{V_y} ((n-m-1) \frac{\Delta}{(m+1)\Delta - y_{i-1}^k} + \frac{(m+1)\Delta - y_{i-1}^k}{\Delta}). \end{aligned} \tag{78}$$

Since the MT error $d_{x,i} > 0$, then the velocity $V_{x,i}$ is increasing and $V_{x,i}^k \geq V_{x,2}^k$ $\forall i \geq 2$ is valid.

$$\begin{aligned} V_{x,1}^k &= \frac{\Delta + \delta_{x,0}}{\|T_0\|^2} t_0^k = \frac{\Delta + \delta_{x,0}}{n} \frac{V_y}{\Delta} \\ V_{x,2}^k &= \frac{d_{x,1}}{\|T_1\|^2} t_1^k + V_{x,1}^k \\ V_{x,i}^k &\geq V_{x,1}^k + \frac{\delta_{x,0}}{\|T_1\|^2} t_1^k > \frac{\Delta + \delta_{x,0}}{n} \frac{V_y}{\Delta}, \end{aligned} \tag{79}$$

where $\|T_0\|^2 = \sum_{k=1}^{f} t_0^{k^2} = n(\frac{\Delta}{V_y})^2$. Since the first condition in the Lemma implies that $V_{x,1}^k \leq V_{x,i}^{k+1}$, we substitute $V_{x,i}^{k+1}$ with $V_{x,i}^1$ in (78) to get:

$$\begin{aligned} \lambda_{x,i} &\geq V_{x,i}^{k+1} \frac{\Delta}{V_y} ((n-m-1) \frac{\Delta}{(m+1)\Delta - y_{i-1}^k} + \frac{(m+1)\Delta - y_{i-1}^k}{\Delta}) \\ &\geq V_{x,1}^k \frac{\Delta}{V_y} ((n-m-1) \frac{\Delta}{(m+1)\Delta - y_{i-1}^k} + \frac{(m+1)\Delta - y_{i-1}^k}{\Delta}) \\ &\geq \frac{\Delta + \delta_{x,0}}{n} ((n-m-1) \frac{\Delta}{(m+1)\Delta - y_{i-1}^k} + \frac{(m+1)\Delta - y_{i-1}^k}{\Delta}). \end{aligned} \tag{80}$$

Moreover, $\alpha_i^q \leq 1$ is true $\forall C^q$. Applying the error dynamics (62), then $0 \leq d_{x,j}$ and $x_j^f \leq x^*$ $\forall j \leq i$. Hence $\lambda_{x,i} < \delta_{x,0}$ holds. It follows:

$$\frac{\Delta + \delta_{x,0}}{n} [(n-m-1) \frac{\Delta}{(m+1)\Delta - y_{i-1}^k} + \frac{(m+1)\Delta - y_{i-1}^k}{\Delta}] < \delta_{x,0}. \tag{81}$$

Now we look for a lower bound for (81). It is given that $n-m-1 \geq 1$ and $m\Delta \leq y_{i-1}^k \leq (m+1)\Delta$. Thus $\frac{\Delta}{(m+1)\Delta - y_{i-1}^k} > 0$. Let κ be $\kappa = \frac{(m+1)\Delta - y_{i-1}^k}{\Delta}$ and the function $g(\kappa) : (0,1] \to \Re_+$ defined as follows:

$$g(\kappa) = (n-m-1)\frac{1}{\kappa} + \kappa. \tag{82}$$

Concerning the roots of the derivative of $\dot{g}(\kappa) = 0$, are

$$\dot{g}(\kappa) = -\frac{(n-m-1)}{\kappa^2} + 1 = 0. \tag{83}$$

Since $\kappa > 0$ then the root of $\dot{g}$ is $\kappa^* = \sqrt{(n-m-1)}$. Recalling that $n-m-1 > 0$ and $n, m \in \mathcal{N}$, then $n-m-1 \geq 1$, $\dot{g}(\kappa) \leq 0$ and $\kappa^* = \sqrt{(n-m-1)} \geq 1$. However, we know that $0 \leq \kappa \leq 1$, then $g(\kappa) \geq g(1) = (n-m-1)+1$.

$$\frac{\Delta + \delta_{x,0}}{n} g(1) = \frac{\Delta + \delta_{x,0}}{n}[(n-m-1)+1] \leq \frac{\Delta + \delta_{x,0}}{n}(n-m) < \delta_{x,0}. \tag{84}$$

Consequently, a lower bound for $\delta_{x,0}$ is:

$$\frac{\Delta}{m}(n-m) < \delta_{x,0}. \tag{85}$$

□

The second inequality is stated in the following lemma:

Lemma 3.3.4. *Let the predicted flow be updated according to (28). Suppose Assumptions 3.1.1, and 3.3.1 hold. Let cells C^k and C^{k+1} correspond to $C^{(h,m)}$ and $C^{(h+1,m)}$ respectively and $t_i^{k+1} \geq t_i^k$ holds, then $\delta_{x,0} \leq \frac{\Delta(n-m)}{2m}$ is valid.*

Proof. Since the crossed set of cells is constant starting from iteration $i = 1$, $\mathcal{C}_i = \mathcal{C}_1$ and $\mu_0 = \Delta$, μ_i is decreasing, see the proof of Lemma (3.3.3) but still positive $\mu_i > 0$:

$$\mu_i = \Delta - \sum_{j=0}^{j=i} m \frac{d_{x,j}}{\|T_j\|^2} \frac{\Delta}{V_y}^2 \tag{86}$$

$$\mu_2 = \Delta - m\frac{\Delta + \delta_{x,0}}{\|T_0\|^2} \frac{\Delta}{V_y}^2 - m\frac{\delta_{x,0}}{\|T_1\|^2} \frac{\Delta}{V_y}^2. \tag{87}$$

Hence,

$$\mu_i \leq \Delta - m\frac{\Delta + \delta_{x,0}}{\|T_0\|^2}\frac{\Delta}{V_y}^2 - m\frac{\delta_{x,0}}{\|T_1\|^2}\frac{\Delta}{V_y}^2. \tag{88}$$

Furthermore, we can simplify $\|T_i\|^2 = \sum_{k=1}^{f} t_i^{k2}$ as follows:

$$\begin{aligned}
\|T_0\|^2 &= n\frac{\Delta}{V_y}^2 \\
\|T_i\|^2 &= (n-1)\frac{\Delta}{V_y}^2 + t_i^{k2} + t_i^{k+1\,2} \\
&= (n-1)\frac{\Delta}{V_y}^2 + \frac{\mu_i}{V_{x,i}^k}^2 + (\frac{\Delta}{V_y} - \frac{\mu_i}{V_{x,i}^k})^2 \\
&= n\frac{\Delta}{V_y}^2 + 2\frac{\mu_i}{V_{x,i}^k}(\frac{\mu_i}{V_{x,i}^k} - \frac{\Delta}{V_y}).
\end{aligned} \tag{89}$$

Since $t_i^{k+1} \geq t_i^k$, then we apply $\frac{\Delta/2}{V_y} \geq \frac{\mu_i}{V_{x,i}^k}$, see (68) in the above equation:

$$\|T_i\|^2 < n\frac{\Delta}{V_y}^2. \tag{90}$$

Hence, we simplify as follows (88):

$$\mu_i \leq \Delta - m\frac{\Delta + \delta_{x,0}}{n} - m\frac{\delta_{x,0}}{n} - m\frac{\delta_{x,1}}{m}. \tag{91}$$

Adding to that $\mu_i > 0$ implies

$$m\frac{\Delta + \delta_{x,0}}{n} + m\frac{\delta_{x,0}}{n} \leq \Delta. \tag{92}$$

Hence,

$$\delta_{x,0} \leq \frac{\Delta(n-m)}{2m}. \tag{93}$$

□

Lemma 3.3.5. *Let the predicted flow be updated according to (28). Suppose Assumptions 3.1.1, 3.3.1 hold. Let cells C^k and C^{k+1} correspond to $C^{(h,m)}$ and $C^{(h+1,m)}$, then $V_{x,i}^{k+1} \leq V_{x,i}^k$, $\forall i$.*

Proof. We prove the Lemma by Induction:

Since $V_{x,0}^k = 0$, the AUV crosses cell C^k according to first case of trajectory tracing, in vertical direction. Hence, $V_{x,1}^k = \frac{d_{x,0}}{\|T_0\|^2} t_1^k = \frac{d_{x,0}}{\|T_0\|^2} \frac{\Delta}{V_y}$ and the flow in cell C^{k+1} is not updated $V_{x,1}^{k+1} = 0$. $d_{x,0} \geq 0$ results in $V_{x,0}^{k+1} \leq V_{x,0}^k$ and the statement is initially valid. Suppose that $V_{x,i-1}^{k+1} \leq V_{x,i-1}^k$ and let us prove $V_{x,i}^{k+1} \leq V_{x,i}^k$.

We notice from Figure 8 that two scenarios can happen: The first case occurs when the traveling time in cell k, t_i^k, exceeds the traveling time in cell $k+1$, t_i^{k+1}. Since $t_i^{k+1} + t_i^k = \frac{\Delta}{V_y}$, then we have:

$$\begin{aligned} t_i^k &= \frac{y_i^k - m\Delta}{V_y} \\ t_i^{k+1} &= \frac{\Delta}{V_y} - \frac{y_i^k - m\Delta}{V_y}. \end{aligned} \tag{94}$$

The flow update implies:

$$\begin{aligned} V_{x,i}^{k+1} - V_{x,i}^k &= V_{x,i-1}^{k+1} - V_{x,i-1}^k + \frac{d_{x,i-1}}{\|T_{i-1}\|^2}(t_{i-1}^{k+1} - t_{i-1}^k) \\ &= V_{x,i-1}^{k+1} - V_{x,i-1}^k + \frac{d_{x,i-1}}{\|T_{i-1}\|^2}(\frac{\Delta}{V_y} - 2\frac{y_{i-1}^k - m\Delta}{V_y}). \end{aligned} \tag{95}$$

Since the first scenario implies $(y_{i-1}^k - m\Delta) \geq \frac{\Delta}{2}$ and given $V_{x,i-1}^{k+1} \leq V_{x,i-1}^k$ then $V_{x,i}^{k+1} \leq V_{x,i}^k$.

The second scenario is more challenging: The traveling time in cell k t_i^k is less than the traveling time in cell $k+1$, t_i^{k+1} $t_i^{k+1} \geq t_i^k$. We use the principle of contradiction to prove the second position. Assume, for the sake of contradiction that $V_{x,1}^k \leq V_{x,i}^{k+1}$. For clarity, let us first assume that $n - m - 1 \geq 1$. On the one hand, Lemma 3.3.3 implies:

$$\frac{\Delta}{m}(n-m) < \delta_{x,0}. \tag{96}$$

On the other hand, Lemma 3.3.4 provides:

$$\delta_{x,0} \leq \frac{\Delta(n-m)}{2m}. \tag{97}$$

Combining the two inequalities results in:

$$\frac{\Delta}{m}(n-m) < \delta_{x,0} \leq \frac{\Delta(n-m)}{2m} \tag{98}$$

Obviously $2m < m$ is not true because $m > 0$ and this contradiction shows that $V_{x,1}^{k} \leq V_{x,i}^{k+1}$ must be false. Accounting for $V_{x,j}^{1} < V_{x,i}^{k}$, then $V_{x,i}^{k+1} < V_{x,i}^{k}$ holds. For completeness, let us consider the case $n = m + 1$. Since $t_i^{k+1} + t_i^k = \frac{\Delta}{V_y}$, $V_{x,i}^{k+1}$ is maximum increased when the corresponding travel time t^{k+1} in cell C^{k+1} tends to $\frac{\delta}{V_y}$, $t_i^{k+1} \to \frac{\delta}{V_y}$ and $t_i^k \to 0$. It is to notice that we require $t_i^k > 0$ so that the AUV crosses the same cell C^{k+1}. Elsewhere, it does not enter cell C^{k+1}. Concerning the MT error $d_{x,i}$ we apply in (78) $t_i^k \to 0$ and $t_i^{k+1} \to \frac{\delta}{V_y}$ to get:

$$d_{x,i} = \delta x,0 - \lambda_{x,i} = \delta x,0 - V_{x,i}^{k+1} t_i^{k+1}. \tag{99}$$

Plugging $t_i^{k+1} = \frac{\Delta}{V_y}$ in (69) leads to:

$$\begin{aligned} V_{x,i}^{k+1} &= \sum_{j=2}^{i-1} \frac{(m+1)\Delta - y_j^k}{V_y} \frac{d_{x,j}}{\|T_j\|^2} \\ &\leq \frac{\Delta}{V_y} \sum_{j=2}^{i} \frac{d_{x,j}}{\|T_j\|^2} \\ &\leq \frac{\Delta}{V_y} \sum_{j=2}^{i} \frac{\delta x,0 - V_{x,j}^{k+1} \frac{\Delta}{V_y}}{n(\frac{\Delta}{V_y})^2}. \end{aligned} \tag{100}$$

Let us define $\bar{\lambda}_{x,i}$ $\forall 2 \leq i$ with $\bar{\lambda}_{x,0} = \bar{\lambda}_{x,1} = \lambda_{x,0} = 0$:

$$\begin{aligned} \bar{\lambda}_{x,i} &= \frac{\Delta}{V_y} V_{x,i}^{k+1} \\ &= \sum_{j=2}^{i-1} \frac{\delta x,0 - V_{x,j}^{k+1} \frac{\Delta}{V_y}}{n} \\ &= \sum_{j=2}^{i-2} \frac{\delta x,0 - V_{x,j}^{k+1} \frac{\Delta}{V_y}}{n} + \frac{\delta x,0 - V_{x,i-1}^{k+1} \frac{\Delta}{V_y}}{n} \\ &= \bar{\lambda}_{x,i-1} + \frac{\delta x,0 - \bar{\lambda}_{x,i-1}}{n} \\ &= (1 - \frac{1}{n})\bar{\lambda}_{x,i-1} + \frac{\delta x,0}{n} \end{aligned}$$

$$
\begin{aligned}
&= \sum_{j=0}^{i-2}(1-\frac{1}{n})^j\frac{\delta x,0}{n} + (1-\frac{1}{n})^i\bar{\lambda}_{x,0} \\
&= \sum_{j=0}^{i-2}(1-\frac{1}{n})^j\frac{\delta x,0}{n} \\
&= (1-[1-\frac{1}{n}]^{i-1})\delta x,0. \qquad (101)
\end{aligned}
$$

Adding to that, (91) provides:

$$
\begin{aligned}
\mu_i &= \Delta - \sum_{j=0}^{j=i} m\frac{d_{x,j}}{\|T_j\|^2}\frac{\Delta}{V_y}^2 \\
&\leq \Delta - (n-1)\frac{\Delta+2\delta_{x,0}}{n} - (n-1)\sum_{j=2}^{i-1}\frac{\delta x,0 - V_{x,j}^{k+1}\frac{\Delta}{V_y}}{n} \\
&\leq \Delta - (n-1)\frac{\Delta+2\delta_{x,0}}{n} - (n-1)(1-[1-\frac{1}{n}]^{i-1})\delta x,0. \qquad (102)
\end{aligned}
$$

Finally, we recall that $z_1^k = y_1^k - (n-1)\Delta < \frac{\Delta}{2}$, hence, applying Triangle Intercept Theorem on the green dashed triangle in Figure 9 yields:

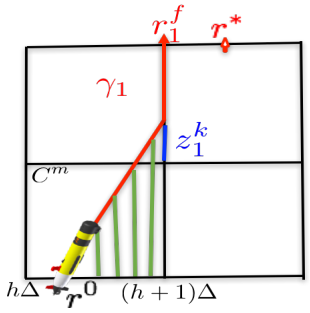

Figure 9: Illustration of trajectory tracing for $n = m + 1$.

$$
\begin{aligned}
\frac{z_1^k}{z_1^k+(n-1)\Delta} &= \frac{\mu_1}{\Delta} \\
\frac{z_1^k}{z_1^k+(n-1)\Delta} &= \frac{\Delta - \frac{n-1}{n}(\Delta+\delta_{x,0})}{\Delta} \\
\frac{\Delta}{z_1^k+(n-1)\Delta} &= \frac{(\Delta+\delta_{x,0})}{n\Delta}. \qquad (103)
\end{aligned}
$$

Applying $z_1^k < \frac{\Delta}{2}$ yields:

$$
\frac{n\Delta}{n-\frac{1}{2}} - \Delta < \delta_{x,0}
$$

$$\frac{\Delta}{2n-1} < \delta_{x,0}. \tag{104}$$

Plugging (103) in (102):

$$\begin{aligned}\mu_i &\leq \Delta - (n-1)\frac{\Delta}{n} - \frac{n-1}{n}((1-[1-\frac{1}{n}]^{i-1}) + 2)\delta x,0 \\ &\leq \Delta - (n-1)\frac{\Delta}{n} - \frac{n-1}{n}(3-[1-\frac{1}{n}]^{i-1})\frac{\Delta}{2n-1}\end{aligned} \tag{105}$$

Let us choose $i = n+1$. On the one hand, we get:

$$\lambda_{x,i} < \bar{\lambda}_{x,i} \leq \lim_{i\to\infty}((1-[1-\frac{1}{n}]^{i-1})\delta x,0 < \delta x,0. \tag{106}$$

On the other hand, we get:

$$\begin{aligned}\lim_{i\to\infty}\mu_i &\leq \lim_{i\to\infty}\Delta - (n-1)\frac{\Delta}{n} - \frac{n-1}{n}(3-[1-\frac{1}{n}]^{i-1})\frac{\Delta}{2n-1} \\ &\leq \frac{\Delta}{n}[1-3\frac{n-1}{2n-1}]\end{aligned} \tag{107}$$

Since $n \geq 2$, then $\lim_{i\to\infty}\mu_i \geq 0$, hence $\mu_i \leq 0$, which means that the cell $C^{(h+1,m)}$ is no more included in the set of traced trajectory. However, $\lambda_{x,i} < \delta_{x,0}$. If the travel time in cell C^k is less than the travel time in cell C^{k+1}, the AUV traced trajectory changed the set of cells before the MT error changes the sign. Hence, m is decreased so that $m < n-1$ and the required condition to prove $V^k_{x,i} \geq V^{k+1}_{x,i}$ becomes valid.

□

Theorem 3.3.1. *Let the traced trajectory be formulated according to (28). Suppose Assumptions 3.1.1 and 3.3.1 hold, then the MT error $d_{x,i}$ converges to* 0*, as $i \to \infty$.*

Proof. The key idea of the proof is to analyze the norm of the MT error when the AUV enters new cells or when the traced trajectory evolves in the same set of cells. We use the Induction method to prove the convergence and we assume w.l.o.g. that $l\Delta \leq x_0 < (l+1)\Delta$ and $p\Delta \leq x^* \leq (p+1)\Delta$; $p \geq l$. As initially the flow $F^k_{x,0} = 0$, then the AUV velocity is constant along the trajectory with $V^k_{x,0} = 0$, $\forall k$. Furthermore, we

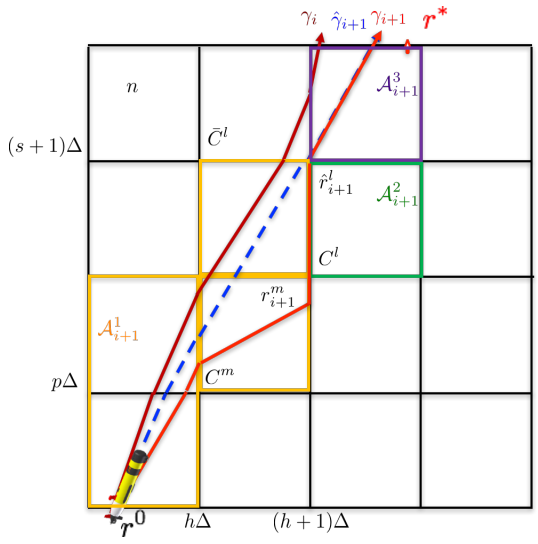

Figure 10: Illustration of trajectory tracing in new set of cells

know the error dynamic $d_{x,1}$ (62) is valid for $\mathcal{C}_1 \cap \mathcal{C}_0 = \mathcal{C}_0$. So if $l = p$, Lemma 3.3.2 implies $d_{x,1} = 0$ and the MT error converges from the first iteration. However if $p > l$ and as $V^k_{x,0} = 0$, then $x^f_0 = x^0 < (l+1)\Delta$. Adding to that, $V^k_{x,1} > 0$ and $\mathcal{C}_1 \cap \mathcal{C}_0 \neq \mathcal{C}_0$, then $x^f_1 = (l+1)\Delta$

$$\begin{aligned} d_{x,1} &= x^* - x^f_1 \\ &= x^* - (l+1)\Delta < d_{x,0}. \end{aligned} \tag{108}$$

Hence the initial value satisfies the statement: $d_{x,1} < d_{x,0}$. Suppose that $0 \leq d_{x,i} < d_{x,i-1}$ and let us prove $0 \leq d_{x,i+1} < d_{x,i}$.

Two scenarios can happen: The first one is if $\mathcal{C}_{i+1} \cap \mathcal{C}_i = \mathcal{C}_i$. Recalling the dependency of error dynamics on $\beta^k_i = 1 - \prod_{j=k}^{f} \alpha^j_i$ and the escalation of α^j_i for horizontal crossing:

$$\alpha^j_i = \frac{V^j_{x,i}}{V^{j-1}_{x,i}} \alpha^{j-1}_i. \tag{109}$$

Since Lemma 3.3.5 guarantees that $V^{k+1}_{x,i} \leq V^k_{x,i}$ is valid, $\forall i$ and $\forall$ cells that are in the same row, then $\alpha^j_i < 1$ $\forall j \leq f$ and $0 \leq \beta^k_i = 1 - \prod_{j=k}^{f} \alpha^j_i < 1$ hold. Consequently the error dynamics imply $0 \leq d_{x,i+1} < d_{x,i}$.

The second scenario is when $\mathcal{C}_{i+1} \cap \mathcal{C}_i \neq \mathcal{C}_i$ which means the AUV enters new cells.

Again two cases may occur:

Let us split the set $\mathcal{C}_{i+1}$ into three parts, where the cells are successively crossed by the AUV as follows: $\mathcal{A}^1_{i+1} = \mathcal{C}_{i+1} \cap \mathcal{C}_i = \{C^1, \cdots, C^m\}$, $\mathcal{A}^2_{i+1} = \mathcal{C}_{i+1} \setminus \mathcal{C}_i \cap \mathcal{C}_{i+1} = \{C^{m+1}, \cdots, C^l\}$ and $\mathcal{A}^3_{i+1} = \mathcal{C}_{i+1} \cap \mathcal{C}_i = \{C^{l+1}, \cdots, C^f\}$. Notice that $m \geq 1$, the initial position is constant, and if $\mathcal{C}_{i+1} \cap \mathcal{C}_i \neq \mathcal{C}_i$ then both $\mathcal{A}^1_{i+1} \neq \emptyset$ and $\mathcal{A}^2_{i+1} \neq \emptyset$ hold. Hence, the first case is when $\mathcal{A}^3_{i+1} = \emptyset$, then $C^l = C^f$. Let cell $C^m = C^{(h,p)}$. As $C^{m+1} \notin \mathcal{C}_i$ then $x^f_i < (h+1)\Delta \leq x^* \ \forall i > 0$ and accordingly $d_{x,i} > 0$. Therefore, the flow is increasing in cells $C^k \in \mathcal{C}_i$. In other terms, the AUV velocity remains null in cells $C^k \in \mathcal{A}^2_{i+1}$ and increases in $C^k \in \mathcal{A}^1_{i+1}$. $C^{m+1} = C^{(h+1,s)}$ implies $x^f_{i+1} = (h+1)\Delta > x^f_i$ and $x^f_{i+1} \leq x^*$. This case satisfies the induction claim.

The second case is when $\mathcal{A}^3_{i+1} \neq \emptyset$. For better understanding, we provide Figure 10 to illustrate the case. Concerning the velocity $V^k_{x,i+1}$, it varies in different parts as follows:

$$V^k_{x,i+1} = \begin{cases} F^k_{x,i} + \frac{(t^k_i)^2}{\|T_i\|^2} d_{x,i} & \text{if} \quad C^k \in \mathcal{A}^1_{i+1} \\ 0 & \text{if} \quad C^k \in \mathcal{A}^2_{i+1} \\ F^k_{x,i} + \frac{(t^k_i)^2}{\|T_i\|^2} d_{x,i} & \text{otherwise} \end{cases} \tag{110}$$

Let $\hat{x}^l_{i+1} = (h+1)\Delta = x^m_{i+1}$ and $\hat{y}^l_{x,i+1} = (s+1)\Delta$. Applying that $\sum_{k=m+1}^{l} t^k_{i+1} F^k_{x,i+1} = \sum_{k=m+1}^{l} t^k_{i+1} 0 = 0$, the AUV final position $x^f_{x,i+1}$ can be expressed as follows:

$$\begin{aligned} x^f_{i+1} &= x_0 + \sum_{k=1}^{m} t^k_{i+1} F^k_{x,i+1} + \sum_{k=m+1}^{l} t^k_{i+1} F^k_{x,i+1} + \sum_{k=l+1}^{f} t^k_{i+1} F^k_{x,i+1} \\ &= x^m_{i+1} + \sum_{k=l+1}^{f} t^k_{i+1} F^k_{x,i+1} = \hat{x}^l_{i+1} + \sum_{k=l+1}^{f} t^k_{i+1} F^k_{x,i+1}. \end{aligned} \tag{111}$$

Let us define $\hat{\mathcal{C}}_i$ as $\hat{\mathcal{C}}_i = \mathcal{A}^1_{i+1} \cup \mathcal{A}^2_i \cup \mathcal{A}^3_{i+1}$ and $\mathcal{A}^2_i = \{C^{m+1}, \cdots, C^l\} \in \mathcal{C}_i$ and let $\hat{d}_{x,i}$ be the MT error and $\hat{F}_{x,i+1}$ computed as follows:

$$\hat{F}^k_{x,i+1} = \begin{cases} F^k_{x,i} + \frac{(t^k_i)^2}{\|T_i\|^2} \hat{d}_{x,i} & \text{if} \quad C^k \in \mathcal{A}^1_{i+1} \cup \mathcal{A}^2_i \\ F^k_{x,i} + \frac{(t^k_i)^2}{\|T_i\|^2} d_{x,i} & \text{if} \quad C^k \in \mathcal{A}^3_{i+1} \end{cases} \tag{112}$$

$\hat{d}_{x,i}$ is chosen such that $\hat{\gamma}_{i+1}$ evolves according to $\hat{F}^k_{x,i+1}$. The key features of this constructed trajectory that $\hat{\gamma}_i = \gamma_i$, $\hat{\gamma}_{i+1}$ includes the point ($\hat{x}^l_{i+1}$,$\hat{y}^l_{i+1}$) and $\hat{\gamma}_{i+1} = \gamma_{i+1}$ in $\mathcal{A}^3_{i+1}$, see the blue dashed line in Figure 10. In other terms, $\hat{\gamma}_{i+1}$ evolves in set of cells $\hat{\mathcal{C}}_{i+1} = \mathcal{C}_i$, where it crosses the cell $C^{(s+1,h)}$ in only one point ($\hat{x}^l_{i+1}$,$\hat{y}^l_{i+1}$). Figure 10 illustrates that $\hat{\gamma}_{i+1}$ crosses the cell $C^{(s+1,h)} \in \mathcal{C}_i$ in $\hat{r}^l_{i+1}$. Furthermore, we know if the AUV starts from the same position and reaches different final positions, we can deduce the flow variation and accordingly the MT error. While $y = \hat{y}$ and $x \geq \hat{x}$ implies $d_x \geq \hat{d}_x$, $x = \hat{x}$ and $y \geq \hat{y}$ implies $d_x \leq \hat{d}_x$. We notice that $x^m_{i+1} = \hat{x}^l_{i+1}$ and $y^m_{i+1} \leq \hat{y}^l_{i+1}$. Hence, $\hat{d}_{x,i} \leq d_{x,i}$ holds. Let $\hat{\alpha}^k_{i+1}$, defined in (59) be the coefficient embedded in error dynamics (62) for trajectory $\hat{\gamma}_{i+1}$. As $\hat{\mathcal{C}}_{i+1} = \hat{\mathcal{C}}_i$, $\hat{\gamma}_{i+1}$ evolves in the same set of cells, we can apply the trajectory tracing dynamics (61) and Lemma 3.3.5 ensures if C^p and C^{p+1} follow the notation $p = (h,m)$ and $p+1 = (h+1,m)$, then $V^{k+1}_{x,i} \leq V^k_{x,i}$, $\forall i$. Hence, both $0 \leq \alpha^k_{i+1} \leq 1$ and $0 \leq \hat{\alpha}^k_{i+1} \leq 1$. Thus we deduce:

$$\begin{aligned} x^f_{i+1} &= x^m_{i+1} + \sum_{k=l+1}^{f} t^k_{i+1} F^k_{x,i+1} \\ &= x^0 + \sum_{k=1}^{l} \hat{t}^k_{i+1} \hat{F}^k_{x,i+1} + \sum_{k=l+1}^{f} t^k_{i+1} F^k_{x,i+1} \\ &= x^f_i + \sum_{k=1}^{l} \frac{\hat{t}^{k2}_i}{\|\hat{T}_i\|^2} \hat{\alpha}^k_{i+1} \hat{d}_{x,i} + \sum_{k=l+1}^{f} \frac{t^{k2}_i}{\|T_i\|^2} \alpha^k_{i+1} d_{x,i}. \end{aligned} \tag{113}$$

Since $\hat{d}_{x,i} \leq d_{x,i}$, we get:

$$\begin{aligned} x^f_{i+1} &\leq x^f_i + \sum_{k=1}^{f} \frac{t^{k2}_i}{\|T_i\|^2} d_{x,i} \\ &\leq x^f_i + d_{x,i} \leq x^* \end{aligned} \tag{114}$$

Furthermore, since the MT error $d_{x,i} > 0$, it follows that $x^l_{i+1} > x^l_i$, the flow and the explored distance along x-axis $\psi_{x,i}$ in $\mathcal{A}^3_{i+1}$ increases.

$$\psi_{x,i+1} = \sum_{k=l+1}^{f} t^k_{i+1} F^k_{x,i+1} \geq \psi_{x,i} = \sum_{k=l+1}^{f} t^k_i F^k_{x,i}. \tag{115}$$

Hence,

$$x_{i+1}^{f} = x_{i+1}^{l} + \sum_{k=l+1}^{f} t_{i+1}^{k} F_{x,i+1}^{k} > x_{i}^{f}. \tag{116}$$

Finally, we obtain by combining (114) and (116) $x_i^f < x_{i+1}^f \leq x^*$ which implies $0 \leq d_{x,i+1} < d_{x,i}$.

□

3.4 Simulations and Results

In this section, we present a simulation example applying MT to a discontinuous flow field. We empirically choose small threshold ε_F as a stopping criteria for the flow field estimation Algorithm 2, for example $\varepsilon = 10^{-14}$. F^* denotes the true flow field and F the estimated flow. We simulate a flow field such that the strength of the flow is varying from one column to another. In the first part of the grid, it decreases from $2.5m/s$ to $1m/s$ and increases in the second part from $1m/s$ to $2.5m/s$. Considering the control velocity S, we choose it to be equal to $2.5m/s$, the maximum true flow. Figure 11 illustrates the evolution of traced trajectory. As expected, only the cells that are crossed by the AUV are updated, which explains why the predicted trajectory includes a vertical part by iteration one. Figure 11b shows another feature of tracing mechanism. As the flow keeps increasing in X-direction, the slope of the AUV velocity decreases leading the AUV to enter new cells. We can remark that the dashed line in Figure 11b goes through the third and fourth cells in column 2 instead of 1. Furthermore, Figure 12 depicts the final computed trajectory, where the final position converges to the real position.

Concerning the estimated flow, it is not a surprise that the flow in Y-direction remains constant since the algorithm involves only one MT error in X-direction; we see blue dashed arrows only in the cells that the AUV crossed. Furthermore, Figure 13a reflects the discontinuity of estimated flow, only the first column is equally updated by iteration 1 because of the constant traveling time $t = \frac{\Delta}{V_y}$. Another interesting

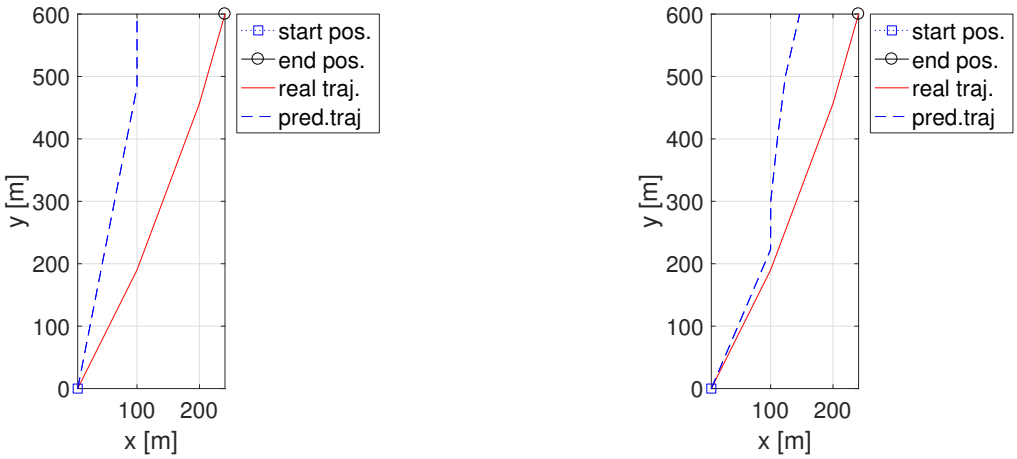

(a) After one iteration

(b) After two iterations

Figure 11: Evolution of predicted trajectories between starting positions (blue rectangles) and target positions (black circles).

property that we have explained in Chapter 3 is the discrepancy in flow strength between cells. We can confirm Lemma 3.3.5 through Figure 14 ; the dashed arrow, representing the estimated flow in X-direction decreases along the traced trajectory, crossing successive columns of the grid.

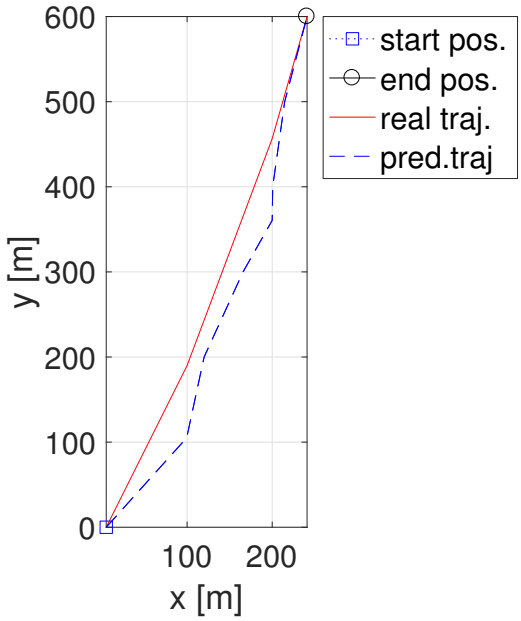

Figure 12: Real and predicted trajectories between starting positions (blue rectangles) and target positions (black circles).

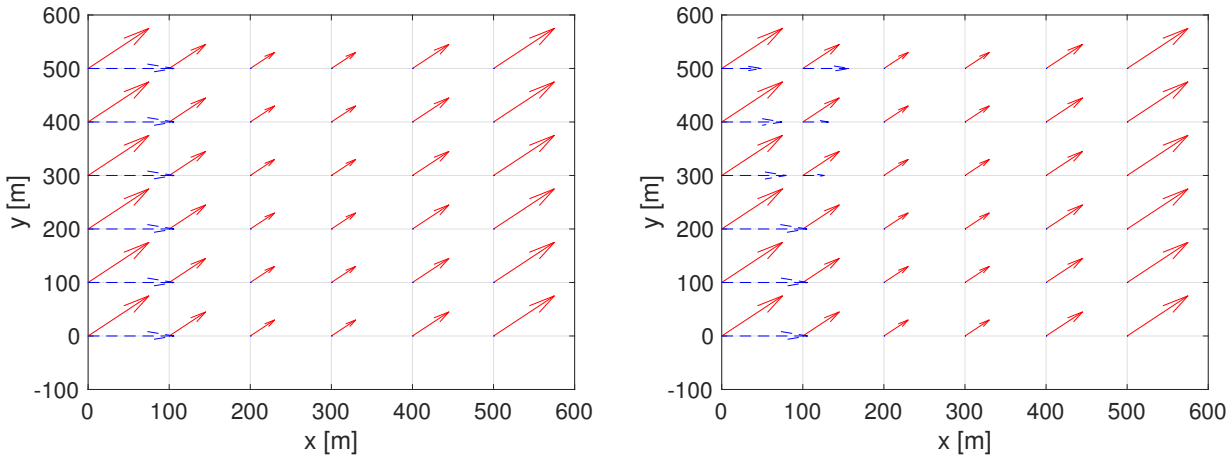

(a) After one iteration

(b) After two iterations

Figure 13: Evolution of predicted flow field (blue dashed line).

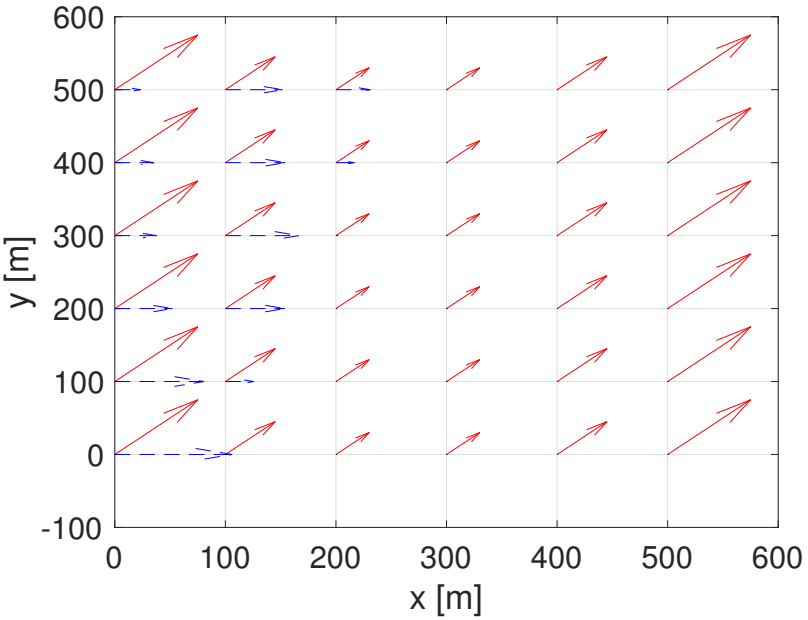

Figure 14: A simulated true flow (red solid lines) and predicted flow field (blue dashed line).

CHAPTER IV

INCORPORATION OF VEHICLE TRAVELING TIME

In this chapter, we extend the MT algorithm with a new phase by incorporating time of travel to improve the accuracy of the strength of the predicted flow $\bar{F}$ obtained from the proposed MT algorithm in Chapter 3.

4.1 Extension of MT by Travel Time

Additionally to the final position, the GPS provides highly accurate time of travel t^*. This extension improves the accuracy of the flow estimate. Let $\bar{F}^k$ be the predicted flow obtained from MT algorithm and $\bar{V}^k = S + \bar{F}^k$ the corresponding AUV velocity. Based on the underlying flow $\bar{F}^k$, the traced trajectory provides the final travel time t^f. Similar to MT error, we define the estimated MT time error e_i as follows:

$$e_{t_i} = t^* - t_i^f, \tag{117}$$

where t^* is the measured time of travel and t_i^f the simulated time of travel at iteration i. Accounting for the piecewise linearity of the traced trajectory, we can formulate the final travel time t_i^f as the sum of travel duration in set of crossed cells $\mathcal{C} = \{C^1, \cdots, C^f\}$ as follows:

$$t_i^f = \sum_{k=1}^{f} t_i^k. \tag{118}$$

The first goal from this part is to keep using the predicted traced trajectory, obtained from MT algorithm $\bar{\gamma}$. The direction of AUV velocity remains constant so that the MT error does not increase. The second goal is to estimate the AUV speed V along $\bar{\gamma}$ such that the simulated travel time converges to the measured travel time. Therefore, We suggest to tune the norm of the velocity $\bar{V}^k$ with adaptive parameter $\lambda^k \in \mathbb{R}$:

$V^k = \lambda^k \bar{V}^k$ and we keep updating λ^k until the time error converges.

Concerning the predicted flow from previous step not using timing information, we use the equation $V^{k*} = S + F^{k*}$. We obtain the solution F^{k*} by subtracting the AUV control velocity S from the final velocity V^{k*}. Since we define t_i^k as the duration of travel in cell C^k such that when the AUV reaches one side of cell C^k $(x_i^k - h\Delta).(y_i^k - s\Delta) = 0$ holds. However, accounting for the symmetry we simplify w.l.g. the equality to $x(t_i^k) - h\Delta = 0$. Similarly to the MT analysis, presented in Chapter 3, we compute an approximation of the gradient of travel time, defined locally in the crossed cells. Let us consider $\frac{\partial x(t_i^k)}{\partial F_{x,i}^k}$

$$\frac{\partial x(t_i^k)}{\partial F_{x,i}^k} = \frac{\partial t_i^k F_{x,i}^k}{\partial F_{x,i}^k} = t_i^k + F_{x,i}^k \frac{\partial t_i^k}{\partial F_{x,i}^k}. \tag{119}$$

Applying the chain rule on $x(t_i^k) - h\Delta = 0$ results in

$$\frac{\partial (x(t_i^k) - h\Delta)}{\partial F_{x,i}^k} = \frac{\partial x(t_i^k)}{\partial t_i^k} \frac{\partial t_i^k}{\partial F_{x,i}^k} = 0. \tag{120}$$

Since $x(t_i^k) - h\Delta = 0$ means that the AUV reaches the vertical side before the horizontal one from cell C^k, then the travel time is locally a function of $F_{x,i}^k$. Thus, $\frac{\partial t_i^k}{\partial F_{x,i}^k} \neq 0$, then $\frac{\partial x(t_i^k)}{\partial t_i^k} = 0$. Finally, we obtain

$$\frac{\partial t_i^k}{\partial F_{x,i}^k} = -\frac{t_i^k}{F_{x,i}^k}. \tag{121}$$

Since the vehicle trajectory is fix, the set of visited cells $\mathcal{C}^*$ is constant. Hence, we can define λ_i for all i as $\lambda_i = [\lambda_i^1, \cdots, \lambda_i^f]$ where $\lambda_i^k \in \Re$ is the corresponding tuning parameter for cell C^k. Concerning the computation of λ^k, we approximate the final time $t_i^f = \sum_{k=1}^{f} t_i^k$ using first order Taylor expansion expanded around λ_i^k.

$$\begin{aligned} t^f((\lambda^k)\bar{V}^k) &= t^f((\lambda_i^k)\bar{V}^k) + \frac{\partial(\lambda^k \bar{V}^k)}{\partial \lambda^k} \frac{\partial t^f}{\partial((\lambda_i^k)\bar{V}^k)}(\lambda^k - \lambda_i^k) \\ &= t^f((\lambda_i^k)\bar{V}^k) + \bar{V}^{k\top} \frac{\partial t^f}{\partial(\lambda_i^k \bar{V}^k)}(\lambda^k - \lambda_i^k). \end{aligned} \tag{122}$$

Then we plug $\lambda^k = \lambda_{i+1}^k$ and $t^f = t^*$:

$$t^* = t_i^f + \bar{V}^{k\top} \frac{\partial t^f}{\partial(\lambda_i^k \bar{V}^k)}(\lambda_{i+1}^k - \lambda_i^k), \tag{123}$$

Since $\frac{\partial t^f}{\partial(\lambda_i^k \bar{V}^k)}$ is not invertible, we use the technique proposed in [24]. We define the required terms as follows:

$$\|H_i\|^2 = \|\bar{V}^\top \frac{\partial t_i^f}{\partial((\lambda_i^k)\bar{V}^k)}\|^2 = \sum_{j=1}^{f} (\frac{t_i^j}{\lambda_i^j})^2 \tag{124}$$

$$h_i^k = \bar{V}^{k\top} \frac{\partial t_i^k}{\partial(\lambda_i^k \bar{V}^k)} = \frac{t_i^k}{\lambda_i^k}. \tag{125}$$

So the adaptive factor $\lambda^k{}_i$ follows:

$$\lambda_{i+1}^k = \lambda_i^k + \frac{h_i^k}{\|H_i\|^2} e_{t_i}, \tag{126}$$

When λ_i^k converges to λ^{k*}, equation (126) implies the convergence of error time e_t. The final solution V^{k*} guarantees that both MT error d and e_t converge to zero. Recalling that $V = F + S$, then we obtain F^* as follows:

$$F^{k*} = V^{k*} - S = \lambda^{k*} \bar{V}^k - S \tag{127}$$

To ensure the convergence of MT time error, we modify the underlying algorithm with a factor $\omega > 0$ such that the adaptive parameter evolves according to the following recursion:

$$\begin{aligned} \lambda_{i+1}^k &= \lambda_i^k + \omega \frac{h_i^k}{\|H_i\|^2} e_{t_i} \\ &= \lambda_i^k - \omega \frac{t_i^k}{\lambda_i^k} \frac{t^* - \sum_{j=1}^{f} t_i^j}{\sum_{j=1}^{f} (\frac{t_i^j}{\lambda_i^j})^2}. \end{aligned} \tag{128}$$

One merit from splitting the problem into two parts, convergence of MT error first and then time error problem, is that the length of the trajectory within one cell is constant as we do not change the direction of the velocity. Thus, the following relationship holds, $\forall i$ and $\lambda_i^k \neq 0$:

$$\begin{aligned} \lambda_i^k \bar{V}^k t_i^k &= \lambda_{i+1}^k \bar{V}^k t_{i+1}^k \\ t_{i+1}^k &= t_i^k \frac{\lambda_i^k}{\lambda_{i+1}^k} \end{aligned} \tag{129}$$

Combining the MT algorithm, introduced in Chapter 3, with the time extension, the new MT algorithm comprises two phases: While we use the motion integration error in the first part to trace the AUV trajectory and accordingly to estimate the flow field, we increase the accuracy of flow estimation in the second part by employing the travel time.

Algorithm 3: MT flow field estimation

Data: Measured final position r_i^*
Time of travel t_i^*
Set $i = 0$. Initialize the flow $F_0^k = \mathbf{0} \in \Re^2$; **repeat**
  Trajectory tracing to get T_i, t_i^k and d_i
  Update the flow in all cells k according to (28)

$$F_{i+1}^k = F_i^k + \frac{t_i^k}{\|T_i\|^2} d_i. \tag{130}$$

until $\| d_i\| \leq \epsilon_{\mathbf{f}}, \quad V^k \to \bar{V}^k$
Set $i = 0$. Initialize ${\lambda^k}_0 = 1$; **repeat**
until $\| e_{t_i}\| \leq \epsilon_{\mathbf{f}}, \quad F^* \to V^* - S$
for $i = 1$ **to** N **do**
  Compute H_i, h_i and e_{t_i} according to (129) and (124)
  Update the flow in all cells k

$$\begin{aligned} \lambda_{i+1}^k &= \lambda_i^k + \omega \frac{h_i^k}{\|H_i\|^2} e_{t_i} \\ V_{i+1}^{k*} &= \lambda_{i+1}^k \bar{V}^k \end{aligned} \tag{131}$$

end

4.2 Convergence Analysis of Time Integration Error

As outlined above, the proposed algorithm incorporates measured time data to estimate the norm of the flow. We compute the adaptive parameter λ^k that ensures the convergence of the predicted time of the flight $t_i^f = \sum_{k=1}^f t_i^k$ to the measured time t^* using the traced trajectory (12). For convenience, we rewrite (126) as follows:

$$\lambda_{i+1}^k = \lambda_i^k + \omega \frac{h_i^k}{\|H_i\|^2} e_{t_i}$$

$$= \lambda_i^k - \omega \frac{t_i^k}{\lambda_i^k} \frac{t^* - \sum_{j=1}^{f} t_i^j}{\sum_{j=1}^{f} (\frac{t_i^j}{\lambda_i^j})^2}. \tag{132}$$

Furthermore, t_i^k evolves according to the following

$$\lambda_i^k \bar{V}^k t_i^k = \lambda_{i+1}^k \bar{V}^k t_{i+1}^k$$
$$t_i^k = t_{i+1}^k \frac{\lambda_{i+1}^k}{\lambda_i^k}. \tag{133}$$

Substituting t_i^k in (132) provides a formulation of the problem as nonlinear discrete mapping $G(\lambda_i^k) = \lambda_{i+1}^k$.

$$G(\lambda_i^k) = \lambda_i^k - \omega \frac{t_0^k}{(\lambda_i^k)^2} \frac{t^* - \sum_{j=1}^{f} \frac{t_0^j}{\lambda_i^j}}{\sum_{j=1}^{f} \frac{(t_0^j)^2}{(\lambda_i^j)^4}}, \lambda_i^k \neq 0. \tag{134}$$

We pick $\lambda_0^k = 1$ as initial condition. Our goal is to compute the fix points λ^* of G such that: $G(\lambda^*) = \lambda^*$ for $t_i^k > 0$. Note $\lambda = [0, \cdots, 0]$ is a singular point to be treated separately as shown below:

$$\begin{aligned}
\lim_{\lambda_i^k \to 0} \lambda_{i+1}^k &= \lim_{\lambda_i^k \to 0} \lambda_i^k - \omega \frac{t_i^k}{\lambda_i^k} \frac{t^* - \sum_{j=1}^{f} t_i^j}{\sum_{j=1}^{f} (\frac{t_i^j}{\lambda_i^j})^2} \\
&= \lim_{\lambda_i^k \to 0} \lambda_i^k - \omega \frac{t_i^k}{\lambda_i^k} \frac{A_i - \frac{t_0^k}{(\lambda_i^k)^2}}{B_i + \frac{(t_0^k)^2}{(\lambda_i^k)^4}} \\
&= \lim_{\lambda_i^k \to 0} \lambda_i^k - \omega t_i^k \lambda_i^k \frac{A_i (\lambda_i^k)^2 - t_0^k}{(\lambda_i^k)^3 B_i + (t_0^k)^2} = 0,
\end{aligned} \tag{135}$$

where $B_i = \sum_{j=1, j\neq k}^{f} (\frac{t_i^j}{\lambda_i^j})^2$ and $A_i = t^* - \sum_{j=1, j\neq k}^{f} t_i^j$. This case implies that the velocity of the vehicle is zero. Adding to $\lambda = [0, \cdots, 0]$, $G(\lambda^*) = \lambda^*$ implies $e_{t^*} = 0$ for $\lambda^* \neq 0$. Ultimately, the fix points set λ^* is:

$$\lambda^* = \{0_{1\times f} \cup \lambda \in \Re^{1\times f} \mid e_{t^*} = 0\}. \tag{136}$$

The questions about a possible definition for the stability region of G and the convergence of time integration error e_{t_i} are yet to be answered. So, we establish an explicit formula for e_{t_i} in the following Lemma

Lemma 4.2.1. *Let λ_i^k be defined in equation (126), then the time error e_{t_i} evolves according to*

$$e_{t_{i+1}} = \sum_{k=1}^{f}(1-\gamma_i^k)(\frac{t_i^k}{\lambda_i^k})^2\frac{e_{t_i}}{H_i}, \tag{137}$$

with $\gamma_i^k = \omega\frac{2-\omega\beta_i^k}{\left(1-\omega\beta_i^k\right)^2}$, $\beta_i^k = \frac{t_i^k}{(\lambda_i^k)^2}\frac{e_{t_i}}{H_i}$ and $H_i = \sum_{j=1}^{f}(\frac{t_i^j}{\lambda_i^j})^2$.

Proof.

$$\begin{aligned}
e_{t_{i+1}} &= t^* - t_{i+1}^f \\
&= t^* - \sum_{k=1}^{f} t_{i+1}^k \\
&= t^* - \sum_{k=1}^{f} t_i^k\frac{\lambda_i^k}{\lambda_{i+1}^k} \\
&= t^* - \sum_{k=1}^{f} t_i^k\frac{\lambda_i^k}{\lambda_i^k - \omega\frac{t_i^k}{\lambda_i^k}\frac{t^*-\sum_{j=1}^{f}t_i^j}{\sum_{j=1}^{f}(\frac{t_i^j}{\lambda_i^j})^2}} \\
&= t^* - \sum_{k=1}^{f}\frac{1}{\left(1-\omega\frac{t_i^k}{\lambda_i^{k2}}\frac{e_{t_i}}{H_i}\right)^2}t_i^k \\
&= t^* - \sum_{k=1}^{f}\frac{1}{\left(1-\omega\beta_i^k\right)^2}t_i^k,
\end{aligned} \tag{138}$$

where $\beta_i^k = \frac{t_i^k}{(\lambda_i^k)^2}\frac{e_{t_i}}{H_i}$. Now we add and subtract t_i^f in order to extract e_{t_i} :

$$\begin{aligned}
e_{t_{i+1}} &= t^* - t_i^f + t_i^f - \sum_{k=1}^{f}\frac{1}{\left(1-\omega\beta_i^k\right)^2}t_i^k \\
&= e_{t_i} + \sum_{k=1}^{f}(1-\frac{1}{\left(1-\omega\beta_i^k\right)^2})t_i^k \\
&= e_{t_i} - \sum_{k=1}^{f}\frac{2-\omega\beta_i^k}{\left(1-\omega\beta_i^k\right)^2}\omega(\frac{t_i^k}{\lambda_i^k})^2\frac{e_{t_i}}{H_i} \\
&= \sum_{k=1}^{f}(1-\gamma_i^k)(\frac{t_i^k}{\lambda_i^k})^2\frac{e_{t_i}}{H_i},
\end{aligned} \tag{139}$$

with $\gamma_i^k = \omega\frac{2-\omega\beta_i^k}{\left(1-\omega\beta_i^k\right)^2}$ and $H_i = \sum_{j=1}^{f}(\frac{t_i^j}{\lambda_i^j})^2$. □

Based on the deduced error dynamics, we can state the main result of this chapter in the following theorem:

Theorem 4.2.1. *Consider the discrete, nonlinear mapping* $G(\lambda_i) = \lambda_{i+1}$ *and its subset of fix points* $\lambda^* = \{\lambda \in \mathbb{R}^{1\times f} \mid e_{t^*} = 0\}$. *Let* $\omega = \frac{1}{2}$, $\lambda_0^k > 0$, $\forall k$ *such that* $e_{t_0} \leq 0$ *then,* $e_{t_i} \leq 0$, $\forall i$ *and the time integration error converges to zero.*

Proof. We prove by induction the Lemma. First we choose λ so that $e_{t_0} \leq 0$. Now, assuming that $e_{t_n} \leq 0$. Let us consider the error dynamics $e_{t_{n+1}}$:

$$e_{t_{n+1}} = \sum_{k=1}^{f}(1-\gamma_i^k)(\frac{t_i^k}{\lambda_i^k})^2\frac{e_{t_i}}{H_i}. \tag{140}$$

Obviously the term $1-\gamma_n^k$, determines the sign of $e_{t_{n+1}}$. We suppose that $0 \leq 1-\gamma_n^k < 1$ holds in order to define the conditions for the validity of the claim.

$$\begin{aligned} 0 &\leq 1-\gamma_n^k < 1 \\ 0 &\leq \omega\frac{2-\omega\beta_i^k}{\left(1-\omega\beta_i^k\right)^2} < 1 \end{aligned} \tag{141}$$

We substitute ω with $\omega = \frac{1}{2}$ and since $\beta_n^k = \frac{2t_i^k}{(\lambda_n^k)^2}\frac{e_{tn}}{H_n} \leq 0$, the left side of (141) is valid. Considering the right side of (141):

$$\begin{aligned} 2-\frac{1}{2}\beta_i^k &< 2-2\beta_i^k+\frac{1}{2}(\beta_i^k)^2 \\ 0 &< \beta_i^k(\frac{1}{2}\beta_i^k-\frac{3}{2}) \end{aligned} \tag{142}$$

$e_{t_n} < 0$ implies (142) is valid. Therefore, if $e_{t_n} < 0$ is true, $0 \leq 1-\gamma_n^k < 1$ holds. Since $e_{t_{n+1}} = \sum_{k=1}^{f}(1-\gamma_n^k)(\frac{t_n^k}{\lambda_n^k})^2\frac{e_{tn}}{H_n}$ and $e_{t_n} \leq 0$ implies $0 < 1-\gamma_n^k < 1$ then $e_{t_{n+1}} \leq 0$. Hence, $e_{t_{n+1}} \leq 0$ is valid. Furthermore, using $0 \leq 1-\gamma_n^k < 1$ yields:

$$\begin{aligned} \|e_{t_{n+1}}\| &\leq \sum_{k=1}^{f}\|(1-\gamma_n^k)\|(\frac{t_n^k}{\lambda_n^k})^2\frac{\|e_{t_n}\|}{H_n} \\ &< \sum_{k=1}^{f}(\frac{t_n^k}{\lambda_n^k})^2\frac{\|e_{t_n}\|}{H_n} \end{aligned}$$

$$< \|e_{t_n}\|. \tag{143}$$

This completes the proof of the claim. □

4.3 Simulations and Results

In this section, we modify the simulation example, introduced in Chapter 3. We improve the accuracy of flow estimation by applying Algorithm 3 instead of Algorithm 2 to incorporate the measured traveling time. In Algorithm 3, we keep the direction of the previous AUV velocity $\bar{V}$. Hence, Figures 16a and 15 are identical. However, we correct the norm of AUV velocity so that the measured and estimated traveling time are equal. Hence, the flow F is updated as follows:

$$F^k = V^{k*} - S = \lambda^{k*}\bar{V}^k - S$$

Therefore, the estimated flow in Figure 16b exhibits change in both norm and direction along the traced trajectory which leads to better accuracy comparing to Figure 14. However there exists noticeable difference between the predicted and the true flow, the red and the blue arrows. This fact urges the deployment of multiple vehicles as we will show in the following chapter.

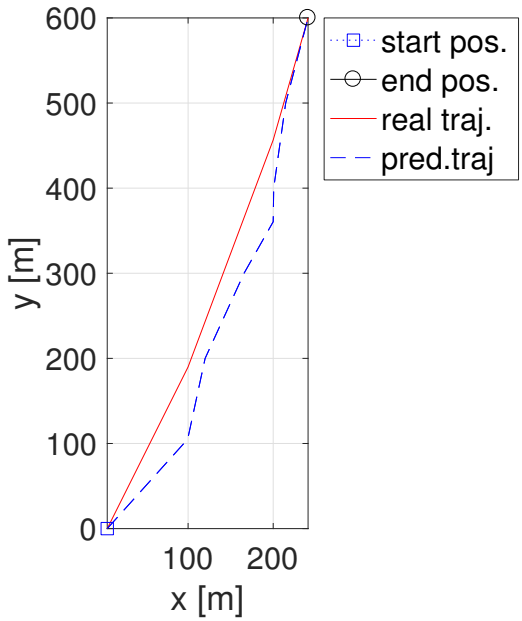

Figure 15: Real and predicted trajectories between starting positions (blue rectangles) and target positions (black circles).

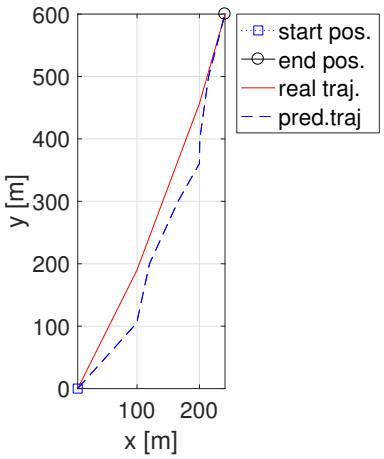

(a) Estimated and true Traced trajectory

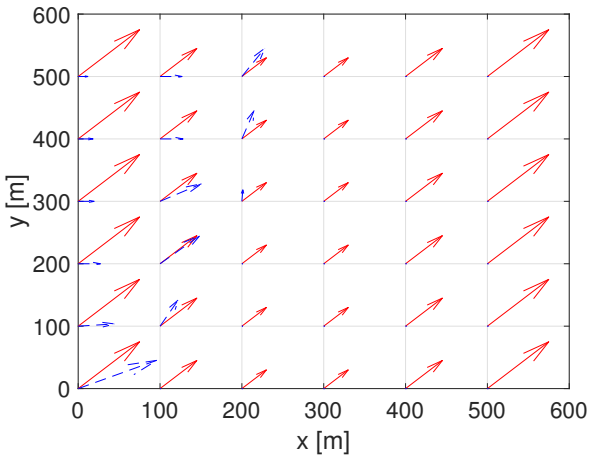

(b) Estimated and true Flow field mapping

Figure 16: A simulated true flow (red solid lines) and predicted flow field (blue dashed line) with travel time incorporation.

CHAPTER V

MUTLI VEHICLE MOTION TOMOGRAPHY

The MT method can be formulated as an optimization problem, where multiple vehicles are involved to cover the studied area. In this chapter we utilize multiple AUVs to estimate the underlying flow. We propose two versions of MT algorithm, we discuss the underlying features and we establish the convergence of the MT error.

5.1 Previous Works

In recent years, different reconstruction algorithms have been developed. Accounting for its promising results, Algebraic Reconstruction Technique (ART) has been widely used in computerized tomography see [19, 27]. As a matter of fact, ART owes much of its success to the use of Kaczmarz algorithm as one of the most efficient iterative method for image reconstruction in computerized tomography. There is a considerable volume of research on this method: A modified ART for THz tomography has been developed in [38]. Strohmer and Vershynin [35] proposed randomized version of the Kaczmarz method for consistent, overdetermined linear systems and Kamath et al. suggested a parallel algorithm for a randomized Kaczmarz algorithm [20]. The convergence of both algorithms is proved. Nonetheless, the challenge in MT arises by the inherent nonlinear characteristics of the MT problem. Chang et al. proposes a Kaczmarz-Type Method to solve the MT problem for multiple vehicles and explains the approach with regard to MT error, see [20].

Concerning the solution structure, ART has been considered in various forms, where the correction is applied in different stages of the algorithm. Reference [8] proposes and compares four reconstruction methods based on simulated data.

In this chapter, we compare these approaches. Based on the followed evaluation, we

implement the appropriate version to solve MT problem. For self containment, we recall some technical words used in ART and we redefine it with respect to MT. A cycle is defined in [8] as a stage of reconstruction in which all projection data are considered once. As V AUVs are deployed, a cycle comprises V projections, where one projection denotes one traced ray. It is worth to underline that in contrast to Acoustic tomography, where the projection diffuses different rays, the MT projection is represented by one traced ray. This fact reduces the four modifications, discussed in [8] into two: While the Correction per Cycle updates the estimated flow $\mathbf{F}$ after one cycle, the Averaged Correction per Projection corrects the latter after every projection. Note that the Averaged Correction per Projection collapses into a simple Correction per Projection since we have only one ray for one vehicle.

Chang et al. uses the Correction per Cycle in distributed fashion. The MT problem is considered as a joint optimization problem where vehicle v solves the vth optimization problem and then computes a common estimate of the flow field $\mathbf{F}$. The decentralized MT allows vehicle v to share its estimate ${}^{v}\mathbf{F}$ with only a subset of other vehicles, referring it as Neighbors and eventually reaches the consensus $\mathbf{F}$. Nonetheless, this approach suffers from scalability, when the solution vector that needs to be communicated among neighbors is large. We focus in this thesis on the the correction per cycle or per projection, which can be seen as centralized methods and we leave the distributed formulation for further work.

5.2 Multiple Vehicle MT

As discussed in Chapter 1, Chang et al. derived an iterative flow field estimation algorithm referred to as a Kaczmarz-type method based on the Kaczmarz method, an iterative method for solving a linear system of equations. We follow the same principle, though we apply the centralized approach, Correction per Cycle (CC) and Correction per Projection (CP).

In this chapter, we suppose V vehicles are involved in MT, where we assign to every vehicle v the MT error ${}^{v}d$. Hence, ${}^{v}t_i^k$ denotes the time that the AUV v spends to cross the cell k by iteration i, $\|{}^{v}T_i\|^2 = \sum_{k=1}^{f} {}^{v}t_i^{k\,2}$ and η^k the number of vehicles that enters the cell k. Consequently, the estimated flow $\mathbf{F}_{i+1}$ is updated at step $i+1$ in different ways as follows:

- Motion Tomography Correction per Cycle (MTCC): All AUV trajectories are constructed through simulation that involves the current estimated flow F_i and hence the resulted MT error ${}^{v}d_I$ is computed for each AUV. Then, the flow is updated again using the average of flow modifications as follows:

$$F_{i+1}^k = F_i^k + \sum_{v=1}^{\eta^k} \frac{{}^{v}t_i^k}{\eta^k \|{}^{v}T_i\|^2} {}^{v}d_i, \tag{144}$$

  Based on the Kaczmarz-type method for MT in Equation (144), we obtain a flow field estimation algorithm (Algorithm 4). In the algorithm, we check the norm of MT error as a criteria for the convergence. We continue updating the solutions until the Euclidean norms of MT errors ${}^{v}d_i, \forall v \leq V$ are sufficiently small (i.e., below a threshold ϵ_F).

- Motion Tomography Correction per Projection (MTCP): The traced trajectory ${}^{v}\tilde{\gamma}$ for the AUV v is obtained by simulating the vehicle trajectory using current estimate of the flow F_{i+1}, updated by AUV $v-1$ as follows:

$${}^{v}\tilde{\gamma} = \int_{t_0}^{t^f} \left({}^{v}S + {}^{v-1}F_i({}^{v}r) \right) \mathrm{d}t, \tag{145}$$

  Hence the resulted MT error ${}^{v}d_i$ is computed for AUV v. Then, the flow is updated again using the newest MT error as follows:

$${}^{v}F_i^k = {}^{v-1}F_i^k + \frac{{}^{v}t_i^k({}^{v-1}F_i)}{\|{}^{v}T_i({}^{v-1}F_i)\|^2} {}^{v}d_i, \tag{146}$$

  Based on the Kaczmarz-type method for MT in Equation (146), we obtain a flow field estimation algorithm (5). In the algorithm, the same operation recurs

untill $v = V$, then the iteration number increases $i + 1$ we check the norm of MT error as a criteria for the convergence. We continue updating the solutions until the Euclidean norms of MT errors ${}^{v}d_i, \forall v \leq V$ are sufficiently small (i.e., below a threshold ϵ_F).

In the next section, we analyze the convergence of the MTCC and we omit the proof for the MTCP because the two methods have similar analysis. It is worth to underline that [8] addressed ray-tracing and compared results on four reconstruction methods based on simulated data. However, only experimental results are shown, which are in good agreement with the theoretical study. The work does not prove the convergence of the proposed approach.

Algorithm 4: MTCC flow field estimation

Data: Measured final positions ${}^{v}r^*$ where v $\{1, \cdots, V\}$

Set $i = 0$. Initialize the flow $F_0^k = \mathbf{0} \in \Re^2$; **repeat**

  Trajectory tracing to get ${}^{v}T_i$, ${}^{v}t_i^k$ and ${}^{v}d_i$

  Update the flow in all cells k:

$$F_{i+1}^k = F_i^k + \sum_{v=1}^{\eta^k} \frac{{}^{v}t_i^k}{\eta^k \|{}^{v}T_i\|^2} {}^{v}d_i,$$

until $\| {}^{v}d_i \| \leq \epsilon_F, \quad \forall v \leq V$

5.3 Convergence Analysis of one Dimension MTCC and Simulation Results

Recognizing the difficulty associated with ray tracing as discussed in Chapter 3, we divide the analysis into two parts. In the first part, we limit the scope on one axis flow estimation. In other terms, we place the AUVs along one axis and we prove the convergence for the proposed case.

In the second part, we consider the general case, where the AUVS are launched from the horizontal and vertical axis, and we prove the convergence of MTCC using the first part.

Algorithm 5: MTCP flow field estimation

Data: Measured final positions ${}^{v}r^{*}$ where v $\{1, \cdots, V\}$

Set $i = 0$. Initialize the flow $F_0^k = \mathbf{0} \in \Re^2$; **repeat**

until $\| {}^{v}d_i \| \leq \epsilon_{\mathbf{f}}, \quad \forall v \leq V$

for $v = 1$ **to** V **do**

Trajectory tracing to get ${}^{v}T_i$, ${}^{v}t_i^k$ and ${}^{v}d_i$ Update the MT error by

$$ {}^{v}d_i = {}^{v}\, r^{*} - {}^{v}\, r({}^{v-1}F_i), $$

Update the flow in all cells k crossed by vehicle v

$$ {}^{v}F_{i+1}^k = {}^{v-1}\, F_i^k + \frac{{}^{v}t_i^k({}^{v-1}F_i)}{\|{}^{v}T_i({}^{v-1}F_i)\|^2} {}^{v}d_i, $$

Let $v = v + 1$.

end

5.3.1 Convergence Analysis of one Dimension MTCC

We keep the same problem setup described in Chapter 3 and we place V AUVs along the horizontal axis. Note that the symmetry of the grid implies the same analysis for the ordinate Axis as well. Accounting for the multiple vehicle navigation, we extend Assumption 3.3.1 as follows:

Assumption 5.3.1. *Let the AUV v be one of the launched V AUVs. The AUV velocity ${}^{v}S_x = 0$, ${}^{v}S_y > \max(F_x^k) \geq 0$, ${}^{v}r^0 = [{}^{v}x^0, 0]^\top$ and ${}^{v}x^{*} >^{v} x^0$*

In order to establish the analysis of multi vehicle MT algorithm, we need to extend the MT error dynamics. Let us define $\varepsilon_{x,i}^k = \sum_{v=1}^{\eta^k} \frac{{}^{v}t_i^k}{\eta^k \|{}^{v}T_i\|^2} {}^{v}d_{x,i}$, $\varepsilon_{y,i}^k = 0$, and $\varepsilon_i^k = [\varepsilon_{x,i}^k, \varepsilon_{y,i}^k]^\top$. Applying the flow update on the error dynamics (60) results in:

$$ \begin{aligned} {}^{v}d_{x,i} &= {}^{v}\, d_{x,i-1} + \sum_{k=1}^{f} {}^{v}t_{i-1}^k \prod_{j=k}^{f} {}^{v}\alpha_i^j \times^{v} \varepsilon_{i-1}^k, \\ &= {}^{v}\, d_{x,i-1} - \sum_{k=1}^{f} {}^{v}t_{i-1}^k \prod_{j=k}^{f} {}^{v}\alpha_i^j \Big(\sum_{p=1}^{\eta^k} \frac{{}^{p}t_{i-1}^k}{\eta^k \|{}^{p}T_{i-1}\|^2} {}^{p}d_{x,i-1}\Big), \end{aligned} \tag{147} $$

where

$$\alpha_i^j = \begin{cases} 1 & \text{if} \quad y_i^j - y_i^{j-1} = \Delta \cup x_i^j - x_i^{j-1} = \Delta \\ \frac{V_{y,i}^j}{V_{x,i}^j} & \text{if} \quad y_i^j = h\Delta \cap x_i^{j-1} = s\Delta \\ \frac{V_{x,i}^j}{V_{y,i}^j} & \text{otherwise} \end{cases} \tag{148}$$

Before stating the convergence theorem, it is worth to notice that if the cell C^k is crossed only by one AUV v, we showed in Chapter 4 that the flow F_x^k will be updated such that the MT error ${}^v d$ decreases. However, if multiple vehicles cross the same cell, at least the MT error of one vehicle can increase.

Example: For clarity, let us consider the following example, where two vehicles share the same crossed cells. The flow update follows:

$$F_{x,i+1}^k = F_{x,i}^k + \sum_{v=1}^{2} \frac{{}^v t_i^k}{2\|{}^v T_i\|^2} {}^v d_{x,i}. \tag{149}$$

Let us choose w.l.o.g. $\frac{{}^1 t_i^k}{\|{}^1 T_i\|^2} {}^1 d_{x,i} \neq \frac{{}^2 t_i^k}{\|{}^2 T_i\|^2} {}^2 d_{x,i}$ and $\frac{{}^1 t_i^k}{\|{}^1 T_i\|^2} {}^1 d_{x,i} < \frac{{}^2 t_i^k}{\|{}^2 T_i\|^2} {}^2 d_{x,i}$, then it follows $\frac{{}^1 t_i^k}{\|{}^1 T_i\|^2} {}^1 d_{x,i} < \sum_{v=1}^{2} \frac{{}^v t_i^k}{2\|{}^v T_i\|^2} {}^v d_{x,i} < \frac{{}^2 t_i^k}{\|{}^2 T_i\|^2} {}^2 d_{x,i}$. This increase of flow results in overshoot of MT error ${}^2 d_{x,i+1}$. Motivated by the example, we discuss the impact of time weight included in flow prediction in the following Lemma.

Lemma 5.3.1. *Let the traced trajectory be formulated according to (144). Suppose Assumptions 3.1.1, 5.3.1, V is the number of AUVS, ${}^V\mathcal{C}_i \cap {}^v\mathcal{C}_i = {}^v\mathcal{C}_i$ and ${}^v r^0 < {}^{v+1} r^0$ $\forall v < V$ and $\sum_{v=1}^{V} {}^v d_{x_i} \geq 0$ hold, then*

$$({}^{p+1}t_i^{k+1})({}^V t_i^{k+1}) + ({}^{p+1}t_i^k)({}^V t_i^k) \geq ({}^p t_i^{k+1})({}^V t_i^{k+1}) + ({}^p t_i^k)({}^V t_i^k) \tag{150}$$

and

$$\sum_{k=1}^{f} \frac{({}^p t^k)({}^V t^k)}{\|{}^p T\|^2} \leq \sum_{k=1}^{f} \frac{({}^{p+1}t^k)({}^V t^k)}{\|{}^{p+1}T\|^2} \tag{151}$$

$$\sum_{k=1}^{f} \prod_{j=k}^{f} \alpha^j \frac{({}^p t^k)({}^V t^k)}{\|{}^p T\|^2} \leq \sum_{k=1}^{f} \prod_{j=k}^{f} \alpha^j \frac{({}^{p+1}t^k)({}^V t^k)}{\|{}^{p+1}T\|^2} \tag{152}$$

are valid $\forall k \leq f$ and $1 \leq p \leq V$.

Proof. Recalling that ${}^{v}\mathcal{C}_i = {}^{V}\ \mathcal{C}_i\ \forall 1 \leq v \leq V$, then all the traced trajectories cross the same side of involved cells. Since the AUV trajectories are parallel inside the explored cells and there exist three different ways of cell crossing, we can infer the following comparison:

- If the AUVs cross the cell in vertical direction, case 1 of trajectory tracing, then ${}^{v}t_i = \frac{\Delta}{V_y}\ \forall 1 \leq v \leq V$
- As $V_y \geq V_x$ case two and case 3 occur successively such that ${}^{v}t_i^k + {}^{v}\ t_i^{k+1} = \frac{\Delta}{V_y}$. Since the traced trajectories are parallel and cross the same side of the cell, the travel time can be formulated as follows:

$$\begin{aligned} {}^{v}t_i^k &= \frac{(h+1)\Delta - {}^{v}\ x_i^{k-1}}{V_x^k} \\ {}^{v}t_i^{k+1} &= \frac{\Delta}{V_y} - {}^{v}\ t_i^k, \end{aligned} \tag{153}$$

  where $C^k = C^{(h,s)}$ and $C^{k+1} = C^{(h+1,s)}$. Adding to that, ${}^{v}r^0 <^{v+1} r^0\ \forall v < V$ implies ${}^{v}x_i^{k-1} \leq^{v+1} x_i^{k-1}$ resulting in ${}^{v+1}t_i^k \leq^{v}\ t_i^k$ and ${}^{v}t_i^{k+1} \leq^{v+1}\ t_i^{k+1}$

Therefore, ${}^{V}t_i^k$ is the minimum then ${}^{V}t_i^{k+1}$ the maximum and ${}^{V}t_i^{k+1} \geq^{V}\ t_i^k = \frac{\Delta}{V_y} - {}^{V}t_i^k$. Suppose that $({}^{V}t_i^k)({}^{p}t_i^k)+({}^{N}t_i^{k+1})({}^{p}t_i^{k+1}) \leq ({}^{N}t_i^k)({}^{p+1}t_i^k)+({}^{N}t_i^{k+1})({}^{p+1}t_i^{k+1})\ \forall V-N+1 \leq p \leq V-1$, and let us prove the claim $\forall V-N \leq p \leq V-1$. Based on the previous reasoning, ${}^{V-N}t_i^k$ is the maximum and ${}^{V-N}t_i^{k+1}$ the minimum.

$$\begin{aligned} {}^{V}t_i^{k+1} &\geq^{V}\ t_i^k \\ {}^{V}t_i^{k+1}({}^{V-N-1}t_i^{k+1} - {}^{V-N}t_i^{k+1}) &\geq {}^{V}t_i^k({}^{V-N-1}t_i^{k+1} - {}^{V-N}t_i^{k+1}) \\ {}^{V}t_i^{k+1}({}^{V-N-1}t_i^{k+1} - {}^{V-N}t_i^{k+1}) &\geq {}^{V}t_i^k({}^{V-N-1}t_i^{k+1} - \frac{\Delta}{V_y} + \frac{\Delta}{V_y} - {}^{V-N}t_i^{k+1}) \\ {}^{V}t_i^{k+1}({}^{V-N-1}t_i^{k+1} - {}^{V}t_i^{k+1}{}^{V-N}t_i^{k+1}) &\geq {}^{V}t_i^k({}^{V-N}t_i^k - {}^{V-N-1}t_i^k) \\ ({}^{V-N-1}t_i^{k+1})({}^{V}t_i^{k+1}) + ({}^{V-N-1}t_i^k)({}^{V}t_i^k) &\geq ({}^{V}t_i^k)({}^{V-N}t_i^k) + ({}^{V-N}t_i^{k+1}{}^{V}t_i^{k+1}). \end{aligned} \tag{154}$$

Furthermore, we are interested to compare the time weight, included in flow update ${}^{v}t^k \frac{{}^{p}t^k}{\|{}^{p}T\|^2} {}^{p}d_{x,i}$. Let us consider two AUVs V and p and case 2 and 3 of trajectory

tracing, as case one is constant for both of them. We assume ${}^{V}t_i^k$ is maximal in cell C^k and $\frac{\Delta}{V_y} = 1$ to simplify the calculation:

$$\begin{aligned}\pi &= \frac{{}^{p}t^{k\,V}t^k + {}^{p}t^{k+1\,V}t^{k+1}}{\|{}^{p}T\|^2} \\ &= \frac{{}^{p}t^{k\,V}t^k + (1 - {}^{p}t^k)(1 - {}^{V}t^k)}{\|{}^{p}T\|^2}.\end{aligned} \tag{155}$$

We compute the derivative of π with respect to ${}^{p}t^k$:

$$\dot{\pi} = \frac{(-4{}^{V}t^k + 2){}^{p}t^{k\,2} + 1}{\|{}^{p}T\|^4} = 0. \tag{156}$$

The root of $\dot{\pi}$ is ${}^{p}t^{k*\,2} = \frac{1}{(4({}^{V}t^k) - 2)}$ and we obtain:

$$\begin{cases} \dot{\pi} \geq 0 \quad \text{if} \quad 0 \leq {}^{p}t^{k*} \leq \sqrt{\frac{1}{(4({}^{V}t^k) - 2)}} \\ \dot{\pi} \leq 0 \quad \text{if} \quad \sqrt{\frac{1}{(4({}^{V}t^k) - 2)}} \leq {}^{p}t^{k*} \leq 1 \end{cases} \tag{157}$$

Adding to that, the travel time satisfies the following inequality:

$$0 < {}^{p}t^{k\,2} = \frac{1}{(4({}^{V}t^k) - 2)} \leq 1. \tag{158}$$

Thus, if ${}^{V}t^k \geq \frac{3}{4}$ then $\frac{1}{(4({}^{V}t^k) - 2)} \leq 1$ and π is increasing for $0 \leq {}^{p}t^k \leq \sqrt{\frac{1}{(4({}^{V}t^k) - 2)}}$ and decreasing for $\sqrt{\frac{1}{(4({}^{V}t^k) - 2)}} \leq {}^{p}t^{k*} \leq 1$. Elsewhere, π is increasing. Recalling that ${}^{V}t^k$ is the maximum travel time among all the AUVs, then when ${}^{p}t^k$ increases π increases as well, which means if the AUV is closer to AUV V π is bigger. Since all the AUVs cross the same set of cells $\mathcal{C}_i$, computing the gradient of π with respect of t^k and the corresponding roots t^{k*} implies the aforementioned conclusion for every cell C^k. Hence, we extend the analysis for the AUV trajectory to get:

$$\sum_{k=1}^{f} \frac{({}^{p}t^k)({}^{V}t^k)}{\|{}^{p}T\|^2} \leq \sum_{k=1}^{f} \frac{({}^{p+1}t^k)({}^{V}t^k)}{\|{}^{p+1}T\|^2}. \tag{159}$$

If the cell $C^k = C^{(h,s)}$ and $C^f = C^{(p,q)}$ and recalling that case one of trajectory tracing implies $\frac{V_{x,i}^{j+1}}{V_{x,j}^k} = 1$, then there exists $p - h$ column crossings that are included in $\prod_{j=k}^{f} \alpha_i^j$ as follows:

$$\prod_{j=k}^{f} \alpha_i^j = \prod_{j=h}^{p} \frac{V_{x,i}^{j+1}}{V_{x,j}^k}, \tag{160}$$

where the cells C^j satisfies $C^j = C^{(h,s)}$ and $C^{j+1} = C^{(h+1,s)}$. Consequently, if C^k and C^{k+1} are in the same column then $\prod_{j=k}^{f} \alpha_i^j = \prod_{j=k+1}^{f} \alpha_i^j$. Elsewhere, we have:

$$\prod_{j=k+1}^{f} \alpha_i^j = \prod_{j=h+1}^{p} \frac{V_{x,i}^{j+1}}{V_{x,j}^{k}} = \prod_{j=h}^{p} \frac{V_{x,i}^{j+1}}{V_{x,j}^{k}} \frac{V_{x,i}^{h}}{V_{x,h+1}^{k}}. \tag{161}$$

Let us recall that the MT algorithm ensures that $\frac{V_x^{h+1}}{V_x^h} \leq 1$, if the MT error is positive. Applying $\sum_{v=1}^{V} {}^v d_{x_i} \geq 0$ and that all the vehicles are evolving in the same set of cells, then $\prod_{j=k}^{f} \alpha^j \leq \prod_{j=k+1}^{f} \alpha^j$ holds. Finally, using (154) leads:

$$\sum_{k=1}^{f} \prod_{j=k}^{f} \alpha^j \frac{({}^p t^k)({}^V t^k)}{\|{}^p T\|^2} \leq \sum_{k=1}^{f} \prod_{j=k}^{f} \alpha^j \frac{({}^{p+1} t^k)({}^V t^k)}{\|{}^{p+1} T\|^2}. \tag{162}$$

□

As we are considering multiple vehicles, we define $E_{x,i+1} = \sum_{v=1}^{V} {}^v d_{x_{i+1}}$ and we study the dynamic of the sum of MT errors in the following lemma.

Lemma 5.3.2. *Let the traced trajectory be formulated according to (144). Suppose Assumptions 3.1.1, 5.3.1, V is the number of AUVS, ${}^V d_{x,0} > 0$, ${}^v d_{x,0} = 0$ and ${}^V \mathcal{C}_i \cap {}^v \mathcal{C}_i = {}^v \mathcal{C}_i$ $\forall 1 \leq v \leq V-1$ hold, then $E_{x,i}$ is monotone decreasing such that: $E_{x,i} \to 0$, when $i \to \infty$. and $\underline{m} E_{x,i} \leq E_{x,i+1} \leq \bar{m} E_{x,i}$, where $-1 < \underline{m} < 1$ and $0 < \bar{m} < 1$.*

Proof. Given that all traced trajectories evolve in the same set of cells ${}^V \mathcal{C}_i \cap {}^v \mathcal{C}_i = {}^v \mathcal{C}_i$ $\forall 1 \leq v \leq n$, the MT error dynamics (147) is formulated as follows:

$$\begin{aligned} E_{x,i+1} &= \sum_{v=1}^{V} {}^v d_{x_{i+1}} \\ &= \sum_{v=1}^{V} {}^v d_{x,i} - \sum_{k=1}^{f} {}^v t_i^k \prod_{j=k}^{f} {}^v \alpha_i^j (\sum_{p=1}^{V} \frac{{}^p t_i^k}{V \|{}^p T_i\|^2} {}^p d_i) \\ &= \sum_{v=1}^{V} {}^v d_{x,i} - \sum_{k=1}^{f} {}^v t_i^k \prod_{j=k}^{f} {}^v \alpha_i^j (\sum_{p=1}^{V} \frac{{}^p t_i^k}{V \|{}^p T_i\|^2} {}^p d_i). \end{aligned} \tag{163}$$

Since all the AUVs explore the same set of cells, then ${}^v \alpha_i^j = \alpha_i^j$ and ${}^v t_i^k > 0$. We denote with β^k the coefficient embedded in MT error dynamics $\beta^k = \prod_{j=k}^{f} \alpha_i^j l_i^k$.

$$E_{x,i+1} = \sum_{v=1}^{V} {}^v d_{x,i} - \sum_{k=1}^{f} {}^v t_i^k \prod_{j=k}^{f} {}^v \alpha_i^j (\sum_{p=1}^{V} \frac{{}^p t_i^k}{V \|{}^p T_i\|^2} {}^p d_i)$$

$$
\begin{aligned}
&= \sum_{v=1}^{V} {}^{v}d_{x,i} - \sum_{k=1}^{f} \frac{\prod_{j=k}^{f} \alpha_i^j}{V} {}^{v}t_i^k \sum_{p=1}^{V} \frac{{}^{p}t_i^k}{\|{}^{p}T_i\|^2} {}^{p}d_{x,i} \\
&= \sum_{v=1}^{V} {}^{v}d_{x,i} - \sum_{k=1}^{f} \frac{\beta^k}{V} \sum_{p=1}^{V} {}^{v}t_i^k \frac{{}^{p}t_i^k}{\|{}^{p}T_i\|^2} {}^{p}d_{x,i} \\
&= \sum_{v=1}^{V} {}^{v}d_{x,i} - \sum_{p=1}^{V} \frac{1}{V\|{}^{p}T_i\|^2} \sum_{k=1}^{f} \beta^k ({}^{v}t_i^k)({}^{p}t_i^k) {}^{p}d_{x,i}. \qquad (164)
\end{aligned}
$$

We denote $\|\underline{T_i}\| = \min_p \|{}^{p}T_i\|$, $\|\bar{T_i}\| = \max_p \|{}^{p}T_i\|$, $0 < \underline{\beta} = \min_k \beta^k$, $\bar{\beta} = \max_k \beta^k \leq 1$, $0 <^{v} \underline{t}_i = \min_k {}^{v}t_i^k$, ${}^{v}\bar{t}_i = \max_k {}^{v}t_i^k \leq \frac{\Delta}{V_y}$ and n the total number of cells in one column. As $y^f = \sum_{k=1}^{f} t_i^k V_y = n\Delta$, $\sum_{k=1}^{f} t_i^k = \frac{n\Delta}{V_y}$ holds.

$$
\begin{aligned}
&\sum_{v=1}^{V} {}^{v}d_{x,i} - \sum_{p=1}^{V} \frac{\bar{\beta}\bar{t_i^k}}{V\|\underline{T_i}\|^2} \sum_{k=1}^{f} {}^{p}t_i^{kp} d_{x,i} \leq E_{x,i+1} \leq \sum_{v=1}^{V} {}^{v}d_{x,i} - \sum_{p=1}^{V} \frac{\underline{\beta}\underline{t_i^k}}{V\|\bar{T_i}\|^2} \sum_{k=1}^{f} {}^{p}t_i^{kp} d_{x,i} \\
&\sum_{v=1}^{V} {}^{v}d_{x,i} - \sum_{p=1}^{V} \frac{\bar{\beta}\bar{t_i^k}}{V\|\underline{T_i}\|^2} \frac{n\Delta}{V_y} {}^{p}d_{x,i} \leq E_{x,i+1} \leq \sum_{v=1}^{V} {}^{v}d_{x,i} - \sum_{p=1}^{V} \frac{\underline{\beta}\underline{t_i^k}}{V\|\bar{T_i}\|^2} \frac{n\Delta}{V_y} {}^{p}d_{x,i} \\
&\sum_{v=1}^{V} (1 - \frac{\bar{\beta}\bar{t_i}}{V\|\underline{T_i}\|^2} \frac{n\Delta}{V_y})^{v} d_{x,i} \leq E_{x,i+1} \leq \sum_{v=1}^{V} (1 - \frac{\underline{\beta}\underline{t_i}}{V\|\bar{T_i}\|^2} \frac{n\Delta}{V_y})^{v} d_{x,i}. \qquad (165)
\end{aligned}
$$

Furthermore, we know the traced trajectory AUV includes either vertical cell crossing, case 1 of trajectory tracing, such that $t^k = \frac{\Delta}{V_y}$ or two successive crossings that combine case 2 and 3, such that $t^k + t^{k+1} = \frac{\Delta}{V_y}$. While the first case is distinguished by a constant travel time $\frac{\Delta}{V_y}$, the sum of the square of travel time in the second and third case is varying.

Let us consider the minimum of $(t^k)^2 + (t^{k+1})^2 = (\frac{u}{V_y})^2 + (\frac{\Delta - u}{V_y})^2$. As $u = \frac{\Delta}{2V_y}$ is the root of $\frac{\partial (\frac{u}{V_y})^2 + (\frac{\Delta - u}{V_y})^2}{\partial u} = 2\frac{2u}{V_y} - 2\frac{\Delta}{V_y}$, then $u = \frac{\Delta}{2V_y}$ is the minimum.

Thus $\frac{1}{2}(\frac{\Delta}{V_y})^2 \leq (t^k)^2 + (t^{k+1})^2 \leq (\frac{\Delta}{V_y})^2$ is true $\forall i$. Accounting for $V_y \geq V_x$, then the traced trajectory includes at least $z \geq \frac{n}{2}$ vertical crossings and the rest comprises case 2 ad case 3. Let $\|T_i\|^2 = \sum_{k=1}^{f} t_i^{k2}$ and applying the discussed properties leads to:

$$
\begin{aligned}
\frac{n}{2}(1 + \frac{1}{2}) \frac{\Delta}{V_y}^2 &\leq \|T_i\|^2 \leq n \frac{\Delta}{V_y}^2 \\
\frac{3n}{4} \frac{\Delta}{V_y}^2 &\leq \|T_i\|^2 \leq n \frac{\Delta}{V_y}^2 . \qquad (166)
\end{aligned}
$$

Thus,

$$(1-\frac{\bar{\beta}\bar{t_i}}{V\|\underline{T}_i\|^2}\frac{nV_y}{\Delta})E_{x,i} \leq E_{x,i+1} \leq (1-\frac{\underline{\beta}\underline{t}_i}{V\|\bar{T}_i\|^2}\frac{nV_y}{\Delta})E_{x,i}$$
$$(1-\frac{4\bar{\beta}\bar{t}_i}{V3}\frac{V_y}{\Delta})E_{x,i} \leq E_{x,i+1} \leq (1-\frac{\underline{\beta}\underline{t}_i}{V}\frac{V_y}{\Delta})E_{x,i}. \tag{167}$$

Plugging $\bar{\beta}=1$, $\bar{t}_i=\frac{\Delta}{V_y}$ and $0<\kappa=\underline{\beta}\underline{t}_i\frac{V_y}{\Delta}\leq 1$ yields:

$$(1-\frac{4}{3V})E_{x,i} \leq E_{x,i+1} \leq (1-\frac{\underline{\beta}\underline{t}_i}{V})E_{x,i}$$
$$(1-\frac{4}{3V})E_{x,i} \leq E_{x,i+1} \leq (1-\frac{\kappa}{V})E_{x,i}$$
$$\underline{m}E_{x,i} \leq E_{x,i+1} \leq \bar{m}E_{x,i}$$
$$\|E_{x,i}\| \leq \bar{m}^i E_{x,0}, \tag{168}$$

where $0<\underline{m}=(1-\frac{4}{3V})<1$ and $\underline{m}\leq\bar{m}=1-\frac{\kappa}{V}<1$. Hence, $\underline{m}E_{x,i}\leq E_{x,i+1}\leq \bar{m}E_{x,i}$ implies that $\|E_{x,i}\|$ is monotone decreasing such that: $E_{x,i}\to 0$, when $i\to\infty$. Furthermore, $\underline{m}E_{x,i}\leq E_{x,i+1}\leq\bar{m}E_{x,i}$ and $0<\underline{m}\leq\bar{m}$ results in $E_{x,i}$ and $E_{x,i+1}$ have the same sign. Hence, $0\leq E_{x,0}$ implies $0\leq E_{x,i+1}$. □

Adding to $E_{x,i}=\sum_{v=1}^{V}{}^{v}d_{x_i}$ we denote $\tilde{E}_{x,i}=E_{x,i}-{}^{V}d_{x,i}$ and derive new lemma, which we will use for the analysis later.

Lemma 5.3.3. *Let the traced trajectory be formulated according to (144). Suppose Assumptions 3.1.1, 5.3.1, V is the number of AUVS, ${}^{V}d_{x,0}>0$ and ${}^{v}d_{x,0}=0$ $\forall 1\leq v<V-1$ hold, then the following results hold*

- ${}^{V}d_{x,i}\geq 0$ *and* ${}^{V}d_{x,i}\geq^{V} d_{x,i+1}$
- $\sum_{v=1}^{V-1}{}^{v}d_{x,i}\leq 0$ *and* $\sum_{v=1}^{V-1}{}^{v}d_{x,i}\leq\sum_{v=1}^{V-1}{}^{v}d_{x,i+1}$ $\forall i>0$

Proof. In this proof we extend the claim and use the Induction method for the following recursions:

- ${}^{V}d_{x,i}\geq^{V} d_{x,i+1}\geq 0$

- $\sum_{v=1}^{V-1} {}^{v}d_{x,i} \leq 0 \ \forall i \geq 0$
- ${}^{V}d_{x,i} \leq (1+V)\|\tilde{E}_{x,i}\| \ \forall i > 1$

Let us consider the flow update and apply ${}^{V}d_{x,0} > 0$ and ${}^{v}d_{x,0} = 0 \ \forall 1 \leq v < V-1$, Since the flow along x-axis is initially null we have:

$$F_{x,1}^{k} = F_{x,0}^{k} + \sum_{v=1}^{V-1} \frac{{}^{v}t_i^k}{V\|{}^{v}T_i\|^2} {}^{v}d_{x,0} + \frac{{}^{V}t_i^k}{V\|{}^{V}T_i\|^2} {}^{V}d_{x,0} = \frac{{}^{V}t_i^k}{V\|{}^{V}T_i\|^2} {}^{V}d_{x,0}. \tag{169}$$

As the column that the AUV V crosses for the first time at iteration $i = 1$ is initially zero, the flow is null in ${}^{V}\mathcal{C}\backslash{}^{V}\mathcal{C}_0 \cap {}^{V-1}\mathcal{C}_0$. Adding to that $0 < \frac{{}^{V}t_i^k}{V\|{}^{V}T_i\|^2} {}^{V}d_{x,0} < \frac{{}^{V}t_i^k}{\|{}^{V}T_i\|^2} {}^{V}d_{x,0}$, then ${}^{V}x_1^f <^{V} x^*$ which means ${}^{V}d_{x,0} >^{V} d_{x,1} \geq 0$.

Concerning the other AUVs, as $F_{x,0}^k$ guarantees ${}^{v}x_1^f =^{v} x^* \ \forall 1 \leq v < V$ and $F_{x,0}^k \leq F_{x,1}^k$, then ${}^{v}x_1^f \geq^{v} x^* \ \forall 1 \leq v < V$, ${}^{v}d_{x,1} \leq 0 \ \forall 1 \leq v < V$. Suppose that for $i = n$, the claim holds and there exists $V_1 > v \geq 0$ AUVs such that ${}^{v}d_{x,i} \geq 0$ and $V_1 \leq v \leq V-1$ AUVs such that ${}^{v}d_{x,i} \leq 0$, and let us prove the validity of the claim for $i = n+1$. We reformulate the error dynamics:

$$\begin{aligned} {}^{V}d_{x,n+1} &=^{V} d_{x,n} - \sum_{k=1}^{f}\prod_{j=k}^{f} \alpha_{n+1}^{j} \Big(\sum_{p=1}^{V} \frac{{}^{V}t_n^{kp}t_n^k}{V\|{}^{p}T_n\|^2} {}^{p}d_{x,n}\Big) \\ &=^{V} d_{x,n} - \frac{1}{V}\Big(\sum_{p=1}^{V_1} {}^{Vp}\underline{\kappa}_n {}^{p}d_{x,n} + \sum_{p=V_1}^{V-1} {}^{Vp}\bar{\kappa}_n {}^{p}d_{x,n} + {}^{V}\kappa_n {}^{V}d_{x,n}\Big), \end{aligned} \tag{170}$$

where ${}^{V}\kappa_n = \sum_{k=1}^{f}\prod_{j=k}^{f} \alpha_{n+1}^{j}(\frac{{}^{V}t_n^{k\,2}}{V\|{}^{V}T_n\|^2})$, $\underline{\kappa}_n = \sum_{k=1}^{f}\prod_{j=k}^{f} \alpha_{n+1}^{j}(\frac{{}^{V}t_n^{kp}t_n^k}{V\|{}^{p}T_n\|^2}) \ \forall 1 \leq p \leq V_1$ and $\bar{\kappa}_n = \sum_{k=1}^{f}\prod_{j=k}^{f} \alpha_{n+1}^{j}(l_{n+1}^k \frac{{}^{V}t_n^{kp}t_n^k}{V\|{}^{p}T_n\|^2}) \ \forall V_1 - 1 \leq p \leq V-1$.

Since all AUVs cross the same set of cells and $E_{x,n} = \sum_{p=1}^{V} {}^{p}d_{x,n} \geq 0$, Lemma 5.3.1 implies:

$$\sum_{k=1}^{f}\prod_{j=k}^{f} \alpha_{n+1}^{j}\Big(\frac{{}^{V}t_n^{kp}t_n^k}{V\|{}^{p}T_n\|^2}^{p+1} d_{x,n}\Big) \geq \sum_{k=1}^{f}\prod_{j=k}^{f} \alpha_{n+1}^{j}\Big(\frac{{}^{V}t_n^{kp}t_n^k}{V\|{}^{p}T_n\|^2}^{p} d_{x,n}\Big). \tag{171}$$

Hence we deduce $\underline{\kappa}_n \leq \bar{\kappa}_n \leq {}^{V}\kappa_n \leq 1$. Adding to that, the induction recursion ensures that $\tilde{E}_{x,i} \leq 0$, which means $\sum_{p=1}^{V_1-1} \|{}^{p}d_{x,n}\| \leq \sum_{p=V_1}^{V-1} \|{}^{p}d_{x,n}\|$. Based on the

above reasons, we insert $\tilde{E}_{x,n} = \sum_{p=1}^{V-1} {}^{p}d_{x,n} \leq 0$ to get a lower bound for ${}^{V}d_{x,n+1}$:

$$\begin{aligned}
{}^{V}d_{x,n+1} &=^{V} d_{x,n} - \frac{1}{V}(\sum_{p=1}^{V_1} {}^{Vp}\underline{\kappa}_n{}^{p}d_{x,n} + \sum_{p=V_1}^{V-1} {}^{Vp}\bar{\kappa}_n{}^{p}d_{x,n} + {}^{V}\kappa_n{}^{V}d_{x,n}) \\
&\geq^{V} d_{x,n} - \frac{1}{V}(\sum_{p=1}^{V-1} {}^{Vp}\underline{\kappa}_n{}^{p}d_{x,n} + {}^{V}\kappa_n{}^{V}d_{x,n}) \\
&\geq^{V} d_{x,n} - \frac{{}^{V}\kappa_n}{V}{}^{V}d_{x,n} \geq (1 - \frac{1}{V})^{V}d_{x,n}. \qquad (172)
\end{aligned}$$

And we plug $E_{x,n} \geq 0$ to get an upper bound for ${}^{V}d_{x,n+1}$:

$$\begin{aligned}
{}^{V}d_{x,n+1} &=^{V} d_{x,n} - \frac{1}{V}(\sum_{p=1}^{V_1} {}^{Vp}\underline{\kappa}_n{}^{p}d_{x,n} + \sum_{p=V_1}^{V-1} {}^{Vp}\bar{\kappa}_n{}^{p}d_{x,n} + {}^{V}\kappa_n{}^{V}d_{x,n}) \\
&\leq^{V} d_{x,n} - \frac{1}{V}(\sum_{p=1}^{V-1} {}^{Vp}\bar{\kappa}_n{}^{p}d_{x,n} + {}^{V}\kappa_n{}^{V}d_{x,n}) \\
&\leq^{V} d_{x,n} - \frac{1}{V}({}^{Vp}\bar{\kappa}_n\tilde{E}_{x,n} + {}^{V}\kappa_n{}^{V}d_{x,n}) \\
&\leq^{V} d_{x,n} - \frac{1}{V}({}^{V}\kappa_n\tilde{E}_{x,n} + {}^{V}\kappa_n{}^{V}d_{x,n}) \\
&\leq^{V} d_{x,n} - \frac{1}{V}{}^{V}\kappa_n E_{x,n} \leq^{V} d_{x,n}. \qquad (173)
\end{aligned}$$

Hence, ${}^{V}d_{x,n} \geq^{V} d_{x,n+1} \geq 0$, first part of the Lemma is valid. Furthermore, combining both inequalities (168) and (172), then it follows that:

$$\begin{aligned}
E_{x,n+1} &\leq (1 - \frac{\kappa}{V})E_{x,n} \\
{}^{V}d_{x,n+1} + \tilde{E}_{x,n+1} &\leq (1 - \frac{\kappa}{V})({}^{V}d_{x,n} + \tilde{E}_{x,n}) \\
\tilde{E}_{x,n+1} &\leq (\frac{1}{V} - \frac{\kappa}{V})({}^{V}d_{x,n}) + (1 - \frac{\kappa}{V})\tilde{E}_{x,n} - {}^{V}d_{x,n+1} \\
&\leq (1 - \frac{\kappa}{V})({}^{V}d_{x,n} + \tilde{E}_{x,n}) \\
&\leq \frac{1}{V}{}^{V}\kappa_n E_{x,n} + (1 - \frac{\kappa}{V})({}^{V}d_{x,n} + \tilde{E}_{x,n}) \\
&\leq \frac{{}^{V}\kappa_n - \kappa}{V}{}^{V}d_{x,n} + (1 + \frac{{}^{V}\kappa_n - \kappa}{V})(\tilde{E}_{x,n}) \\
&\leq \frac{1}{V}{}^{V}d_{x,n} + (1 + \frac{1}{V})(\tilde{E}_{x,n}). \qquad (174)
\end{aligned}$$

We use ${}^{V}d_{x,n} \leq (1 + V)\|\tilde{E}_{x,n}\|$, the third induction statement:

$$\tilde{E}_{x,n+1} \leq \frac{1}{V}{}^{V}d_{x,n} + (1 + \frac{1}{V})(\tilde{E}_{x,n}) \leq 0. \qquad (175)$$

Hence, $\tilde{E}_{x,n} \leq 0$ is satisfied as well. Finally we confirm the last part of claim ${}^{V}d_{x,n} \leq (1+V)\|\tilde{E}_{x,n}\|$ by using Lemma (5.3.2) and $V > 1$:

$$\begin{aligned}
E_{x,n+1} &\leq E_{x,n} \\
{}^{V}d_{x,n+1} &\leq -\tilde{E}_{x,n+1} + E_{x,n} \\
{}^{V}d_{x,n+1} &\leq -\tilde{E}_{x,n+1} + (\tilde{E}_{x,n} + {}^{V}d_{x,n}) \\
{}^{V}d_{x,n+1} &\leq -\tilde{E}_{x,n+1} + \frac{V}{1+V}{}^{V}d_{x,n} \\
{}^{V}d_{x,n+1} &\leq -\tilde{E}_{x,n+1} + \frac{V}{1+V}{}^{V}d_{x,n}. \qquad (176)
\end{aligned}$$

Applying $(1-\frac{1}{V}){}^{V}d_{x,n} \leq {}^{V}d_{x,n+1}$ results in:

$$\begin{aligned}
\frac{V-1}{V(1+V)}{}^{V}d_{x,n} &\leq \|\tilde{E}_{x,n+1}\| \\
{}^{V}d_{x,n+1} &\leq (1+V)\|\tilde{E}_{x,n+1}\|. \qquad (177)
\end{aligned}$$

□

Based on Lemma 5.3.3, we show the convergence of one axis MTCC algorithm in the following theorem.

Theorem 5.3.1. *Let the traced trajectory be formulated according to (144). Suppose Assumptions 3.1.1, 5.3.1 and V is the number of AUVS, then the MT error ${}^{v}d_{x,i}$ converges to 0, as $i \to \infty$.*

Proof. We prove the theorem by Induction:
Let the number of AUV be one, $V = 1$ then Theorem 3.3.1 implies that ${}^{1}d_{x,i}$ converges to 0, as $i \to \infty$. Hence the statement is initially valid.
Suppose that for $V = n$ $\forall v, 1 \leq v \leq n$ ${}^{v}d_{x,i}$ converges to 0, as $i \to \infty$ and let us prove for $V = n+1$ $\forall v, 1 \leq v \leq n+1$ ${}^{v}d_{x,i}$ converges to 0, as $i \to \infty$.
Let ${}^{n+1}\mathcal{C}_0$ be the set of crossed cells by AUV $n+1$ and ${}^{n+1}r^0$ its initial position such that ${}^{n+1}r^0 > {}^{n}r^0$. Since the traced trajectories are parallel inside the cells and the

velocity along x-axis is positive, the end position of AUV $n+1$ satisfies the inequality ${}^{n+1}r_i^k \geq^v r_i^k \; \forall 1 \leq v \leq n$. Hence, ${}^{n+1}\mathcal{C}_i \cap^v \mathcal{C}_i =^{n+1} \mathcal{C}_i \cap^n \mathcal{C}_i \; \forall 1 \leq v \leq n$.

Suppose ${}^{n+1}\mathcal{C}_0 \cap {}^n\mathcal{C}_0 = \emptyset$ and as the velocity along x-axis is positive, then the AUV $n+1$ does not cross the cells $C^k \in {}^v\mathcal{C}_i \; \forall 1 \leq v \leq n$. Consequently, the flow in $C^k \in^v \mathcal{C}_i$ remains constant such that $F_{x,i} = F_{x,0}$ and ${}^v dx,i = 0 \; \forall 1 \leq v \leq n$. Concerning the AUV $n+1$, Theorem 3.3.1 implies that ${}^1d_{x,i}$ converges to 0, as $i \to \infty$. Hence the statement is valid.

If the cell C^k is crossed only by one AUV v, we showed in Chapter 4 that the flow F_x^k will be updated such that the MT error ${}^v d$ decreases. However, if multiple vehicles cross the same cell, at least the MT error of one vehicle can increase, see the aforementioned Example 5.3.1. Therefore, the worst case is when ${}^v\mathcal{C}_i =^{n+1} \mathcal{C}_i \; \forall 1 \leq v \leq n$. We will show that the MT error converges also when all the cells are crossed between the AUVs.

Based on Lemma 5.3.3, ${}^V d_{x,i} \geq 0$ and ${}^V d_{x,i+1} \leq^V d_{x,i}$. Hence the MT error is decreasing or constant. Let us suppose that ${}^V d_{x,i} =^V d_{x,j}$, $j \leq i$, and since $E_{x,i}$ converges to zero, then $\tilde{E}_{x,i} \to -{}^V d_{x,j}$ and the resulted flow is constant along the crossed cells ${}^V\mathcal{C}_i$. However, if the flow keeps increasing (or decreasing) at least in one cell the associated AUV will leave the cell from new direction. As ${}^V d_{x,i} > 0$ the flow will increase at least in one cell such that after couple of iterations K, ${}^V\mathcal{C}_i \neq^V \mathcal{C}_{i+K}$.

Since AUV position ${}^V r^0 >^v r^0 \; \forall v$, the cells ${}^V\mathcal{C}_{i+K} \setminus {}^V\mathcal{C}_i \cap^V \mathcal{C}_{i+K}$ are only updated by AUV V resulting in decrease of ${}^V d_{x,i}$. The reciprocal effect is that the norm of $\tilde{E}_{x,i}$ will decrease as well because $\|E_{x,i}\| = \|{}^V d_{x,i} + \tilde{E}_{x,i}\|$ is decreasing. Hence, the MT error of all AUVs will converge to zero.

Concerning the case that the flow remains constant in all cells C^k in ${}^V\mathcal{C}_i$ requires:

$$\sum_{v=V}^{1} \frac{{}^v t_i^k}{V \|{}^v T_i\|^2} {}^v d_i = 0. \tag{178}$$

However Lemma 5.3.1 implies ${}^V t_i^k$ is the maximum and then the minimum in two consecutive cells. Let ${}^V t_i^j$ be the maximum travel time in cell C^j, then ${}^v t_i^j <^{V-1} t_i^j <$

${}^{V}t_i^j \ \forall 1 \leq v < V$ and $\sum_{v=1}^{V} \frac{{}^{v}t_i^k}{V\|{}^{v}T_i\|^2} {}^{v}d_i = 0$ leads to:

$$\|{}^{V}d_i\| \leq \frac{{}^{V-1}t_i^j}{{}^{V}t_i^j} \| \sum_{v=1}^{V-1} {}^{v}d_{x,i} \| < \|\tilde{E}_{x,i}\| \tag{179a}$$

$$\|{}^{V}d_i\| \geq \frac{{}^{V-1}t_i^{j+1}}{{}^{V}t_i^{j+1}} \| \sum_{v=1}^{V-1} {}^{v}d_{x,i} \| > \|\tilde{E}_{x,i}\|. \tag{179b}$$

Since (179a) does not contradict (179b), if ${}^{V}d_i = 0$ $\tilde{E}_{x,i} = 0$ or if $\|{}^{V}d_i\| - \|\tilde{E}_{x,i}\| = 0$ and the travel time of all AUVs is overall equal. Hence ${}^{V}\mathcal{C}_i$ is one column such that ${}^{V}t_i^j = {}^{v}t_i^j = \frac{\Delta}{V_y} \ \forall 1 \leq v < V$ However, the MT errors have different signs which contradicts again the parallelism principle. Based on the above analysis, we deduce that ${}^{V}d_{x,i}$ is decreasing and ${}^{V}d_{x,i} \geq 0$. Hence ${}^{V}d_{x,i}$ converges to zero. Adding to that $\tilde{E}_{x,i} = E_{x,i} - {}^{V} d_{x,i} \to 0$ for $i \to \infty$.

Since $\tilde{E}_{x,i}$ involves only $V-1$ AUVs and the induction claim holds for $V-1$ AUVs, then the MT error ${}^{v}d_{x,i}$ converges $\forall 1 \leq v < V$. Hence the MT error is overall decreasing. This completes the proof. □

5.3.2 Simulations and Results of one Dimension MTCC

We simulate multiple vehicles that navigate under flow in a domain of interest and implement the proposed MTCC method to construct a trajectory that fulfills the final time and position constraint and accordingly estimate the underlying flow field. We raise the challenge by subjecting the mapping to strongly discontinuous flow and a limited number of vehicles. We randomly generate flow field with different directions and speeds that varies between $0.35m/s$ and $2.5m/s$. The maximum flow strength is located in the center and equal to the AUV control velocity which is $3m/s$.

For better understanding, we simulate the one dimension flow field mapping, which requires the AUV departure from one desired axis e.g. the X-axis. This enables us to understand the theoretical analysis discussed in previous section. We use 9 AUVS so that we increase the intersections between the traced trajectories and we apply MTCC algorithm, without incorporating traveling time. While the distribution of

blue dashed arrows in Figure 17a shows the evolution of the simulated flow field that covers all the cells, Figure 17b depicts the final trajectories which converge to the measured positions. Following the traced trajectories, we can identify the estimated flow that leads to the convergence of MT error. Obviously, the Y-component F_y is zero, see Figure 17a because the underlying algorithm MT algorithm in this scenario is only subject to MT error along the X-axis. Incorporating traveling time in the second case provides a considerable improvement as illustrated in Figure 18a. The second constraint raises the blue arrows to present the estimated flow in Y direction, such that the AUV velocity is updated in two dimensions. Although this fact is not reflected on traced trajectory, Figures 18b and 17b are identical, there is a noticeable difference in the estimated flow between Figures 18a and 17a.

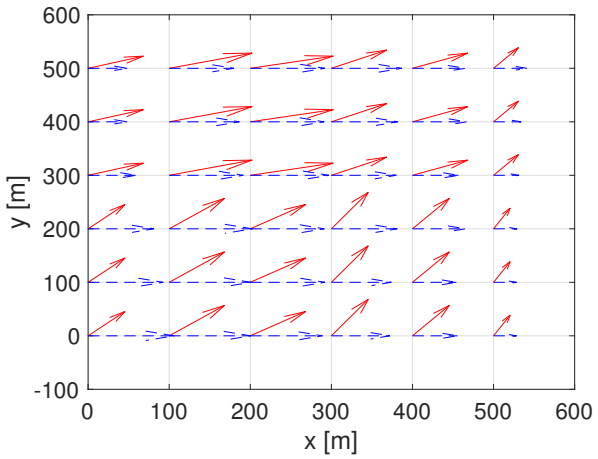

(a) Estimated and true Flow field mapping

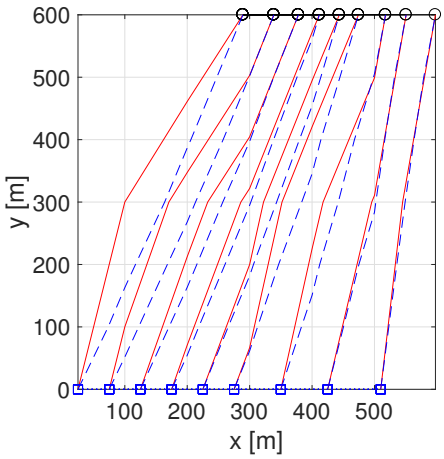

(b) Estimated and true traced trajectories

Figure 17: One axis MTCC without travel time incorporation.

5.4 Convergence Analysis of MTCC and Simulation Results

5.4.1 Convergence Analysis of MTCC

After studying the one axis case, we analyze the convergence of MTCC algorithm, where we place vehicles on both Axis to provide two dimensions flow field mapping.

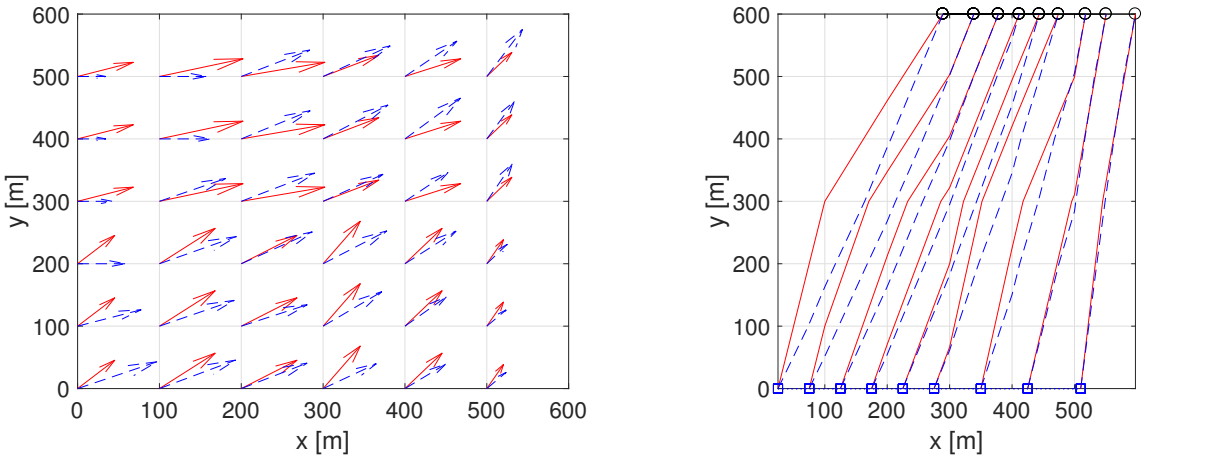

(a) Estimated and true Flow field mapping (b) Estimated and true traced trajectories

Figure 18: One axis MTCC with travel time incorporation.

Hence, the algorithm updates both F_y and F_x, which requires an extension of Assumption (3.3.1).

Assumption 5.4.1. *We assume that for AUVs that their initial position* $r^0 = [x^0, 0]^\top$ *the velocity* $S_x = 0$, $S_y > F_x^k \geq 0$, $r^* = [x^*, L]^\top$, *and* $x^* \geq x^0$
and for AUVs that their initial position $r^0 = [0, y^0]^\top$ *the velocity* $S_y = 0$, $S_x > F_y^k \geq 0$, $r^* = [L, y^*]^\top$, *and* $y^* \geq y^0$

One major problem in convergence analysis, as shown in Chapter 3 is coefficient $\beta_i^k = 1 - \prod_{j=k}^{f} \alpha_i^j$ involved in MT error dynamics. The possible increase of α_i^j, when the AUV crosses the cell in horizontal way, can cause an overshoot of MT error. For better understanding, let us state the definition of α_i^j as follows:

$$\alpha_i^j = \begin{cases} 1 & \text{if} \quad y_i^j - y_i^{j-1} = \Delta \cup x_i^j - x_i^{j-1} = \Delta \\ \frac{V_{y,i}^j}{V_{x,i}^j} & \text{if} \quad y_i^j = h\Delta \cap x_i^{j-1} = s\Delta \\ \frac{V_{x,i}^j}{V_{y,i}^j} & \text{otherwise} \end{cases} \tag{180}$$

For clarity, we refer to crossing consecutive sides from one cell, see Figure 6 case 2, as horizontal transition. Since we restricted the scope on one axis flow field mapping,

the velocity in $y-$ direction was equal to the control velocity $V_y = S_y$, which allows to simplify $\frac{V^j_{x,i}}{V^j_{y,i}} \frac{V^{j-1}_{y,i}}{V^{j-1}_{x,i}} = \frac{V^j_{x,i}}{V^{j-1}_{x,i}}$. Considering the two dimension flow field mapping, the simplification does not hold because $V^j_{y,i}$ varies from one cell to another. This fact urges to reconsider the MT convergence without assuming a constant flow F_y. However, Assumption 5.4.1 implies:

$$\begin{aligned} \frac{V^{j-1}_{y,i}}{V^j_{y,i}} &= \frac{S_y + F^{j-1}_{y,i}}{S_y + F^{j-1}_{y,i}}, \\ &\leq \frac{S_y + F_{max}}{S_y} \leq 2. \end{aligned} \tag{181}$$

Since $\frac{V_{y,i}{}^{j-1}}{V^j_{y,i}} \leq 2$ holds, we need to study the variation of α^k_i under the influence of $\frac{V_{y,i}{}^{j-1}}{V^j_{y,i}}$ and accordingly to ensure that the MT error $d_{x,i}$ decreases. We showed in Chapter 3 that when the AUV crosses new column, the flow along X-axis increases in previous columns, making the AUV change the crossed set of cells. Hence, the AUV enters new cells before it reaches the final position under the influence of flow update. Recalling the expression of α^k_i, we can reformulate it as follows:

$$\alpha^k_i = \prod_{j=k}^{L} \frac{V^j_{x,i}}{V^j_{y,i}} \frac{V^{j-1}_{y,i}}{V^{j-1}_{x,i}}, \tag{182}$$

where L is the last column crossed by the AUV and j denotes the first crossed cell in every column starting from column k. Thus, crossing successive columns, where the flow along X-axis is initially zero, $V_x = 0$, implies a sink of the traced trajectory and accordingly $\alpha^k_i = \prod_{j=k}^{L} \frac{V^j_{x,i}}{V^j_{y,i}} \frac{V^{j-1}_{y,i}}{V^{j-1}_{x,i}} = 0$. Hence, we can consider entering new cell in horizontal way as a decrease or reset to α^k_i as cell C^L is updated after the previous ones, see Chapter 3 for further explanation. Now when the AUV reaches the final column, the MT error shrinks and the frequency to explore new cell decreases. Hence, if the traced trajectory keeps evolving in the same consecutive cells that have the same ordinate, it is still to confirm that α^k_i remains less than 2. However this condition is conservative: The error dynamics is the sum of update parts along the traced

trajectory:

$$d_{x,i} = \sum_{k=1}^{f} (1 - \prod_{j=k}^{f} \alpha_i^j) \frac{t_{i-1}^{k2}}{\|T_{i-1}\|^2} d_{x,i-1}. \tag{183}$$

If only one cell has $\alpha_i^1 > 2$, but $\alpha_i^k \leq 1$ in the other cells, the MT error still decreases. Therefore, we will focus on the convergence of MT error and not on the condition $\alpha_i^k < 2$. Before considering the general case, we want to introduce a key feature of the predicted flow map that we will exploit it later for the convergence analysis. Based on the flow distribution property, we study the convergence of MT error without assuming constant flow F_y in the following Lemma:

Lemma 5.4.1. *Let the traced trajectory be formulated according to Algorithm 2. Suppose Assumptions 3.1.1 and 5.4.1 hold, then the MT error $d_{x,i}$ converges to 0 as $i \to \infty$.*

Proof. It is to notice that the following error dynamic is valid for $\mathcal{C}_i = \mathcal{C}_{i-1}$:

$$d_{x,i} = \sum_{k=1}^{f} (1 - \prod_{j=k}^{f} \alpha_i^j) \frac{t_{i-1}^{k2}}{\|T_{i-1}\|^2} d_{x,i-1}. \tag{184}$$

and nonlinear. Hence, we need to deal with two possible cases.

For the first scenario is when $d_{x,i} \geq 0 \; \forall i > 0$, we use the derived analysis from Chapter 3. The first part of Proof 3.3 of Theorem 3.3.1 shows as long as $d_{x,i} \geq 0$, the MT error is decreasing for any embedded α. And since the flow is initially zero, whenever the AUV enters new cell $d_{x,i} \geq 0$. Therefore, if $d_{x,i} \geq 0 \; \forall i > 0$ the MT error decreases when it enters new cells or when $\mathcal{C}_i$ is constant.

Since the MT error is initially positive, the second scenario is when $d_{x,t} \geq 0 \; \forall t > 0$ and then $d_{x,t+1} < 0$. Recalling if $d_{x,t} \geq 0 \; \forall t > 0$, then the AUV traced trajectory deviates in the clockwise rotation, due to the flow increase. This means, the new embedded cells are not updated by the MT algorithm. In this case The second part of Proof 3.3 allows us to consider the new crossed cells as equivalent for the previous

crossed set of cells. Since the new embedded ones have null value, we can apply the error dynamics piece wise and simplify the calculation when the flow is zero. Hence, this case is considered as a special case of the final scenario that we will consider now: $\mathcal{C}_i = \mathcal{C}_t$, $\forall i \leq t \leq h$ and $\|d_{x,t}\|$ is decreasing till $\|d_{x,h}\| \geq \|d_{x,h-1}\|$. This result stems from the increase of α_i^k in some cells. Suppose w.l.o.g. that $d_{x,h-1} > 0$ and $d_{x,h} < 0$ and $\|T_{h-1}\|^2 \approx \|T_h\|^2$, as $\mathcal{C}_h = \mathcal{C}_{h-1}$. Let us consider the cells where $\frac{V_y^{j-1}}{V_y^j} > 1$ and we can write $d_{x,h} = -(d_{x,h-1} + \lambda_h)$, $\lambda_h > 0$.

$$\begin{aligned}
\alpha_{h+1}^k &= \prod_{j=k}^{L} \frac{V_{x,h+1}^j}{V_{x,h+1}^{j-1}} \frac{V_y^{j-1}}{V_y^j} \\
&= \prod_{j=k}^{L} \frac{V_y^{j-1}}{V_y^j} \frac{V_{x,h-1}^j + \frac{t_{h-1}^j}{\|T_{h-1}\|^2} d_{x,h-1} + \frac{t_h^j}{\|T_h\|^2} d_{x_h}}{V_{x,h-1}^{j-1} + \frac{t_{h-1}^{j-1}}{\|T_{h-1}\|^2} d_{x,h-1} + \frac{t_h^{j-1}}{\|T_h\|^2} d_{x_h}} \\
&= \prod_{j=k}^{L} \frac{V_y^{j-1}}{V_y^j} \frac{V_{x,h-1}^j + \frac{t_{h-1}^j - t_h^j}{\|T_{h-1}\|^2} d_{x,h-1} - \frac{t_h^j \lambda_h}{\|T_{h-1}\|^2}}{V_{x,h-1}^{j-1} + \frac{t_{h-1}^{j-1} - t_h^{j-1}}{\|T_{h-1}\|^2} d_{x,h-1} - \frac{t_h^{j-1} \lambda_h}{\|T_{h-1}\|^2}}.
\end{aligned} \tag{185}$$

Let $C^{j-1} = C^{(h,s)}$. Based on the previous analysis, we know if $\alpha_{h-1}^{j-1} > 2$, then $t_h^{j-1} < t_h^j$. Furthermore, $d_{x,h-1} > 0$ and $d_{x,h} < 0$ implies that $y_{h-1}^{j-1} > y_h^{j-1}$ and $x_{h-1}^{j-2} < x_h^{j-2}$, see Figure 19. Therefore, while the travel time in cell C^{j-1} increases, it decreases in cell C^j such that $t_{h-1}^{j-1} - t_h^{j-1} > 0$ and $t_{h-1}^j - t_h^j < 0$ holds. Plugging the two results yields:

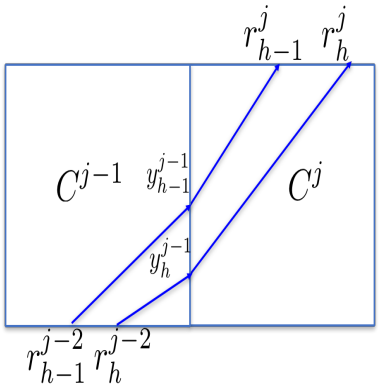

Figure 19: Illustration of trajectory tracing at iteration h and $h-1$.

$$\frac{t_{h-1}^{j-1} - t_h^{j-1}}{\|T_{h-1}\|^2} d_{x,h-1} - \frac{t_h^{j-1} \lambda_h}{\|T_{h-1}\|^2} > \frac{t_{h-1}^j - t_h^j}{\|T_{h-1}\|^2} d_{x,h-1} - \frac{t_h^j \lambda_h}{\|T_{h-1}\|^2}, \tag{186}$$

and consequently,

$$\alpha_{h+1}^k < \alpha_{h-1}^k < \alpha_h^k. \tag{187}$$

Since α_{h-1}^k leads to $\|d_{x,h-2}\| > \|d_{x,h-1}\|$, then $\|d_{x,h}\| > \|d_{x,h+1}\|$ holds. And whenever the MT error increases , α^k decreases until d_x converges.
Based on the aforementioned reasoning, we conclude that both cases lead to MT error convergence. □

While analyzing the mutual effect of multi vehicle trajectory tracing, we encountered a difficulty to determine the crossed cells if F_y and F_x are changing simultaneously. We redesigned MTCC Algorithm 4 to overcome the problem by updating the flow sequentially e.g. estimating F_x and then F_y. We repeat the same step until the MT error converges for all AUVs and we increment the iteration j after completing part 1 and 2. Let us denote $F_{x,j}$ the final solution after running part 1 and $F_{y,j}$ the final solution after running part 2. Moreover, we will define an average flow $\bar{F}$ such that $\bar{F}_x = \frac{\sum_{k=1}^{f} F_x^k}{f}$, $\bar{F}_y = \frac{\sum_{k=1}^{f} F_y^k}{f}$ and S the maximal control velocity. Finally, we state the main Theorem for this chapter:

Theorem 5.4.1. *Let the traced trajectory be formulated according to Algorithm 6. Suppose Assumptions 3.1.1, 5.4.1 hold and the average flow fulfills* $S/2 < \bar{F}_x, \bar{F}_y < S$, *then the MT error* ${}^v d_i$ *converges to* 0, $\forall v$ *as* $i \to \infty$.

Proof. Since Lemma 5.4.1 guarantees the convergence of one vehicle MT error, we can consider part 1 or 2 in Algorithm 6 separately and apply Theorem 5.3.1 to prove the convergence of the underlying part. Hence, we need to look in the overall algorithm typically the transition between the two parts. We focus on slope variation due to transition from part 1 to part 2. As initially $F_y = 0$ and the real flow $F_y^* \geq 0$, part 2 will lead to increase in $F_{y,j}$ which implies a retreat of final estimated position ${}^v x^f$ for AUVs placed on X-axis. In other terms, we have ${}^v x^f \leq^v x^*$ and MT error ${}^v d_x \geq 0$

$\forall 1 \leq v \leq V_x$. Therefore, running part 1 results in increase of $F_{x,j}$. Following the same reasoning and because of symmetry, $F_{x,j}$ and $F_{y,j}$ are increasing between part 1 and 2, which results in drift $\Delta^k_{y,j}$ and $\Delta^k_{x,j}$ from the solution trajectory in crossed cells.

Let us consider the slope after part 1 $\frac{S_y+F^k_{y,j-1}}{F^k_{x,j}}$ and after part 2 $\frac{S_y+F^k_{y,j}}{F^k_{x,j}}$ at iteration j and the slope$\frac{S_y+F^k_{y,j-1}}{F^k_{x,j-1}}$ at iteration $j-1$, then the drift $\Delta^k_{x,j}$ is defined as follows:

$$\begin{aligned}\Delta^k_{x,j} &= \Delta\frac{F^k_{x,j}}{S_y+F^k_{y,j-1}} - \Delta\frac{F^k_{x,j-1}}{S_y+F^k_{y,j-1}} \\ &= \Delta\frac{F^k_{x,j}-F^k_{x,j-1}}{S_y+F^k_{y,j-1}}.\end{aligned} \tag{188}$$

We can substitute $\frac{F^k_{y,j-1}}{S_x+F^k_{x,j-1}} = \frac{F^k_{y,j}}{S_x+F^k_{x,j}}$ to describe the drift $\Delta^k_{y,j}$ as follows:

$$\begin{aligned}\Delta^k_{y,j} &= \Delta\frac{F^k_{y,j}}{S_x+F^k_{x,j}} - \Delta\frac{F^k_{y,j-1}}{S_x+F^k_{x,j}} \\ &= \Delta\frac{F^k_{y,j-1}}{S_x+F^k_{x,j-1}} - \Delta\frac{F^k_{y,j-1}}{S_x+F^k_{x,j}} \\ &= \Delta\frac{F^k_{y,j-1}(F^k_{x,j}-F^k_{x,j-1})}{(S_x+F^k_{x,j})(S_x+F^k_{x,j-1})}.\end{aligned} \tag{189}$$

Applying (188) yields:

$$\begin{aligned}\Delta^k_{y,j} &= \Delta^k_{x,j}\frac{F^k_{y,j-1}(S_y+F^k_{y,j})}{(S_x+F^k_{x,j})(S_x+F^k_{x,j-1})} \\ &= \Delta^k_{x,j}\frac{F^k_{y,j-1}(S_y+F^k_{y,j})}{(S_x+F^k_{x,j})(S_x+F^k_{x,j-1})}.\end{aligned} \tag{190}$$

We can consider the MT error as the sum of the drift along the traced trajectory:

$$^v d_{y,j} = \sum_{k=1}^{f} \Delta^k_{y,j}. \tag{191}$$

Since the flow is varying from one cell to another we can use the average flow $\bar{F}$ and according an average of MT error $\bar{d}$ as approximation of MT error d. As we assumed that $S_{y,x} > \bar{F}_{x,y} > (1/2)S_{y,x}$ hence:

$$^v \bar{d}_{y,j} = \sum_{k=1}^{f} \bar{\Delta}^k_{y,j}$$

$$
\begin{aligned}
&= \sum_{k=1}^{f} \bar{\Delta}_{x,j}^{k} \frac{\bar{F}_{y,j-1}^{k}(S_y + \bar{F}_{y,j}^{k})}{(S_x + \bar{F}_{x,j}^{k})(S_x + \bar{F}_{x,j-1}^{k})} \\
&\leq \sum_{k=1}^{f} \bar{\Delta}_{x,j}^{k} \frac{\bar{F}_y(S_y + \bar{F}_y)}{(S_x + \bar{F}_x)^2} \\
&< \sum_{k=1}^{f} \bar{\Delta}_{x,j}^{k} \frac{S_y(S_y + S_y)}{(S_x + (1/2)S_x)^2} \\
&< \sum_{k=1}^{f} \bar{\Delta}_{x,j}^{k} \frac{8}{9}. \qquad (192)
\end{aligned}
$$

This decrease in ${}^{v}\bar{d}_{y,j}$ occurs during the transition from part 1 to part 2. The same principle results in the decrease of ${}^{v}\bar{d}_{x,j}$ as well.

$$
\begin{aligned}
{}^{v}\bar{d}_{y,j} &< \frac{8}{9}{}^{v}\bar{d}_{x,j} \\
&< (\frac{8}{9})^2{}^{v}\bar{d}_{y,j-1}. \qquad (193)
\end{aligned}
$$

Hence, the average MT error ${}^{v}\bar{d}_{y,j}$ is decreasing. Since ${}^{v}\bar{d}_{y,j} \geq 0 \forall j$ then ${}^{v}\bar{d}_{y,j}$ will converge to zero as $j \to \infty$. The same result applies on ${}^{v}\bar{d}_{x,j}$.

Furthermore, $F_{x,j}^{k} \geq F_{x,j-1}^{k}$ $\forall 1 \leq k \leq f$ implies $\bar{F}_{x,j} \geq \bar{F}_{x,j-1}$. Hence, $\bar{\Delta}_{x,j}^{k} = \Delta\frac{\bar{F}x,j-\bar{F}_{x,j-1}}{S_y+F_{y,j-1}^{k}} \geq 0$. Therefore, the convergence of ${}^{v}\bar{d}_{x,j}$ means $\bar{\Delta}_{x,j}^{k} \to 0$ and $\bar{F}_{x,j} - \bar{F}_{x,j-1} \to 0$ as $j \to \infty$. Recalling that $\bar{F}_{x,j} = \frac{\sum_{k=1}^{f} F_{x,j}^{k}}{f}$ then it follows:

$$
\bar{F}_{x,j} - \bar{F}_{x,j-1} = \frac{\sum_{k=1}^{f} F_{x,j}^{k} - F_{x,j-1}^{k}}{f}. \qquad (194)
$$

Combining that $F_{x,j}^{k} - F_{x,j-1}^{k} \geq 0$ $\forall 1 \leq k \leq f$ and $\sum_{k=1}^{f} F_{x,j}^{k} - F_{x,j-1}^{k} \to 0$ as $j \to \infty$ implies that $F_{x,j}^{k} - F_{x,j-1}^{k} \to 0$. Finally, applying the same analysis leads to $F_{y,j}^{k} - F_{y,j-1}^{k} \to 0$. Hence, MT error ${}^{v}d_j$ converges to zero as $j \to \infty$. This completes the proof. □

5.4.2 Simulations and Results of MTCC

Now we navigate 15 vehicles, where the first 6 travel from the left of the domain to the right and the other 9 from the bottom to the top. We assign horizontal or vertical

Algorithm 6: Modified MTCC Algorithm

Data: Measured final positions ${}^{v}r^{*} = \{1, \cdots, V_x\}$
Measured final positions ${}^{v}r^{*} = \{1, \cdots, V_y\}$

Set $j = 0$. Initialize the flow $F_0^k = \mathbf{0} \in \Re^2$; **repeat**
  repeat
    Trajectory tracing to get ${}^{v}T_i$, ${}^{v}t_i^k$ and ${}^{v}d_i$
    Update the flow in all cells k:

$$F_{x,i+1}^k = F_{x,i}^k + \sum_{v=1}^{\eta^k} \frac{{}^{v}t_i^k}{\eta^k \| {}^{v}T_i \|^2} {}^{v}d_{x,i},$$

  until $\| {}^{v}d_i \| \leq \epsilon_F, \quad \forall v_x \leq V$
  repeat
    Trajectory tracing to get ${}^{v}T_i$, ${}^{v}t_i^k$ and ${}^{v}d_i$
    Update the flow in all cells k:

$$F_{y,i+1}^k = F_{y,i}^k + \sum_{v=1}^{\eta^k} \frac{{}^{v}t_i^k}{\eta^k \| {}^{v}T_i \|^2} {}^{v}d_{y,i},$$

  until $\| {}^{v}d_{y,i} \| \leq \epsilon_F, \quad \forall v \leq V_y$
until $\| {}^{v}d_{x,j} \| \leq \epsilon_F, \quad \forall v \leq V_x$ *and* $\| {}^{v}d_{y,j} \| \leq \epsilon_F, \quad \forall v \leq V_y$

velocity with constant control speed $3m/s$ and we keep the same simulated flow field. While the first scenario includes the MT errors in both axis, we incorporate traveling time in the second case. Recalling that MTCC algorithm alternates between two steps: First X-axis MTCC then Y-axis MTCC until the MT error converges for all the AUVS, we will plot different stages to show the evolution of traced trajectories of part 1 under the influence of part 2. Figures 20b and 20a are obtained after running MTCC for MT error along X-axis and then for Y-axis. Changing the velocity along the Y-direction leads to a noticeable MT error in Figure 20b, although the first part is successfully completed. Running the loop for second time reduces the incurred MT error which confirms the claim that the MT error decreases, see Figure 21b. Finally, we run MTCC for five iterations and as expected the MT error converges for all AUVS. A comparison between Figures 21a, 22a does not reveal considerable difference in flow

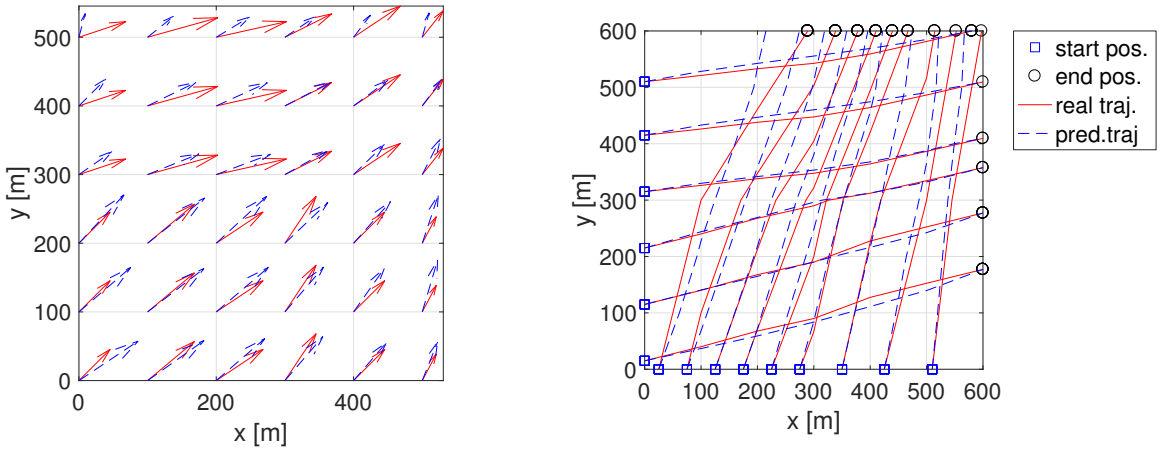

(a) Estimated and true Flow field mapping (b) Estimated and true traced trajectories

Figure 20: MTCC without travel time incorporation after 1 Iteration.

estimation and accordingly the corresponding traced trajectories which shows the fast convergence of MTCC. As planned before, we include the measured travel time as new constraint in MTCC. We will focus on Figure 23a since the traced trajectories remain intact by time constraint. It is worth to underline that this scenario is subject to MT error along both axis, which damps the impact of including measured time that we have noticed in one axis MTCC, see Figure 18a. However, a thorough observation shows that the estimated flow field in the second case is more accurate than in case one. Furthermore let us define δ_F as follows:

$$\delta_F = \max_k \|F^{k*} - F^k\| \quad \forall k \tag{195}$$

We choose δ_F as a criteria to evaluate the performance of the applied algorithms. As a matter of fact, δ_F decreases from $1.7m/s$ to $0.72m/s$ when we incorporate the travel time, proving the contribution of time travel constraint.

5.5 Comparison between MTCP and MTCC

Finally, we conclude the chapter by a comparison between MTCC and MTCP. It is worth to mention that while the MTCC algorithm performs one iteration by cycle, the MTCP updates the flow after every MT error projection, such that the information

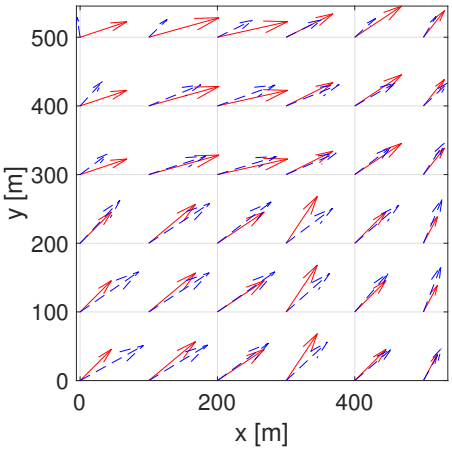

(a) Estimated and true Flow field mapping

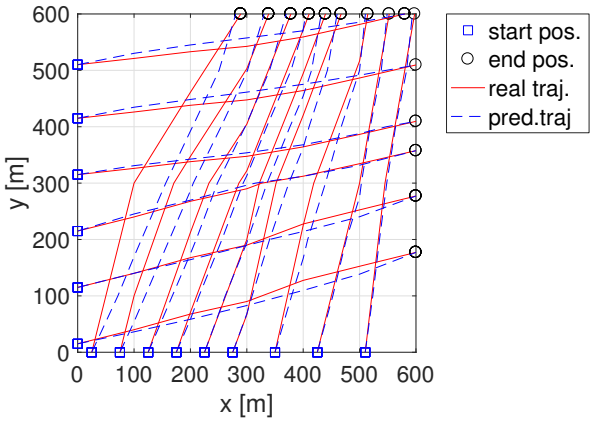

(b) Estimated and true traced trajectories

Figure 21: MTCC without travel time incorporation after 2 Iterations.

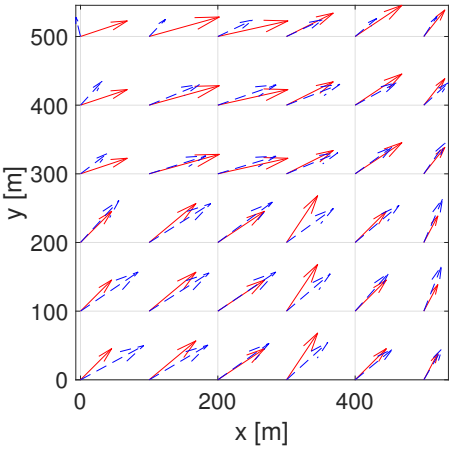

(a) Estimated and true flow field mapping

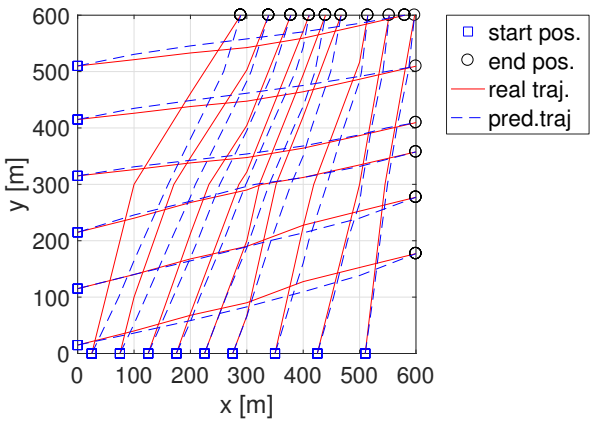

(b) Estimated and true traced trajectories

Figure 22: MTCC without travel time incorporation after 5 Iterations.

used for trajectory tracing is always the most recent one. It seems that MTCC is not optimal; indeed, a complete calculation of all new AUVs MT errors is completed before the correction step. The traced trajectories resulted from MTCP are similar to the ones obtained from MTCC. However, we can not draw definitive conclusion on the efficiency of the algorithm due to the inherent discontinuity of the underlying problem, which urges the running of different simulations to evaluate both approaches. We propose the same scenario described above and we get the following results: The

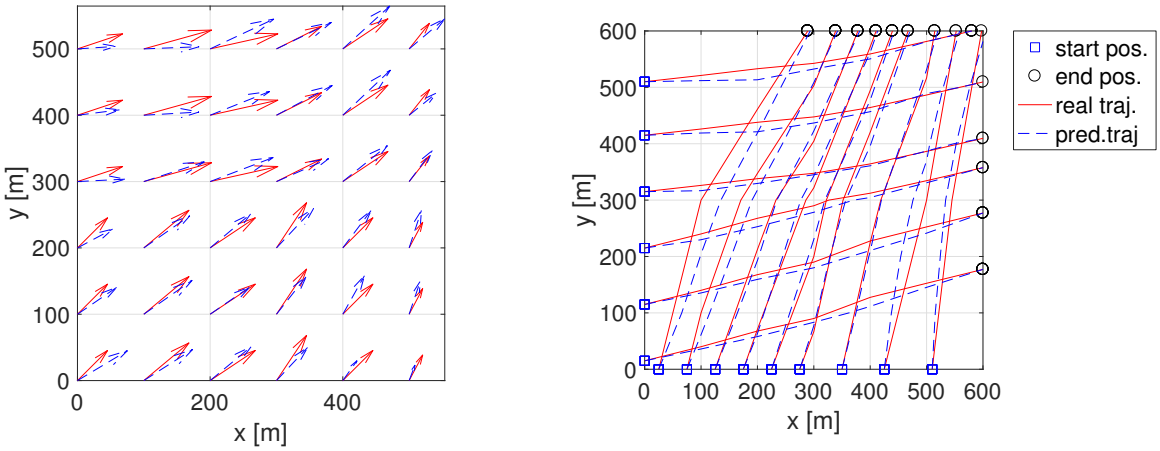

(a) Estimated and true flow field mapping (b) Estimated and true traced trajectories

Figure 23: MTCC with travel time incorporation.

estimated flow field shows some differences in several cells, see Figures 23a, 24a. For example MTCC outperforms MTCP in the first row, however it exhibits lower accuracy in the first column though. It seems difficult to asses the performance from the flow field mapping solely. Hence, we utilize the average estimation error δ_F and the maximum estimation error $\bar{\delta}_F$ to judge the performance of the proposed algorithm. Concerning MTCP, δ_F is equal to $0.38m/s$ and $\bar{\delta}_F = 1.01$. However, for MTCC δ_F is equal to $0.36m/s$ and $\bar{\delta}_F = 0.72$, which implies that MTCC has better performance than MTCP.

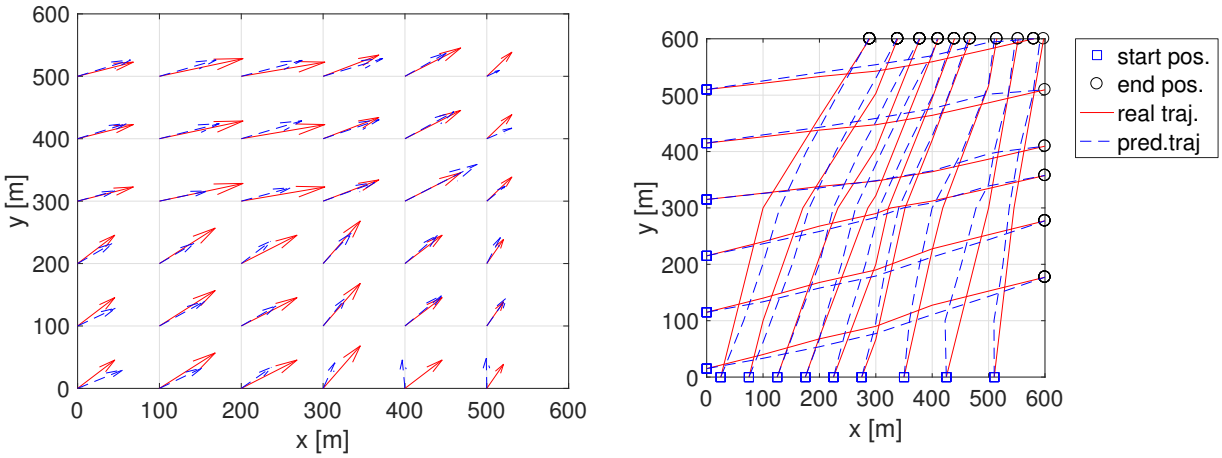

(a) Estimated and true flow field mapping

(b) Estimated and true traced trajectories

Figure 24: MTCP with travel time incorporation.

CHAPTER VI

CONCLUSION

In this thesis we redesigned the motion tomography (MT) algorithm and improved its accuracy in estimating the flow field by incorporating temporal data. In the first part of this thesis, we provided a short review of the MT concept with an emphasis on the shortcomings from the convergence study perspective. Based on the review, we further investigated the proposed proof and found issues with its validity when the Lipschitz assumption does not hold. As a matter of fact, we could not use the available literature which relies on the Lipschitz property in different forms as a fundamental prerequisite to prove the convergence of the inverse problem.

Motivated by the above challenge, we adjusted the MT algorithm to better support further analysis and adopted a new procedure to understand the MT mechanism in order to overcome the difficulty. At first, we focused on one vehicle MT, where we split the algorithm into different steps. After that, we studied the mutual impact between flow update and trajectory tracing. This allowed us to derive local MT nonlinear error dynamics, a standard rule to judge the stability of MT algorithm. Furthermore, we gradually raised the difficulty and enlarged the scope to multiple vehicle MT. In multiple vehicle MT, we looked into the effect of the neighbors on the predicted trajectory of the corresponding vehicle. Based on that, we proved the convergence of MT error. Then, we considered the general case.

Inspired by the Computerized Tomography (CT), we suggested two versions of the MT algorithm in order to fuse the two-dimensional data collected by the AUV: MT Correction per Cycle (MTCC) and MT Correction per Projection (MTCP). We discussed the two methods in regard to the obtained performance and the incurred

computational load. Furthermore, we built on the previous results to establish the convergence of the MTCC algorithm.

A novel part of this thesis is the incorporation of travel times for multiple vehicles in the MT algorithm. As we divided the whole structure into the final position error part and the travel time error part, we were able to study the two problems separately, a good merit from redesigning the MT algorithm. We used Kaczmarz-type methods to solve nonlinear systems of equations constructed for the time error problem and we showed that the simulated travel time converges to the measured one.

The simulations are in good agreement with the theoretical study and show the benefit of taking into account the travel time in the form of a second optimization problem accommodated in the MT algorithm.

In the light of the good performance of the proposed MT algorithm, future work will address some open issues, such as multi-path tracing or the difficulty of choosing an initial value for the reconstruction. Hence, it would be of interest to incorporate some physical insight into the optimization problem to define one unique solution that can be characterized according to oceanography. We also suggest to study the parametric flow model and apply the derived techniques derived in this thesis.

Recalling the primary motivation for flow estimation, we can consider the MT algorithm with respect to the path planning algorithm as a general frame or structure that combines both methods in a harmonized way. Therefore, a map of a flow field estimated by the MT algorithm can be used to guide AUVs in real time. Finally, an issue of practical and of theoretical concern to the control community is the practical applicability of the method to realistic oceanographic features. Therefore, it is interesting to look for the appropriate speed, number, and placement of AUVs and to inquire whether the obtained results are still valid for strong environmental variations.

REFERENCES

[1] Atkinson, C. and Soria, J., "Algebraic reconstruction techniques for tomographic particle image velocimetry," in *16th Australasian fluid mechanics conference*, pp. 191–198, 2007.

[2] Chang, D., Wu, W., Edwards, C. R., and Zhang, F., "Motion tomography: Mapping flow fields using autonomous underwater vehicles," *International Journal of Robotics Research*, vol. 36, no. 3, pp. 320–336, 2017.

[3] Chang, D., Liang, X., Wu, W., Edwards, C. R., and Zhang, F., "Real-time modeling of ocean currents for navigating underwater glider sensing networks," in *Cooperative Robots and Sensor Networks* (Koubâa, A. and Khelil, A., eds.), vol. 507 of *Studies in Computational Intelligence*, pp. 61–75, Springer Berlin Heidelberg, 2014.

[4] Chang, D., Wu, W., and Zhang, F., "Glider CT: Analysis and experimental validation," in *Distributed Autonomous Robotic Systems* (Chong, N.-Y. and Cho, Y.-J., eds.), vol. 112 of *Springer Tracts in Advanced Robotics*, pp. 285–298, Springer Japan, 2016.

[5] Chang, D. and Zhang, F., "Distributed motion tomography for time-varying flow fields," in *OCEANS16 MTS/IEEE Shanghai (OCEANS 2016)*, 2016.

[6] Chang, D. and Zhang, F., "Resolving temporal variations in data-driven flow models constructed by motion tomography," in *10th IFAC Symposium on Nonlinear Control Systems (NOLCOS 2016)*, 2016.

[7] Chen, X. and Yamamoto, T., "Newton-like methods for solving underdetermined nonlinear equations with nondifferentiable terms," *Journal of Computational and Applied Mathematics*, vol. 55, no. 3, pp. 311–324, 1994.

[8] Denis, F., Basset, O., and Gimenez, G., "Ultrasonic transmission tomography in refracting media: reduction of refraction artifacts by curved-ray techniques," *IEEE Transactions on medical imaging*, vol. 14, no. 1, pp. 173–188, 1995.

[9] Epstein, C. L., *Introduction to the mathematics of medical imaging*. Society for Industrial and Applied Mathematics, second ed., 2008.

[10] Fischer, A., "Local behavior of an iterative framework for generalized equations with nonisolated solutions," *Mathematical Programming*, vol. 94, no. 1, pp. 91–124, 2002.

[11] Fischer, A., Herrich, M., Izmailov, A. F., and Solodov, M. V., "Convergence conditions for newton-type methods applied to complementarity systems with nonisolated solutions," *Computational Optimization and Applications*, vol. 63, no. 2, pp. 425–459, 2016.

[12] Geoffroy, M. H., "Iterative solving of generalized equations with calm solution mappings," *Journal of mathematical analysis and applications*, vol. 313, no. 2, pp. 689–699, 2006.

[13] Gordon, R., Bender, R., and Herman, G. T., "Algebraic reconstruction techniques (ART) for three-dimensional electron microscopy and x-ray photography," *Journal of theoretical biology*, vol. 29, no. 3, pp. 471–481, 1970.

[14] Gutiérrez, J. M., Magreñán, Á. A., and Romero, N., "On the semilocal convergence of newton–kantorovich method under center-lipschitz conditions," *Applied Mathematics and Computation*, vol. 221, pp. 79–88, 2013.

[15] Hackbarth, A., Kreuzer, E., and Schröder, T., "Cfd in the loop: Ensemble kalman filtering with underwater mobile sensor networks," in *ASME 2014 33rd International Conference on Ocean, Offshore and Arctic Engineering*, pp. V002T08A063–V002T08A063, American Society of Mechanical Engineers, 2014.

[16] Jakovetić, D., Xavier, J., and Moura, J. M. F., "Fast distributed gradient methods," *IEEE Transactions on Automatic Control*, vol. 59, no. 5, pp. 1131–1146, 2014.

[17] Kaczmarz, S., "Angenäherte auflösung von systemen linearer gleichungen," *Bulletin International de lAcademie Polonaise des Sciences et des Lettres*, vol. 35, pp. 355–357, 1937.

[18] Kaczmarz, S., "Approximate solution of systems of linear equations," *International Journal of Control*, vol. 57, no. 6, pp. 1269–1271, 1993.

[19] Kak, A. C. and Slaney, M., *Principles of computerized tomographic imaging*. SIAM, 2001.

[20] Kamath, G., Ramanan, P., and Song, W.-Z., "Distributed randomized Kaczmarz and applications to seismic imaging in sensor network," in *2015 International Conference on Distributed Computing in Sensor Systems*, pp. 169–178, 2015.

[21] Kinsey, J. C., Eustice, R. M., and Whitcomb, L. L., "A survey of underwater vehicle navigation: Recent advances and new challenges," in *IFAC Conference of Manoeuvering and Control of Marine Craft*, vol. 88, 2006.

[22] Lobel, I. and Ozdaglar, A., "Convergence analysis of distributed subgradient methods over random networks," in *2008 46th Annual Allerton Conference on Communication, Control, and Computing*, pp. 353–360, 2008.

[23] Martínez, J. M. and De Sampaio, R. J., "Parallel and sequential Kaczmarz methods for solving underdetermined nonlinear equations," *Journal of Computational and Applied Mathematics*, vol. 15, no. 3, pp. 311–321, 1986.

[24] Meyn, K.-H., "Solution of underdetermined nonlinear equations by stationary iteration methods," *Numerische Mathematik*, vol. 42, no. 2, pp. 161–172, 1983.

[25] Mueller, J. L. and Siltanen, S., *Linear and nonlinear inverse problems with practical applications*. SIAM, 2012.

[26] Natterer, F., *The mathematics of computerized tomography*. Society for Industrial and Applied Mathematics, 2001.

[27] Natterer, F. and Wübbeling, F., *Mathematical methods in image reconstruction*. Society for Industrial and Applied Mathematics, 2001.

[28] Nedic, A. and Ozdaglar, A., "Distributed subgradient methods for multi-agent optimization," *IEEE Transactions on Automatic Control*, vol. 54, no. 1, pp. 48–61, 2009.

[29] Nesterov, Y. E., "A method for solving the convex programming problem with convergence rate O(1/kˆ2)," *Doklady Akademii Nauk SSSR*, vol. 269, no. 3, pp. 543–547, 1983.

[30] Paull, L., Saeedi, S., Seto, M., and Li, H., "Auv navigation and localization: A review," *IEEE Journal of Oceanic Engineering*, vol. 39, no. 1, pp. 131–149, 2014.

[31] Penrose, R., "A generalized inverse for matrices," *Mathematical Proceedings of the Cambridge Philosophical Society*, vol. 51, no. 3, pp. 406–413, 1955.

[32] Prikopa, K. E., Straková, H., and Gansterer, W. N., "Analysis and comparison of truly distributed solvers for linear least squares problems on wireless sensor networks," in *Euro-Par 2014 Parallel Processing*, Lecture Notes in Computer Science, pp. 403–414, Springer International Publishing, 2014.

[33] Qi, L. and Sun, J., "A nonsmooth version of newton's method," *Mathematical programming*, vol. 58, no. 1, pp. 353–367, 1993.

[34] Schomberg, H., "An improved approach to reconstructive ultrasound tomography," *Journal of Physics D: Applied Physics*, vol. 11, no. 15, pp. L181–L185, 1978.

[35] Strohmer, T. and Vershynin, R., "A randomized Kaczmarz algorithm with exponential convergence," *Journal of Fourier Analysis and Applications*, vol. 15, no. 2, pp. 262–278, 2008.

[36] Sundhar Ram, S., Nedić, A., and Veeravalli, V. V., "Distributed stochastic subgradient projection algorithms for convex optimization," *Journal of Optimization Theory and Applications*, vol. 147, no. 3, pp. 516–545, 2010.

[37] Tarantola, A., *Inverse problem theory and methods for model parameter estimation*. SIAM, 2005.

[38] Tepe, J., Schuster, T., and Littau, B., "A modified algebraic reconstruction technique taking refraction into account with an application in terahertz tomography," *Inverse Problems in Science and Engineering*, pp. 1–26, 2016.

[39] Wu, W., Chang, D., and Zhang, F., "Glider CT: Reconstructing flow fields from predicted motion of underwater gliders," in *Proceedings of the Eighth ACM International Conference on Underwater Networks and Systems*, p. 47, 2013.

[40] Yamamoto, T., "Historical developments in convergence analysis for newton's and newton-like methods," *Journal of Computational and Applied Mathematics*, vol. 124, no. 1, pp. 1–23, 2000.

[41] Zhou, G. and Qi, L., "On the convergence of an inexact newton-type method," *Operations research letters*, vol. 34, no. 6, pp. 647–652, 2006.